Characterization of T2Rs in the vasculature and

Elucidation of T2R4 desensitization mechanism

By
Jasbir Deol Upadhyaya

A thesis submitted to the Faculty of Graduate Studies of
The University of Manitoba

In partial fulfillment of the requirements of the degree of

Doctor of Philosophy

Department of Oral Biology

College of Dentistry

University of Manitoba

Winnipeg, Manitoba, Canada

ABSTRACT

Humans can taste many compounds but are able to distinguish between five basic tastes, bitter, sweet, umami, sour and salt. Bitter taste, which is mediated by 25 bitter taste receptors (T2Rs) in humans, acts as a central warning signal against the ingestion of toxic compounds. In addition to their expression in the oral cavity, T2Rs are expressed in various extra-oral tissues, suggesting that they have additional functions apart from sensing taste. The recent finding that T2Rs, upon activation with bitter tastants, cause muscle relaxation and bronchodilation of pre-contracted airway smooth muscle, has been a topic of consideration. The bronchodilatory role of T2Rs, which was three fold greater than that elicited by currently used beta-adrenergic receptor agonists, has implicated them as potential therapeutic targets for the treatment of asthma. In view of the importance of T2R function in extra-oral tissues, it is of fundamental importance to determine their physiological role in extra-oral regions like the vascular tissues, and understand how T2R signal is regulated.

In this study, two representative bitter taste receptors, T2R1 and T2R4, were selected to elucidate the function and signal regulation of T2Rs. The expression of T2Rs was characterized in pulmonary artery smooth muscle cells, and studies were pursued to explore the effects of dextromethorphan (DXM) on the pulmonary artery. DXM caused vasoconstriction in pulmonary arterial cells by activating endogenous T2R1. The structure-function role of the carboxyl (C)-terminus of T2R4 receptor was characterized by site-directed mutagenesis. A conserved KLK motif was identified in the C-terminus and many residues involved in cell surface targeting and function of T2R4 were revealed. A constitutively active mutant (CAM) was also discovered within the T2R4 C-terminus.

To identify the regulatory proteins involved in T2R4 desensitization, a molecular and pharmacological approach was used. The kinases involved in this process were identified by performing either a knockdown or by using activators and inhibitors. The potential residues of T2R4 involved in desensitization were assessed for function. In addition, the internalization status of few T2Rs was determined by using different bitter compounds. This study provides novel insights into the function and desensitization of T2Rs and reports a pharmacochaperone activity for quinine.

ACKNOWLEDGEMENTS

First and foremost, I offer my sincere gratitude to my supervisor, Dr Prashen Chelikani, whose expertise, understanding and patience added considerably to my graduate experience. I am thankful to him for providing me the resources and a healthy environment for pursuing my graduate work. I would also like to thank my advisory committee members Dr Raj Bhullar, Dr Catalena Birek, and Dr Maria Vrontakis, for their guidance and insightful comments over the years.

The insights and suggestions received from Drs Catalena Birek, Raj Bhullar, and all professors who were a part of the "Cell Biology" course, during my course work are gratefully acknowledged. I am extremely grateful to our collaborator Dr Shyamala Dakshinamurti and thank Anurag Singh Sikarwar for his assistance with isometric myography assays which form part of this thesis project. I also want to thank Linda Delmage for all the help with administrative work. She was always a great help.

I acknowledge and appreciate the financial support provided by the College of Dentistry and the Faculty of Graduate studies for my travel to national and international conferences. I want to thank the Faculty of Graduate Studies for providing me the International Graduate Student Scholarship, and the Manitoba Health Research Council for offering me scholarship for two consecutive years during my PhD study. I am extremely thankful to my lab members Nisha Singh, Sai Prasad Pydi, Raja Chakraborty, Thi Le for their assistance and continuous support during my graduate studies at the University of Manitoba.

I warmly thank my parents and in-laws for their moral and spiritual support in all aspects of my life and for believing in me. I also thank my brother for always being there for me. Last but not the least, I want to express my gratitude and deepest appreciation to my husband and lovely daughter, Ahana, for their patience and understanding. My graduate study would not have been possible without them.

DEDICATION

I dedicate this thesis to my parents and my family for their moral support and unconditional love

TABLE OF CONTENTS **Page**

CHAPTER 4

LIST OF FIGURES

LIST OF TABLES

LIST OF COPYRIGHT MATERIAL FOR WHICH PERMISSION WAS OBTAINED

CHAPTER 1

FIGURE 1.1.1 Reprinted with permission from the *Clinical Therapeutics* ; "The Bad Taste of Medicines: Overview of Basic Research on Bitter Taste", 35(8); 1225-46, 2013. © by Elsevier Ltd.

CHAPTER 4.2 & 5.2: Structure-function role of C-terminus in human bitter taste receptor T2R4 signaling

Reprinted with permission from the *Biochimica et Biophysica Acta-Biomembranes,* 1848(7):1502-1508. *License number*- 3641771415456, © by Elsevier Ltd.

LIST OF ABBREVIATIONS

AHLs	Acyl homoserine lactones
BCML	Nα, Nα-Bis carboxy methy-L-lysine
Ca^{2+}	Calcium
CAMs	Constitutively active mutants
cAMP	Cyclic adenosine monophosphate
CO_2	Carbon dioxide
C-terminus	Carboxyl-terminus
DAG	Diacyl glycerol
DB	Denatonium benzoate
DMEM	Dulbecco's modified Eagle's medium
DMSO	Dimethyl sulfoxide
DXM	Dextromethorphan
ECLs	Extracellular loops
ER	Endoplasmic reticulum
FBS	Fetal bovine serum
FFF	Phenylalanine tripeptide
GABA	γ-Amino butyric acid
GNA	Guanine nucleotide binding protein, alpha subunit
GPCRs	G protein-coupled receptors
GRKs	G protein-coupled receptor kinases
GRK-KD	G protein-coupled receptor kinases knock down

hASMCs	Human airway smooth muscle cells
3HDC	3β-Hydroxydihydrocostunolide
HEK cells	Human Embryonic Kidney cells
3HP	3β-Hydroxypelenolide
hPASMCs	Human pulmonary artery smooth muscle cells
ICLs	Intracellular loops
IMNB	N-isopropyl-2- methyl-5-nitrobenzenesulphonamide
IP_3	Inositol triphosphate
LB media	Luria Bertani media
MFI	Mean fluorescence intensity
MLC	Myosin light chain
MLCK	Myosin light chain kinase
nsSNPs	Non-synonymous single nucleotide polymorphisms
N-terminus	Amino-terminus
ON	Overnight
PBS	Phosphate-buffered saline
PDEs	Phosphodiesterases
PIP_2	Phosphatidylinositol 4,5-biphosphate
PKA	Protein kinase A
PKC	Protein kinase C
PLC	Phospholipase C
PROP	6-n-propyl-2-thiouracil
PTC	Phenylthiocarbamide

T1R	Sweet/Umami taste receptor
T2R	Bitter taste receptor
TAS1R	Sweet/Umami taste receptor gene
TAS2R	Bitter taste receptor gene
TMs	Transmembranes
TRCs	Taste receptor cells
TRPM5	Transient receptor potential melastatin-5
WT	Wild type

CHAPTER 1

1.0 INTRODUCTION

1.1 Overview

The ability to perceive, recognize, and respond to stimuli is essential for the survival of organisms. The gustatory system has evolved to recognize essential nutrients as well as for protection against poisonous or harmful compounds in ingested food. Taste is one of the basic senses through which we receive information about the presence of chemicals in food. Humans, and probably other mammals, can taste many compounds but distinguish between five basic tastes which are sweet, bitter, sour, salt and umami. Salt and sour tastes are thought to be mediated via cation channels (Heck et al., 1984; Kinnamon et al., 1988; Ugawa et al., 1998). In contrast, sensation of bitter, sweet and umami tastes is initiated by the interaction of taste molecules with G protein-coupled receptors (GPCRs) (Adler et al., 2000; Gilbertson et al., 2000; Sainz et al., 2001). Recent studies indicate that humans can detect a sixth taste, i.e., the taste of fat, by reaction with free fatty acids present in food (Stewart et al., 2010). Bitter taste is innately aversive and is believed to guard against the ingestion of toxic substances, many of which taste bitter to humans. The molecular events in the perception of taste start at the apical surface of taste receptor cells (TRCs) found in taste buds in the mouth. The interaction of tastants with taste receptors, located in the membrane of TRCs, initiates signaling cascades which are transmitted to the brain through sensory afferents and perceived as taste (Chen et al., 2011).

1.2 Physiology of Taste System

Taste buds are found in taste papillae which are located on the tongue, palate, and to a lesser extent the epiglottis, pharynx and larynx. However, tongue is the main organ of taste and papillae are the primary structures that contain the sensory nerve endings. In humans, around 5,000 taste buds, distributed across these papillae, are present on the dorsal surface of tongue (Miller, 1995). Each taste bud is oval in shape and contains 50-100 TRCs that mediate the sense of taste (Brouwer and Wiersma, 1978; Lalonde and Eglitis, 1961; Miller, 1986) **(Figure 1.1.1)**. Each TRC, containing dozens of taste receptors, projects microvilli to the apical surface of taste bud, where a taste pore is formed.

Humans have four types of papillae: fungiform, foliate, and circumvallate papillae contain taste buds, while filiform papillae transduce touch, temperature, and nociception (Miller and Preslar, 1975). The fungiform papillae are mushroom-shaped structures that protrude from the surface of tongue. Humans have on average 195 human fungiform papillae, majority of which are located on the anterior two-thirds of tongue (Miller, 1986). Foliate papillae are folds on lateral sides of the tongue containing over 100 taste buds, whereas, circumvallate papillae form an inverted V at posterior one-third of the tongue. Bulk of the tongue has filiform papillae which contain trigeminal nerve endings that transmit information about temperature, texture and pain (Miller and Preslar, 1975).

The interaction of taste receptors with the tastants generates signals which are transmitted to the brain via cranial nerves. Three cranial nerves innervate the tongue: chorda tympani (CN VII), glossopharyngeal (CN IX), and trigeminal (CN V). The chorda tympani innervates the anterior fungiform papillae of tongue. The glossopharyngeal innervates the circumvallate and the foliate papillae present on posterior part of the tongue. The trigeminal nerve receives information from the filiform papillae and from various nerve endings

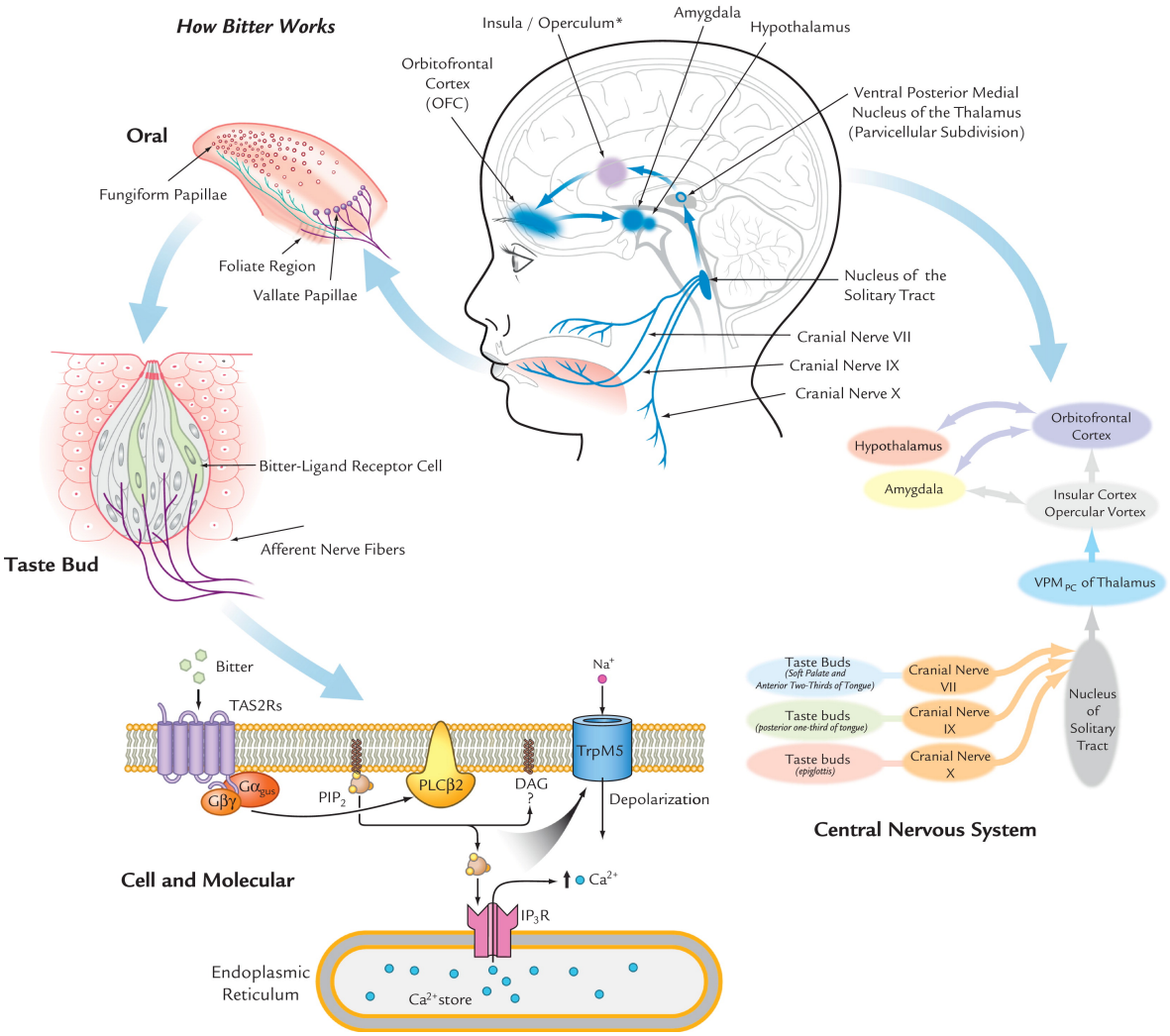

Figure 1.1.1. Mechanism of Bitter Taste Perception. The figure illustrates the bitter taste signal transduction which starts in the oral cavity, after bitter tastants activate bitter taste receptors (T2Rs), and is finally transmitted to the brain via cranial nerves where it is perceived as taste. DAG, Diacylglycerol; $G\alpha_{gust}$, G-protein subunit α-gustducin; Gβγ, G-protein subunits β and γ; IP_3R, inositol triphosphate receptor; PIP_2, phosphatidyl inositol 4,5-biphosphate; PLCβ2, phospholipase C β 2; TRPM5, transient receptor potential ion channel subfamily Member 5; VPMPC, ventral posterior medial nucleus, parvicellular subdivision. (Mennella et al., 2013)

throughout the oral cavity. Taste information from the oral cavity is then projected to the insula of the gustatory cortex region of brain **(Figure 1.1.1)**.

1.3 Taste modalities

Basic tastes comprise of a group of five tastes; sweet, bitter, umami, sour and salt **(Figure 1.3.1)**. Recent studies show that humans have an orosensory system which recognizes dietary fats (Mattes, 2001). Free fatty acids are potent gustatory stimuli which are abundant in the human diet. Specific membrane receptors, like GPR120 and CD36, which are essential for detecting fatty acids are present on taste bud cells (Sclafani et al., 2007). In addition to these well known taste modalities, humans are responsive to CO_2 i.e., the taste of carbonation. Sour-sensing cells act as the taste sensors for carbonation and carbonic anhydrase 4 enzyme functions as the principal CO_2 taste sensor (Chandrashekar et al., 2009). Taste is also commonly confused with somatosensory sensations such as the cool of menthol or the heat of chili peppers. Gustation is the sensory modality generated when chemicals activate oral taste buds and transmit signals to the brain. Capsaicin (the active compound in chilis) and menthol principally stimulate ion channels in somatosensory nerve fibers (Caterina et al., 1997; McKemy et al., 2002). Capsaicin and related compounds may stimulate important interactions between somatosensory trigeminal nerve fibers in the tongue and taste buds, and thus modulate taste (Wang et al., 1995; Whitehead et al., 1999).

1.4 Taste GPCRs

The two best-characterized families of taste receptors, sweet/umami (T1Rs) and bitter receptors (T2Rs), belong to the GPCR superfamily.

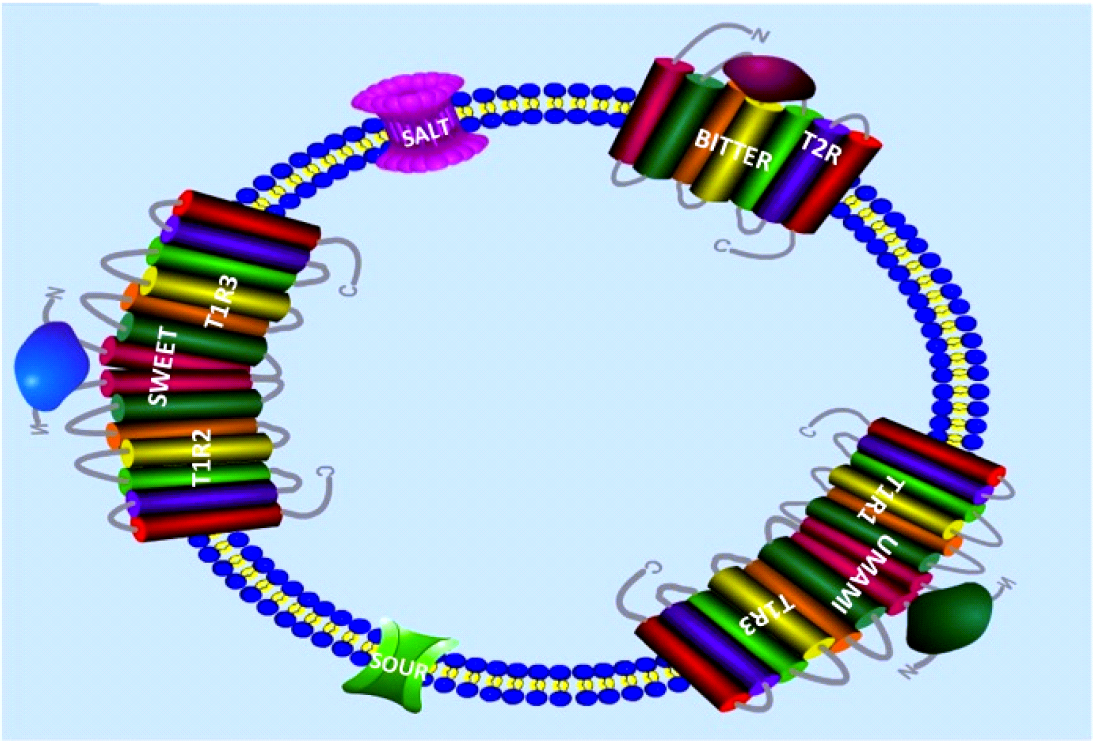

Figure 1.3.1. Schematic representation of the five basic taste modalities. Sour and salt tastes are sensed by ion channels. Sweet, umami and bitter tastes are mediated by G protein-coupled receptors. Bitter taste receptors are referred to as T2Rs, whereas, sweet/umami receptors are known as T1Rs. T1R1 and T1R3 combine to form a umami taste receptor, and heterodimer of T1R2 and T1R3 senses sweet tasting molecules. The ligand for sweet/umami taste receptor binds to the N-terminal domain. In contrast, bitter tasting compounds bind within the extracellular and transmembrane domains of the bitter taste receptor. The figure was generated using Pathway Builder Tool version 2: *www.proteinlounge.com*.

1.4.1 Sweet and Umami taste receptors: T1Rs

Sweet and umami tastes are mediated by a family of three GPCRs, T1R1, T1R2 and T1R3, which combine to form heterodimeric receptors (Li et al., 2002; Nelson et al., 2001). Heterodimerization of T1R2 and T1R3 forms a sweet taste receptor which is activated by molecules like sucrose, fructose, artificial sweeteners like acesulfame-K and saccharin (Li et al., 2002; Nelson et al., 2001) **(Figures 1.3.1 and 1.4.1)**. T1R1 and T1R3 combine to form a heterodimer which is activated by monosodium glutamate (MSG, umami) (Nelson et al., 2002). T1Rs belong to class C GPCRs, other members of the family being metabotropic glutamate receptors (mGluRs), a calcium sensing receptor (CaR), γ-aminobutyric $acid_B$ ($GABA_B$) receptors, L-amino acid receptor GPRC6A and pheromone receptors (V2Rs) (Schioth and Fredriksson, 2005). In addition to a heptahelical transmembrane domain (TMD), these receptors share a large N-terminus or Venus flytrap (VFT) domain linked to the TM via cysteine-rich domain (CRD) (Pin et al., 2003) **(Figures 1.3.1 and 1.4.1)**. The large VFT forms the orthosteric or primary ligand binding site which recognizes endogenous ligands. All T1Rs in the anterior tongue and palate are co-expressed with Gα subunit, gustducin (Adler et al., 2000; Kim et al., 2003a). α-gust is expected to activate a phosphodiesterase (PDE) and decrease intracellular cAMP levels. However, studies suggest that, in addition to Gα-gustducin, sweet taste receptor may couple to Gαs and increase cAMP levels in taste receptor cells (Bernhardt et al., 1996; Margolskee, 2002). The role of α-gust in sweet taste is much less clear than for bitter and umami taste. The sweet taste receptor T1R3 is usually not co-expressed with Gα-gust in posterior tongue. Instead it is co-expressed with a Gq family protein, Gα14, in circumvallate and foliate taste buds (Shindo et al., 2008; Tizzano et al., 2008). Furthermore, literature points to a direct coupling of sweet and umami taste

receptors to Gαi/o proteins (Ozeck et al., 2004). However, it is possible that T1Rs, depending on the cell and tissue and in different physiological conditions, might couple to both Gαi/o and Gαs proteins.

1.4.2 Bitter taste receptors: T2Rs

In humans, bitter taste is perceived by 25 members of the GPCR superfamily, referred to as T2Rs, which are 291-334 amino acids long (Adler et al., 2000; Chandrashekar et al., 2000; Matsunami et al., 2000). These taste receptors, discovered a little more than a decade ago, encode for intronless genes which are referred to as TAS2Rs. The HUGO gene nomenclature of TAS2R is used wherever the gene is mentioned. Except for the TAS2R1 gene, which is localized on chromosome 5p, all other TAS2Rs are organized in the genome in clusters on human chromosomes 7q and 12p, and are genetically linked to loci that influence bitter perception (Conte et al., 2002). Additionally, there are a large number of TAS2R pseudogenes and more than 80 single nucleotide polymorphisms (SNPs) among individual TAS2R genes (Conte et al., 2002; Kim et al., 2005b). The classification of T2Rs within the GPCR family is unclear, with some describing them as a separate family (Horn et al., 2003), whereas, other classification systems have grouped them with the frizzled receptors (Fredriksson et al., 2003). The International Union of Basic and Clinical Pharmacology (IUPHAR) list Frizzled receptors as a separate GPCR family, Class F, and this class does not include T2Rs (Sharman et al., 2013). T2Rs are relatively divergent, showing ~ 25-90% amino acid identity (Adler et al., 2000; Matsunami et al., 2000). This variability corresponds well with an ability to interact with chemically diverse ligands associated with bitter tastes. A single bitter compound is capable of activating multiple T2Rs and each T2R

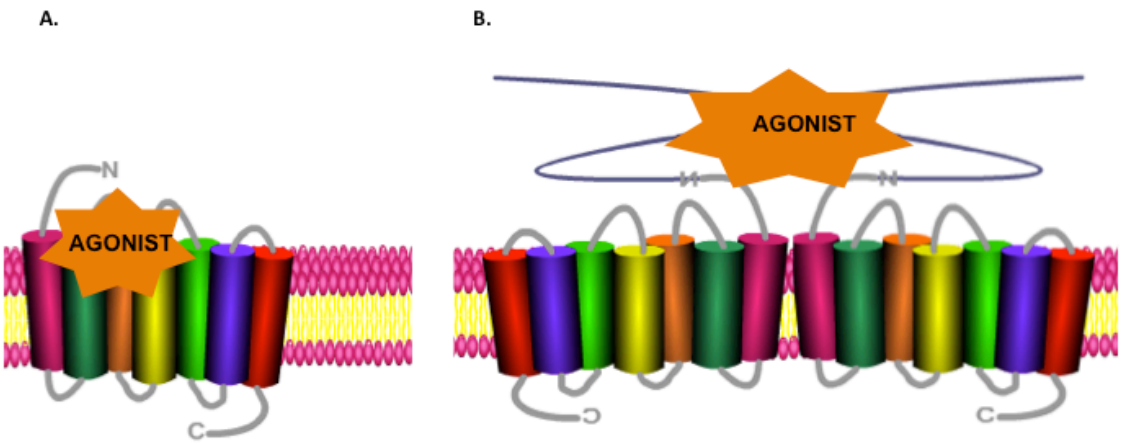

Figure 1.4.1. Taste GPCRs – Bitter and Sweet/Umami receptors. A. Bitter taste receptor (T2R) consists of around 300-330 amino acids, has a short extracellular N-terminus consisting of 7-19 amino acids, an intracellular C-terminus around 7-32 amino acids long, with the extracellular loops and TM regions being the likely sites of agonist binding. T2Rs are localized in clusters on human chromosomes 5, 7 and 12. **B.** Sweet and umami tastes are mediated by a family of three GPCRs, T1R1, T1R2 and T1R3, which combine to form heterodimeric receptors. T1Rs consist of around 850 amino acids, have a long extracellular N-terminus, known as Venus Flytrap, which is believed to mediate ligand binding, and a short intracellular C-terminus. The figure was generated using Pathway Builder Tool version 2: *www.proteinlounge.com*.

can be activated by multiple bitter compounds (Meyerhof et al., 2010). In contrast to the long N-terminus of T1Rs, T2Rs are characterized by a short extracellular N-terminus **(Figure. 1.4.1)**. Sequence conservation is more in the TMs and ICLs of T2Rs, whereas, the N- and C-termini and the ECLs have low amino acid identity. The TMs and ECLs are the predicted regions of ligand binding in T2Rs and ICLs are the regions for G-protein interaction (Adler et al., 2000).

1.5 T2R Signal Transduction

Long before the discovery of T2Rs, the involvement of taste-specific Gα protein, Gα-gustducin, in bitter receptor mediated transduction mechanism was demonstrated (Wong et al., 1996). The generation of α-gustducin knock-out mice resulted in a dramatic reduction in their bitter tasting abilities. Moreover, T2Rs were shown to functionally couple to transducin (He et al., 2002) *in vivo* as well as to other Gi/Go proteins *in vitro* (Ozeck et al., 2004). The mechanism involved in the perception of bitter taste and the second-messengers or other downstream components of T2R signaling pathway were also known before the T2Rs were discovered in 2000 (Chandrashekar et al., 2000; Kurihara et al., 1994; Spielman et al., 1996). A cation channel, transient receptor potential melastatin subtype 5 channel (TRPM5), was found co-expressed with other taste signaling molecules in the taste tissue (Perez et al., 2002).

The canonical T2R signal transduction pathway in a taste receptor cell of the taste bud is described in **Figure 1.5.1**. The binding of a bitter-tasting compound or an agonist, on the extracellular surface of a T2R causes conformational changes in the receptor, and this in turn activates the heterotrimeric G-protein complex, α-gustducin, β1/3 and γ13 on the intracellular

surface of the receptor. The βγ-subunits activate the enzyme phospholipase Cβ2 (PLC β2) which hydrolyzes inositol phospholipid (PIP_2) resulting in the production of 1,4,5-triphosphate (IP_3) and diacylglycerol (DAG). Generation of IP_3 activates IP_3 receptors on the membrane of endoplasmic reticulum (ER), thus opening the calcium release channels and causing transient increase in intracellular calcium. This opens the monovalent selective TRPM5 channels, leading to sodium influx, membrane depolarization and thus release of ATP as a neurotransmitter to activate the gustatory afferents (Finger et al., 2005) **(Fig. 1.5.1)**. In a contrasting pathway, a hypothesis was proposed showing Gα-gustducin to activate the phosphodiesterases (PDEs) which leads to a reduction in cAMP production (McLaughlin et al., 1992; Spielman, 1998).

1.6 Ligand Binding and Activation Mechanisms of T2Rs

Bitter compounds are not only numerous but also structurally diverse. A large number of natural or synthetic molecules which stimulate TAS2Rs include hydroxy fatty acids, peptides, amino acids, amines, N-heterocyclic compounds, urea, thioureas, carbamides, esters, lactones, phenols, alkaloids, glycosides and many more. Several drugs currently marketed for a wide range of indications activate TAS2Rs; these include erythromycin, dapsone, quinine, chloroquine, caffeine, colchicine, flufenamic acid, and azelastine (Meyerhof et al., 2010). In contrast, only 25 T2Rs have been identified, raising the question as to how the vast array of bitter compounds can be detected by such a limited number of receptors. While many T2Rs remain poorly characterized, the ligand specificity of several.

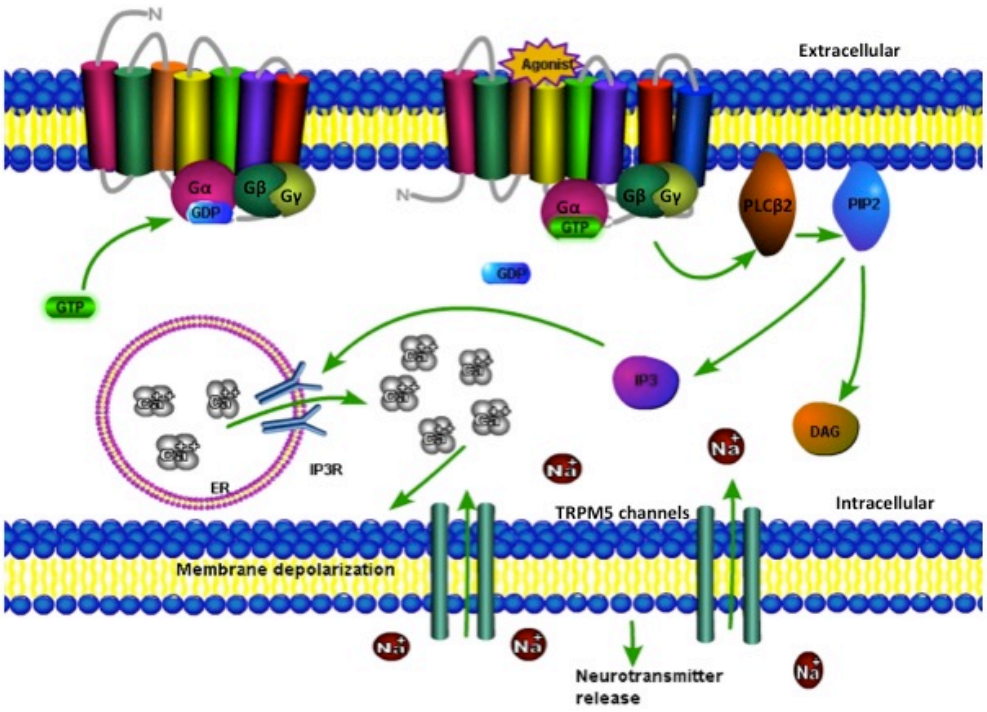

Figure 1.5.1. Bitter taste signaling pathway (IP_3 pathway). Abbreviations: PLCβ2, phospholipase C β2; PIP_2, phospatidyl-inositol-biphosphate; DAG, diacylglycerol; IP_3, inositol triphosphate; ER, endoplasmic reticulum; Ca^{2+}, calcium; Na^{+}, sodium. The figure was generated using Pathway Builder Tool version 2: *www.proteinlounge.com*.

T2Rs was explored in the past decade (Behrens et al., 2004; Brockhoff et al., 2007; Bufe et al., 2002; Chandrashekar et al., 2000; Dotson et al., 2008; Kim et al., 2003b; Kuhn et al., 2004; Maehashi et al., 2008; Meyerhof et al., 2010; Pronin et al., 2004; Sainz et al., 2007; Upadhyaya et al., 2010)

Whereas some receptors recognize only a single or few compounds, others respond to multiple compounds. The affinity of T2Rs for their respective bitter ligands is low, with EC_{50} values in the high micromolar to low millimolar range (Meyerhof et al., 2010). Thus, bitter compounds activate various T2Rs in different concentration ranges, differences usually being in the range of 10-100 fold. However, knowledge of the structural determinants of T2Rs is crucial to provide insights into the molecular basis of bitter sensing and to design new taste modifiers. Molecular modeling and site-directed mutagenesis studies have been pursued to characterize the ligand binding pocket of some T2Rs. The 3D structure of T2R38, also referred to as the phenylthiocarbamide (PTC) receptor, was predicted using computational method *MembStruk* and homology modeling (Floriano et al., 2006). *Hierdock* and *ScanBindSite* computational tools were then used to generate models of PTC bound to T2R38 to predict the binding site and binding energy. According to these models, PTC binds at a site distant from the variant amino acids P49A, A262V and V296I (Floriano et al., 2006). It was also suggested that the inability of humans to taste PTC is due to a failure of G-protein activation, rather than decreased binding affinity of the receptor for PTC. This study emphasized the role of TM6 and TM7 in PTC receptor function. The introduction of bulkier side chains in the non-taster variant altered the packing of TMs 6 and 7, which might render the movement of TM6 more difficult (Biarnes et al., 2010). A recent study predicted the 3D structure of T2R38 using BiHelix and SuperBiHelix Monte Carlo methods (Tan et al., 2012).

This study suggested that the residue 262 is involved in interhelical hydrogen bond network which stabilizes the receptor in tasters (hTAS2R38$_{PAV}$, hTAS2R38$_{AAI}$, and hTAS2R38$_{PVV}$), but not in the non-tasters (hTAS2R38$_{AVI}$) (Tan et al., 2012).

In a study by Pronin *et al,* chimeric receptors for T2R43 and T2R44 were generated in an effort to identify the residues involved in ligand recognition (Pronin et al., 2004). T2R43 is activated by 6-nitrosaccharin and N-isopropyl-2-methyl-5-nitrobenzenesulfonamide (IMNB), a bitter derivative of saccharin. Whereas, T2R44 is activated by denatonium and 6-nitrosaccharin. The amino acid sequences of T2R43 and T2R44 are 89% identical and 15 of the 34 amino acid differences among them are concentrated in ECL1 and ECL2, while ECL3 is completely conserved. T2R43 and T2R44 chimeras were generated by swapping their ECLs-1 and -2. There are only four amino acid differences between T2R43 and T2R44 in ECL1. Functional studies revealed that ECL1 is very important for receptor activation, as replacement of these residues in T2R43 with those of T2R44 was sufficient to render T2R43 insensitive to IMNB. On the other hand, replacing both ECL1 and ECL2 in T2R43 with T2R44 loops eliminated most of the activation by 6-nitrosaccharin. Recently, ligand docking simulations and functional analysis using point mutants of T2R16 were performed to identify binding sites of the receptor for β-glucopyranosides (Sakurai et al., 2010). Seven amino acid residues in TMs 3, 5 and 6 were involved in ligand recognition. Amino acid residues Glu86, Trp94 and Gln177 were involved in salicin recognition, whereas, His181 and hydrophobic residues Phe93, Phe240 and Ile243 likely contributed to formation of the binding site. With the generation of chimeric and mutant receptors, followed by functional analysis, the amino acid residues critical for the activation of T2R46, T2R43 and T2R31 were identified (Brockhoff et al., 2010). The construction of receptor chimeras demonstrated that agonist

selectivity was predominantly determined by TM7 region of the receptors. Exchange of two residues within TM7 between T2R46, activated by strychnine, and T2R31, activated by aristolochic acid, was sufficient to invert the agonist selectivity.

Fermentation of protein-rich foods results in the formation of bitter peptides, which are responsible for the bitter taste of fermented food. Bitter casein digests were shown to activate T2R1, T2R4, T2R14 and T2R16 in a heterologous expression system (Maehashi et al., 2008). Two bitter dipeptides, Gly-Phe (glycine-phenylalanine) and Gly-Leu (glycine-leucine), activated T2R1 more strongly, whereas, they evoked no or weak responses in other receptors. The ability of bitter di- and tri-peptides to activate T2R1 was tested further (Upadhyaya et al., 2010). Results revealed that bitter tri-peptides also activated T2R1 and were more potent than the tested di-peptides. Among all the tested peptides, FFF activated T2R1-expressing cells the most, at concentrations of 0.125-1.0 mM that humans also perceive as bitter, with an EC_{50} value of 370 μM. Phe-Phe-Phe consists of hydrophobic amino acids and the bitter taste of a peptide is more apparent when the hydrophobic amino acid is located at the C-terminus. For the tri-peptides, the middle amino acid residue is considered more important than both the C- and N-terminal amino acids (Wu and Aluko, 2007). In addition, some peptides with ACE (angiotensin-converting enzyme)-inhibitory activity were also able to activate T2R1. Homology modeling and docking studies showed that amino acid residues from TMs 1-3, TM 7 and from ECL1 and ECL2 contributed in forming the ligand binding pocket of T2R1 for the peptide ligands (Upadhyaya et al., 2010). In another study of T2R1, molecular modeling and site-directed mutagenesis studies revealed that two asparagines, Asn66 and the highly conserved Asn24, are important for dextromethorphan (DXM)-induced receptor signaling (Singh et al., 2011a). Asn24 plays a crucial role in receptor activation by mediating

a hydrogen-bond network connecting TM1-TM2-TM7, whereas Asn66 is essential for binding to DXM. The unique signature sequence of T2Rs, the LXXSL motif, plays a predominantly structural role in stabilizing the helical conformation of TM5 at the cytoplasmic end and a functional role by influencing the conformation of ICL3. Replacement of the conserved residues in this motif with bulky β-branched amino acids resulted in protein misfolding and/or non-functional receptor (Singh et al., 2011a).

Recently, the role of ICL3 in quinine-mediated activation of bitter taste receptor T2R4 was demonstrated using alanine scan mutagenesis (Pydi et al., 2014a). ICL3 of T2R4 consists of 23 amino acid residues which were mutated to alanine. Only 14 of the 23 mutants displayed quinine-induced signaling in a concentration-dependent manner. Three mutants, Q216A, T230A and V234A, showed an increased response to quinine. Six mutants, R213A, Q219A, K220A, Q229A, E231A and H233A, showed no detectable or statistically significant increase in intracellular calcium mobilization, suggesting that they may have an important role in receptor activation. Whereas, mutants I215A, F225A and P228A displayed altered receptor activation and/or defective ligand binding. Some mutants showed statistically significant basal signaling or constitutive activity. H214A, which is present in 24 of the 25 human T2Rs, showed the highest constitutive activity (i.e. in the absence of agonist).

1.7 Bitter Taste Perception and T2R Polymorphisms

The sensitivity of humans to the perception of some bitter compounds varies greatly (Bartoshuk, 2000a, b). This variable bitter taste perception is the best known example of genetic variation in oral sensation. A vast number of structurally diverse compounds elicit bitter taste in humans and many bitter substances can be detected at concentrations roughly

1000-fold lower than substances that stimulate other basic tastes (Meyerhof, 2005). Studies on the genetics of taste perception for PTC began in the early 1930s with the accidental finding by A. L. Fox that crystals of PTC tasted very bitter to some people but not to others (Fox, 1932). Thus, 6-n-propyl-2-thiouracil (PROP) and PTC, which share thiocyanate (N-C=S) moiety, taste bitter to some people but are tasteless to others (Fox, 1932).

Sensitivity to PTC/PROP is an inherited trait, and PROP sensitivity was linked with lower acceptability of other bitter compounds and lower reported liking for some bitter foods. Based on the detection thresholds for PTC/PROP solutions, people were categorized into supertasters, tasters and non-tasters. Similarly, inbred mouse strains differ in their ability to detect certain bitter taste stimuli, such as sucrose octaacetate (SOA) and cycloheximide. Genetic studies in humans have demonstrated that the ability to detect PROP is determined by a locus on chromosome 5p15 (Reed et al., 1999).

How humans respond to different bitter tasting compounds is an important question in the field of bitter taste research. Missense mutations were found in the sequences of T2R5 in mouse strains deficient to cycloheximide sensitivity (Chandrashekar et al., 2000). These genetic variants, found in bitter-insensitive mouse strains, also were less responsive in cell-based assays compared with alleles from the bitter-sensitive strains. This demonstrated that alleles of a taste receptor can change both behavioral and cellular responses to bitter compounds. A similar discovery was made in humans when naturally occurring alleles of the TAS2R38 gene, which is localized to chromosome 7q, were reported to be responsible for individual differences in the ability of humans to taste PTC and PROP (Mennella et al., 2005). Three polymorphic variants in T2R38 (proline or alanine at position 49, alanine or valine at position 262, and valine or isoleucine at position 296) gave rise to five common

haplotypes that accounted for 55-85% of the variance in PTC sensitivity (Bufe et al., 2005). The taster haplotype or PROP-sensitive individuals possess one or two dominant alleles (***p***roline-***a***lanine-***v***aline; PAV/PAV), or PAV/AVI (***a***lanine-***v***aline-***i***soleucine), whereas, insensitive individuals are recessive for the trait, AVI/AVI (Bufe et al., 2005). The ability to taste PTC/PROP may protect against cigarette smoking and has also been linked to decreased alcohol consumption (Cannon et al., 2005; Duffy et al., 2004).

Until recently, TAS2R38 was considered the only bitter taste gene that exhibits prominent phenotypic variation in humans. But variation in bitter receptor sequence is not confined to the TAS2R38 locus. Human TAS2Rs have more genetic variation within and between populations than do most other genes (Kim et al., 2005b). One possible explanation is that genes adapt to local conditions especially to the bitter toxins in food. SNPs in some other TAS2R genes have recently been identified. For example, a missense mutation in the TAS2R16 gene, which encodes the β-glucopyranoside receptor or T2R16, reduces sensitivity of the receptor to bitter-taste stimuli which has been associated with risk for alcohol dependence (Bufe et al., 2002; Wang et al., 2007). Polymorphism in the TAS2R43 gene allele makes people very sensitive to bitterness of the natural plant compounds aloin and aristolochic acid (Pronin et al., 2007). TAS2R43 and TAS2R44 gene alleles are also related to the bitterness perception of artificial sweetener, saccharin. Recently an SNP in the cluster of T2Rs on chromosome 12, which contributes to the variation in human bitterness perception of caffeine, was identified (Ledda et al., 2013). Thus, it seems likely that the examination of multiple taste phenotypes might provide a more complete understanding of human eating behavior than a single taste phenotype. Gene variants in TAS2Rs have been related to disease – a polymorphism in TAS2R38 contributes to an increased susceptibility to

respiratory infection (Lee et al., 2012) and a mutation in TAS2R50 has been associated with cardiovascular disease in several population-based prospective studies (Akao et al., 2012; Shiffman et al., 2008). A SNP in TAS2R9 has been linked to deficits in glucose homeostasis (Dotson et al., 2008), whereas, TAS2R14 gene has been associated with increased susceptibility to colorectal cancer (Campa et al., 2010). However, the mechanisms by which the variants of these TAS2R genes influence the pathophysiology of disease are mostly unknown.

1.8 Expression of T2Rs in Extra-oral tissues

With the molecular identification of taste GPCRs, it has become clear that taste signaling is not limited to taste buds, but occurs in many extra-oral tissues and these receptors have additional functions apart from sensing taste. Shortly after the discovery of T2Rs in taste tissue, their expression was demonstrated in the gastrointestinal tract (GIT) and enteroendocrine STC-1 cells of rodents and humans (Rozengurt, 2006; Wu et al., 2002), where they are involved in the chemosensation of nutrients. Gα-gustducin and Gα-transducin were also expressed in these tissues, suggesting that a taste-sensing mechanism existed in the GIT. Addition of bitter compounds like denatonium, PTC, PROP, caffeine and cycloheximide to STC-1 cell cultures promoted rapid $[Ca^{2+}]_i$ responses (Masuho et al., 2005; Wu et al., 2002). In addition, activation of T2Rs stimulated the secretion of hunger hormone ghrelin jvia the gustatory G-protein, α-gustducin (Janssen et al., 2011).

In the airway epithelium, expression of T2Rs was revealed in chemosensory receptor cells of the nasal epithelium and in ciliated epithelial cells (Masuho et al., 2005; Shah et al., 2009; Tizzano et al., 2011). Application of bitter substances to the nasal epithelium activated

the trigeminal nerve and elicited protective reflexes like apnea to prevent inhalation of bacteria further into the respiratory system, or sneezing and coughing to expel bacteria from the nasal cavity. Exposure of T2Rs in motile cilia of human airway epithelial cells with bitter compounds stimulated ciliary beat frequency (Shah et al., 2009), thus initiating a defensive mechanism to eliminate the offending compound. In the human airway smooth muscle (ASM), T2Rs lead to ASM relaxation and bronchodilation (Deshpande et al., 2010). Bitter tastants like denatonium, saccharin and chloroquine caused relaxation of mouse isolated ASM preparations, and dilation of airways that was three-fold greater than the presently used β-agonists. This relaxation by T2Rs was due to increased $[Ca^{2+}]_i$ that was suggested to activate large conductance potassium channels (BK_{Ca}) and resulted in hyperpolarization of the cell membrane. Additional studies showed that bronchodilatory effects of T2R agonists were not impeded by β_2-AR desensitization (An et al., 2012). These findings have reinforced the role of T2Rs as potential novel targets in asthma pharmacotherapy.

Regulation of the mucosal innate defense of human and mouse upper respiratory epithelium by activation of T2R38 was recently demonstrated (Lee et al., 2013; Lee and Cohen, 2013). Gram-negative respiratory pathogens like *Pseudomonas aeruginosa* produce acyl-homoserine lactones (AHLs) as signals for their population density (quorum sensing). AHLs are chemically related to bitter sesquiterpene lactones and activate T2R38 in upper respiratory epithelium. Receptor activation caused calcium and nitric oxide (NO) signaling resulting in stimulation of mucociliary clearance, the major physical respiratory defense against inhaled pathogens. Genetic variation in T2R38 has also been linked to individual differences in susceptibility in respiratory infection (Lee et al., 2012).

Activation of T2Rs in the human pulmonary artery smooth muscle (hPASM) causes

increased $[Ca^{2+}]_i$ release upon stimulation with bitter compounds (Upadhyaya et al., 2014). *Ex vivo* studies using isometric myography on porcine pulmonary arterial and airway rings showed that stimulation with DXM leads to contraction of arterial but relaxation of airway rings. This study suggests that in the pulmonary circuit DXM acts as a vasoconstrictor, and shows that DXM mediated activation of T2R1 in pulmonary tissues leads to vasoconstrictor responses. Thus, T2Rs in pulmonary circuit, upon DXM exposure, might be involved in regulating the vascular tone.

Expression of TAS2R46 was found in mesenchymal stromal cells and vascular smooth muscle cells (Lund et al., 2013). Rats exposed to denatonium, an agonist for T2R46, experienced a significant drop in blood pressure, providing *in vivo* evidence that a bitter compound can modulate vascular tone. The expression of T2Rs has been demonstrated in breast cancer and normal mammary epithelial cells (Singh et al., 2014). In this study, few T2Rs were found to be down-regulated in breast cancer cells, and the chemosensory role of T2Rs in migration and invasion of breast cancer was proposed. In brain, T2Rs were suggested to cause secretion of regulatory peptides involved in the regulation of food intake and other physiological processes (Singh et al., 2011b). Analysis of the rat neonatal heart at multiple time points, from neonatal to 19 months of age, revealed that expression of T2Rs is developmentally regulated in cardiac tissue (Foster et al., 2013). Expression of few T2Rs increased in glucose-deprived rats, and the study suggested the physiological relevance of T2Rs as novel metabolic/nutrient sensors in the heart.

1.9 Nutrigenomics of Taste

The PROP phenotype serves as a general marker for bitterness perception which

influences general food preferences and dietary behavior with subsequent links to body weight and chronic disease risk. Strong bitter taste is aversive and is closely associated with the presence of toxins. However, moderate bitter taste is appealing and expected in a variety of foods including beer, wine, chocolates and many cheeses. Fischer and colleagues noted that PTC tasters tend to manifest a thin and angular body type, whereas non-tasters tend to have generous body proportions (Fischer et al., 1966). Studies in overweight middle-aged women have provided convincing evidence linking PROP status with body weight (Goldstein et al., 2005). Goldstein *et al* showed that non-taster women were heavier than supertaster women by ~ 6 BMI (body mass index) units. Anatomical evidence demonstrates that individuals who differ in taste sensitivity to PTC/PROP also differ in the density of fungiform taste papillae on the anterior surface of tongue (Bartoshuk et al., 1994; Essick et al., 2003; Tepper and Nurse, 1997). Non-tasters have the lowest density of fungiform papillae, whereas supertasters have the highest density.

Isothiocyanates, the breakdown products of glucosinolates that are widely distributed in plants, interfere with the uptake of iodine by the thyroid gland, leading to goiter, and cretinism in its extreme form. Although iodine deficiency is the primary cause of this disease, goitrogens in the food supply can play a contributing role particularly when dietary iodine is low. It was shown that a large percentage of athyroidic cretins in a clinical population in the United States were PTC non-tasters (Shepard, 1961). Investigation of the role of PROP status in children's selection and consumption of vegetables showed that non-taster children consumed more bitter vegetables overall than taster children did (Bell and Tepper, 2006). PROP status has also been linked to sweet taste preferences in children. Taster pre-school children showed greater preferences for sweets than non-taster children (Keller and Tepper,

2004). The perception of oral irritation from capsaicin (chili pepper), cinnamaldehyde (from cinnamon), and carbonation is influenced by PROP sensitivity (Karrer and Bartoshuk, 1991; Prescott et al., 2004; Prescott and Swain-Campbell, 2000). Individual differences in fat perception have been linked to PROP taster status and taste bud density. A study in college students revealed that medium tasters and supertasters reliably discriminated a high-fat from a low-fat dressing, whereas non-tasters could not distinguish the two samples (Tepper and Nurse, 1997). Study by Keller and coworkers in pre-school children demonstrated that this phenotype might have greater influence on preferences for fats in females than males (Keller et al., 2002). Discretionary fat intake did not differ between taster and non-taster boys.

Few studies have examined association between PROP status and disease risk, though the data addressing this issue are scarce. No associations were reported between T2R38 polymorphisms and cardiovascular risk in the elderly women or between PROP status and lipid profiles in the breast cancer patients (Drewnowski et al., 2007; Timpson et al., 2005). However, a modest association between greater sensitivity to PROP and a higher number of colon polyps was found in older men undergoing routine screening for colon pathology (Basson et al., 2005).

Dental caries is the most common chronic disease of childhood that is neither self-limiting nor amenable to short-term pharmacological management (Edelstein and Douglass, 1995). Effective dentistry requires early identification of children at higher risk for caries so they may receive early and intense preventive intervention. The individual differences in PROP sensitivity have been linked to dental caries and can be used as an important tool to determine the taster status in relation to caries experience in children (Hedge and Sharma, 2008; Pidamale et al., 2012; Rupesh and Nayak, 2006; Verma et al., 2006). A comprehensive

review of the role of diet and dental caries reaffirmed that sucrose is the most important dietary item associated with dental caries (Habibian et al., 2001). Non-taster children may have higher concentration and frequencies of sugar intake compared to children who are medium or supertasters and are therefore more susceptible to dental caries (Anliker et al., 1991). Whereas, supertasters and medium tasters are more likely to avoid sweet food, thus making them less prone to dental decay. *Streptococcus mutans* levels were also shown to increase from tasters to non-tasters, thus, placing them at higher risk of developing caries (Verma et al., 2006).

1.10 Oligomerization of T2Rs

Receptor oligomerization has been shown to be necessary for class C GPCRs and also for class A GPCRs. The three members of the mammalian T1R family represent remarkable examples of functional GPCR hetero-oligomerization; combination of T1R1 and T1R3 forms a umami receptor, and that of T1R2 and T1R3 is a sweet taste receptor. Oligomerization has also been studied for the neurotransmitter gamma amino butyric acid, the $GABA_B$ receptor (Jones et al., 1998; Kuner et al., 1999), metabotropic glutamate receptors (Kunishima et al., 2000), rhodopsin (Fotiadis et al., 2003), β_2-adrenergic receptor (Hebert et al., 1996) and opiod receptors (Cvejic and Devi, 1997). Functional consequences of receptor hetero-oligomerization vary from protein maturation and transport to the plasma membrane, differences in signaling pathways, and internalization to pharmacologic effects, for example, alterations in ligand binding affinities and positive or negative binding cooperativity (Hansen and Sheikh, 2004; Maggio et al., 2005; Terrillon and Bouvier, 2004). Hetero-oligomerization may lead to the formation of new, functionally distinct receptors and thereby greatly increase

receptor diversity (Park and Palczewski, 2005). However, studies based on deciphering T2R oligomerization are very scarce. Kuhn *et al,* using biochemical and biophysical approaches, demonstrated that T2Rs exist as oligomers in heterologous expression system (Kuhn et al., 2010). Using coimmunoprecipitation experiments, they demonstrated both homo-oligomerization (for TAS2R5, TAS2R14, TAS2R16, TAS2R44 and TAS2R46) as well as hetero-oligomerization of the remaining TAS2Rs. Supporting evidence for TAS2R oligomerization was provided by bioluminescence resonance energy transfer (BRET) analysis (Kuhn et al., 2010). No obvious effects of TAS2R oligomerization on receptor function were found in this study. Whether T2Rs form oligomeric complexes *in vivo* remains to be elucidated. Given the fact that TAS2Rs are coexpressed in taste receptor cells *in vivo*, it is quite likely that they also form oligomers *in vivo* (Adler et al., 2000; Behrens et al., 2007; Mueller et al., 2005; Zhang et al., 2003).

1.11 Bitter Taste Blockers

The sense of taste has a significant impact on food selection, nutrition and health. It is, therefore, highly desirable to modulate bitter taste perception and bitter taste receptors so that beneficial food and medicines may be rendered more palatable. In addition to having an important role in food and nutraceutical industries, bitter taste blockers could be beneficial as chemical probes to examine the role of T2R function in gustatory and non-gustatory tissues. One of the first reported T2R antagonist, GIV3727, was able to inhibit the activation of T2R44 by saccharin and acesulfame-K (Slack et al., 2010). This compound also inhibited five additional T2Rs, including the closely related T2R43. It appears the -COOH moiety is essential for antagonist activity of GIV3727, since replacement of this group with an ester or

corresponding alcohol abolished its activity. Two residues in TM7 are important for antagonist activity in T2R43/T2R44. Shortly after this study, probenecid, an approved inhibitor of Multidrug Resistance Protein 1 (MRP1) transporter, was shown to inhibit T2R16, T2R38 and T2R43 in a non-competetive (allosteric) mechanism (Greene et al., 2011). Later, two natural sesquiterpene lactones from edible plants, 3β-Hydroxydihydrocostunolide (3HDC) and 3β-Hydroxypelenolide (3HP), were identified which blocked the responses of T2R46 receptor (Brockhoff et al., 2011). Besides T2R46, 3HDC also inhibited T2R30 and T2R40, and 3HP inhibited T2R30, T2R43 and T2R44.

A recent study reported that GABA, an inhibitory neurotransmitter, acts as a T2R4 antagonist (Pydi et al., 2014b). In addition, Nα, Nα-Bis carboxy methy-L-lysine (BCML) was found to be the first reported T2R antagonist to show inverse agonist property. None of the discovered blockers are capable of blocking all the 25 T2Rs and some of them act as agonists for other T2Rs. Taking into account the vast diversity of bitter agonists known for T2Rs, it is highly unlikely that a universal blocker for all T2Rs can be developed. Hence, there is an urgent need to discover more natural or synthetic T2R blockers, with high selectivity and efficacy, so that the consumption of healthy bitter foods and drug compliance can be increased. T2R blockers could, thus, have widespread utility in antioxidant and/or nutrient-fortified food and beverages, and in pharmaceutical and nutraceutical industry.

1.12 Constitutive activity of T2Rs

Constitutive activity of a receptor is the generation of a second messenger response in the absence of agonist stimulation. Several naturally occurring and disease-causing GPCR mutants with increased constitutive activity have been identified (Seifert and Wenzel-Seifert,

2002). Such constitutively active mutants (CAMs) can provide valuable information related to the functional and potential pathophysiological roles of GPCRs. Many class A GPCR family CAMs persist as naturally occurring mutations or SNPs (Chakraborty et al., 2012; Ramon et al., 2003). Though many SNPs have been characterized in T2Rs, none of them are known to exhibit constitutive activity. Recently, a few CAMs were characterized in TM7, ICL3 and C-terminus region of T2R4 (Pydi et al., 2012; Pydi et al., 2014a; Upadhyaya et al., 2015). CAMs are considered important pharmacologic tools for the screening of compounds that act as inverse agonists and decrease the basal level of signaling of these spontaneously active receptors. They are useful reporters for understanding the potential therapeutic differences between neutral antagonists or inverse agonists. Further studies of these class of molecules can allow the full therapeutic potential of T2R receptor family to be realized, which can have implications in the treatment of diseases caused due to such mutations.

1.13 Desensitization of T2Rs

Elucidation of the biochemistry of bitter taste signal transduction plays an important role in understanding how humans perceive bitter taste. The next step includes deciphering as to how the bitter taste receptor is desensitized and taste signal is terminated. Desensitization is loss of receptor responsiveness during continuous or repetitive exposure to the agonist. It is initiated by phosphorylation of serine and/or threonine residues predominantly located in the third intracellular loop and C-terminus of GPCRs (Kohout and Lefkowitz, 2003; Perry et al., 2002). Two types of desensitization occur – homologous and heterologous. Heterologous desensitization is induced by phosphorylation of the receptor by protein kinase A or C, sometimes even without agonist exposure. On the other hand, homologous desensitization is

specific for agonist-occupied receptors and consists in most cases of two steps. First, the receptor is phosphorylated by one of the G protein-coupled receptor kinases (GRKs); then it binds to β-arrestin which exhibit high affinity for agonist-occupied, phosphorylated receptors. β-Arrestin serves to sterically inhibit G protein coupling, thereby terminating the G protein activation, and may also target the receptor to clathrin-coated pits for internalization (Ferguson, 2001; Maudsley et al., 2005). Recent data suggests that members of the GRK4 protein subfamily, especially GRK5 and GRK6, effectively phosphorylate some inactive GPCRs (Li et al., 2015). This activation-independent phosphorylation leads to constitutive arrestin binding, suggesting that GRKs of this subfamily can stimulate basal receptor recycling and/or arrestin mediated signaling in the absence of agonists.

Receptor desensitization, which is initiated by phosphorylation of receptor by different protein kinases (PKA, PKC) or GRKs, can be subsequently followed by receptor internalization. Upon phosphorylation, β-arrestin 1 or 2 not only bind the receptor but also the heavy chain of clathrin, the clathrin adaptor protein AP2 and to phosphoinositides. These interactions direct the phosphorylated receptor to punctate clathrin coated pits in the cell membrane, which are internalized by action of the GTPase dynamin. Upon internalization, receptors can either be rapidly recycled to the plasma membrane, targeted to larger endosomes and slowly recycled, or degraded in lysosomes. In this way, internalization may regulate receptor resensitization and contribute to a positive regulation of receptor signaling (Ferguson, 2001; Pierce et al., 2002; Reiter and Lefkowitz, 2006).

This loss of function caused by receptor desensitization may limit the therapeutic efficacy of agonists by rapidly attenuating the early signal, or by evoking tachyphylaxis during prolonged treatment. So far, only one study by Robinette *et al* has demonstrated a

30% desensitization of T2R function with quinine pre-treatment and subsequent exposure in airway smooth muscle (Robinett et al., 2011). However, current understanding of T2R desensitization is limited, and the potential molecular mechanisms involved in desensitization like receptor internalization, phosphorylation by the respective kinases, and β-arrestin binding leading to uncoupling of receptor-G protein complex, remain poorly characterized. Before the introduction of T2Rs as novel therapeutic targets, it is very crucial that their desensitization mechanisms be probed in detail. Thus, elucidation of the signaling mechanisms utilized downstream of T2Rs, may allow the synthesis of more specific and potent bitter compounds and/or blockers.

CHAPTER 2

2.0 HYPOTHESIS AND OBJECTIVES

2.1 Study Rationale

The human genome encodes 25 bitter taste receptors which are referred to as T2Rs. T2Rs are 291-334 amino acids long and are capable of detecting a vast number of chemically diverse bitter compounds found in nature. The natural or synthetic bitter ligands that activate T2Rs include peptides, thioureas, lactones, phenols, drugs like quinine, colchicine, dapsone and many more (Meyerhof et al., 2010). Initial studies on bitter taste research focused on the deorphanization of T2Rs, followed by structure-function studies to elucidate the receptor-agonist interactions. Successive studies reported the expression of T2Rs in non-gustatory tissues like the respiratory epithelia and smooth muscle (Deshpande et al., 2010; Finger et al., 2003), gastrointestinal tissues (Wu et al., 2002), reproductive organs (Xu et al., 2013), and brain (Singh et al., 2011b), where they mediate protective reflexes. Regulation of mucosal innate defense of upper respiratory epithelium by T2R activation was demonstrated (Lee and Cohen, 2013; Lee et al., 2012). The role of T2Rs in airway muscle relaxation and bronchodilation (Deshpande et al., 2010), and in sinonasal defense has implicated them as potential therapeutic targets in the treatment of asthma and chronic rhinosinusitis (CRS) respectively. Increasing evidence of the functional importance of T2Rs in extra-oral tissues suggests that more studies are required to explore their role in other extra-oral regions.

Molecular modeling and structure-function studies have characterized the activation or ligand binding mechanisms of T2Rs to some extent (Biarnes et al., 2010; Brockhoff et al., 2010; Sakurai et al., 2010). However, molecular and physiological studies aiming at

delineating the mechanism of T2R desensitization and signal termination are very limited. Study by Robinette et al demonstrated 30% T2R desensitization to quinine in airway smooth muscle (Robinett et al., 2011). To elucidate whether this degree of desensitization can limit the therapeutic efficacy of T2Rs, it becomes important to understand in detail their desensitization mechanisms and the regulatory proteins involved in the process.

2.2 Hypothesis

T2Rs are expressed in PASMCs and involved in the regulation of vascular tone. T2Rs, like all GPCRs, undergo a modest amount of desensitization in response to bitter compounds.

2.3 Objectives

To test the hypothesis, I pursued molecular, physiological and pharmacological studies focused on select T2Rs. The specific objectives of my project are:-

2.3.1 DXM-mediated T2R activation in the pulmonary circuit

To characterize the expression of T2Rs in hPASMCs and study the effects of bitter agonist DXM on pulmonary artery by performing knockdown (KD) of endogenous T2R1, and pursuing *ex vivo* studies on porcine arterial rings.

2.3.2 Structure-function role of C-terminus in T2R4 signaling

To obtain mechanistic insights into the role of conserved and receptor specific C-terminus residues of T2Rs by performing site-directed mutagenesis study on C-terminus residues of T2R4.

2.3.3 Characterizing the desensitization mechanism of T2Rs

To determine the desensitization status of T2R4 by pursuing KD studies on GRKs, and assessing T2R trafficking in response to quinine.

2.3.4 Elucidation of the intracellular serine/threonine residues involved in T2R4 signaling

To identify the potential serine and threonine residues involved in T2R4 desensitization by analyzing receptor function and trafficking in response to quinine.

CHAPTER 3

3.0 MATERIALS AND METHODS

3.1 Materials

HEK293T cells were purchased from ATCC (Cat # CRL-3216) and cultured in DMEM/F12 media supplemented with 10% fetal bovine serum (FBS), penicillin (100 mg/ml) and streptomycin (100 mg/ml) at 37ºC in a 95% air and 5% CO_2 chamber. Human airway smooth muscle cells (hASMCs) and hPASMCs (Cat. # PCS-100-023) were either purchased from ATCC or were a kind gift from Dr Andrew Halayko, Dept. of Physiology, University of Manitoba. Cell culture media and growth kit for hPASMCs were purchased from ATCC. FBS, quinine hydrochloride, DXM hydrobromide, chloroquine, nicotine, dapsone, denatonium benzoate (DB), yohimbine, parthenolide, colchicine, thiamine, BCML, other bitter compounds, puromycin for selection of stable GRK-KD clones and poly-L-lysine were purchased from Sigma Aldrich (ON, Canada). The Gα16/gust44 chimera was a gift from Dr. Takashi Ueda, Nagoya City University, Japan. Brefeldin A (BFA) was purchased from Cell Signaling Technology (ON, Canada), phorbol 12-myristate 13-acetate (PMA) from Santa Cruz Biotechnology (TX, USA) and bisindolylmaleimide I (Bis I) was purchased from CalBiochem (MA, USA). Nucleofection kit for smooth muscle cell transfection was purchased from Lonza. DyNazyme hot start was purchased from Thermo Fisher Scientific (Toronto, ON, Canada). Hoechst-33342 and Prolong-antifade gold were purchased from Invitrogen. Restriction enzymes were from New England Biolabs (Ipswich, MA, USA). 96-well black-wall clear-bottom microtiter plates were from BD Biosciences, black dispensing tips and Flexstation 3 were from Molecular devices (Sunnyvale, CA, USA). 96-well

compound plates were from Greiner (Mississauga, ON) and Fluo-4 NW dye was from Invitrogen.

Antibodies: Polyclonal antibodies specific for T2R1, T2R4, T2R38, rabbit polyclonal anti-calnexin antibody, and normal IgG specific rabbit antisera were obtained from Abcam (Cambridge, MA, USA) and Santa Cruz Biotechnology (Dallas, TX, USA) respectively. Phospho-MLC-Ser19 monoclonal antibody and MLC polyclonal antibody were purchased from Cell Signaling technology (Danvers, MA, USA). Mouse monoclonal M2 anti-FLAG antibody was purchased from Sigma Aldrich, anti-GRK, anti-phosphoserine and anti-phosphothreonine antibodies were from Santa Cruz Biotechnology, and Alexa Fluor-488 goat anti-mouse and Alexa Fluor-594 goat anti-rabbit were purchased from Molecular Devices (CA, USA).

shRNA constructs and primers: The shRNA specific for T2R1 was purchased from Qiagen (Toronto, ON, Canada). GRK2 (TRCN0000230149), GRK3 (TRCN0000159482), GRK5 (TRCN0000000842) and GRK6 (TRCN0000199727) specific shRNA constructs were purchased from Sigma Aldrich (ON, Canada). The 25 hTAS2R PCR primers were designed towards the available human sequences from NCBI Genebank using the OligoPerfect software from Invitrogen (Burlington, ON, Canada). The details of the primer sequences are given in **Table 3.1.1**. The short-length DNA primer sequences used for quantitative (q)-PCR are shown in **Table 3.1.2.**

3.1.1 Animals

Newborn piglets (age < 24 hours) were obtained from a pathogen-free farm supplier on the day of experiment. Animals were euthanized with a lethal dose of pentobarbital (480 mg/kg

Table 3.1.1 DNA primer sequences for human bitter taste receptors (TAS2Rs)

Bitter receptor (TAS2R)	Gene Accession ID	Gene size (bp)	Primer Sequence (5'-3')	Expected amplicon size (bp)
TAS2R1	NM_019599	1355	Forward-TGTGGTGGTGAATGGCATTG, Reverse-CAGCACTTACTGTGGAGGAGGAAC	813
TAS2R3	NM_016943	1101	Forward-ACACATGATTCAGGGATAATAATGCAAA, Reverse- TTAGCCATCTTGGTTTTTGGTAGGAAATT	575
TAS2R4	NM_016944	900	Forward-TACAGTGGTCAATTGCAAAACTTGG, Reverse- AATGTCCTGGAGAGTAAAGGGTGG	749
TAS2R5	NM_018980	1150	Forward-TGGTCCTCATATAACCTCATTATCCTGG, Reverse- CTGCCATGAGTGTCTCCCA	667
TAS2R7	NM_023919	1096	TGTTTTATATTGGTGCTATATCCAGATGTCTATGC, GGATAAATGAATGACTTGAGGGGTAGATTAGAG	658
TAS2R8	NM_023918	930	Forward-TTGATATGGTGGTGCACTGG, Reverse-GTGAGTGACCCAAGGGGTAG	471
TAS2R9	NM_023917	1075	Forward-TGAATTGACCATAGGGATTTGGG, Reverse-ATAATTAGAATGAATGAATGGCTTGATGG	807
TAS2R10	NM_023921	924	Forward-GACTTGTAAACTGCATTGACTGTGCC, Reverse- AAAGAGGCTTGCTTTAGCTTGCTG	784
TAS2R13	NM_023920	1637	Forward-GGGTCAGTAAAAGAGAGCTGTCCTC, Reverse- ATCAGAAGAAAGGAGTGGCTTGAAG	742
TAS2R14	NM_023922	954	Forward-GCTTTGGCAATCTCTCGAATTAGC, Reverse-CTCTAAATTCTTTGTGACCTGAGGGC	796
TAS2R16	NM_016945	996	For-CCTGGGAATTTTTTAATATCCTTACATTCTGGT, Reverse-GAAGCGCGCTTTCATGCTT	419
TAS2R38	NM_176817	1143	Forward-ACAGTGATTGTGTGCTGCTG, Reverse-GCTCTCCTCAACTTGGCATT	766
TAS2R39	NM_176881	1017	Forward-TGTCGCCATTTCTCATCACCTTA, Reverse-ATTGAGTGGCTGGCAGGGTAG	841
TAS2R40	NM_176882	972	Forward-AGAGTGCATCACTGGCATCCTT, Reverse-GAGGATGAGAAAGTAGCTGGTGGC	685
TAS2R41	NM_176883	924	Forward-GGTTGCTGCCCTTGGATATGA, Reverse-TGAAGATGAGGATGAAGGGATGG	738
TAS2R42	NM_181429	945	Forward-ATGGCCACCGAATTGGACA, Reverse-GCTTGCTGTTTCCCAGAATGAG	871
TAS2R43	NM_176884	1027	Forward-GGTCTCCAGAGTTGGTTTGC, Reverse-TCTTGTTTCCCCAAATCAGG	698
TAS2R44	NM_176885	1021	Forward-CATTGGTAAATTCCATTGAGC, Reverse-GATATCATTATGGACAGAAAGTAAAC	661
TAS2R45	NM_176886	900	Forward-CTCCTTTGCTGACCAAATTGTC, Reverse-GAACGGGTGGGCTGAAGAAC	709
TAS2R46	NM_176887	930	Forward-GAGTTGAATCCAGCTTTTAAC, Reverse-ATAGCTGAATGCAATAGCTTC	606
TAS2R47	NM_001097643	960	Forward-GGTGTTATTACTACATTGGTATGCAACTC, Reverse- AAGACAGGTTGCTTTTCCAGC	603
TAS2R48	NM_176888	900	Forward-GGTTTACTCTGGGTCATGTTATTC, Reverse- TTTGCTCTGCTGTGTCCTAAG	606
TAS2R49	NM_176889	1914	Forward-GCACTGATAAATTTCATTGCCTGG, Reverse- TTGTTCCCCCAAATCAGAATGAAT	770
TAS2R50	NM_176890	1000	Forward-ATGTGGCTTGCTGCTAACCT, Reverse-CAGCCTTGCTAACCATGACA	514
TAS2R60	NM_177437	957	Forward-CAGGCAATGGCTTCATCACTG, Reverse-TCCCACACCCAGAATTTAAAGTCC	748
GNAT3	NM_001102386	1065	Forward-GTGGCATGACACCTCAACTG, Reverse-GGCCCAGTGTATTCTGGAAA	529
GNAT1	NM_144499	3617	Forward-AGGGAATATCCCTCCCACAC, Reverse-CCAAGAAAGGACAGCTGGAG	843
GAPDH	NM_002046	1310	Forward-TGTGAGGAGGGGAGATTCAG, Reverse-ACCCAGAAGACTGTGGATGG	572

Table 3.1.2 Short-length DNA primer sequences used for quantitative (q)-PCR

Gene	Primer sequence (5'-3')
hGAPDH	Forward-CAATGACCCCTTCATTGACC, Reverse-GACAAGCTTCCCGTTCTCAG
pGAPDH	Forward-CGATGGTGAAGGTCGGAGTG, Reverse-AAGGGGTCATTGATGGCGAC
hTAS2R1	Forward- GTCCGTCACCCACTCTTCAT, Reverse-GGGACCATAAACCCTGCATA
pTAS2R1	Forward- ATCCCTCACCCAATCTTCTC, Reverse-TCCATTTACGTTTGCTCTGG
hGRK2	Forward-ACTTCAGCGTGCATCGCAT, Reverse-GCTTTTTGTCCAGGCACTTCAT
hGRK3	Forward-AGCTGTACCTCAGGTGAAGTT, Reverse-AGCTTGCTTTGAGAAAGGATGT
hGRK5	Forward-GACCACACAGACGACGACTTC, Reverse-CGTTCAGCTCCTTAAAGCATTC
hGRK6	Forward-TAGCGAACACGGTGCTACTC, Reverse-GCTGATGTGAGGGAACTGGA

intraperitoneal). Heart and lungs were removed en bloc into cold Krebs-Henseleit buffer. This protocol is approved by the University of Manitoba, per Canadian Council on Animal Care (Permit Number: 14-008).

3.1.2 Media for mammalian cell culture

LB media : 10 g/l Tryptone, 5 g/l Yeast extract.

SOB media : 2% Bacto-Tryptone, 0.5% Yeast extract, 10 mM NaCl, 2.5 mM KCl (pH 7.0). 10 mM $MgCl_2$ added before use.

SOC media: SOB media containing 20 mM glucose.

DMEM/F12 : Ham's F-12/DMEM High Glucose (1:1, Gibco, Invitrogen) supplemented with 10% FBS, 100 mg/ml Pencillin, 100 mg/ml Streptomycin for culturing HEK293T cells.

DMEM: Dulbecco's modified Eagle's Medium D-Glucose (4.5 g/l, Gibco, Invitrogen) supplemented with 10% FBS, 100 mg/ml Pencillin, 100 mg/ml Streptomycin for culturing hASMCs.

Vascular Cell Basal Media (ATCC, Cat # PCS-100-030): supplemented with growth kit (Cat # PCS-100-042) containing rh FGF-basic (5 ng/ml), rh Insulin (5 µg/ml), Ascorbic acid (50 µg/ml), L-glutamine (10 mM), rh EGF (5 ng/ml), FBS (5%), and antimicrobials penicillin (10 Units/ml), streptomycin (10 µg/ml), amphotericin B (25 ng/ml), phenol red (33 µM). This media was used for culturing hPASMCs.

3.1.3 Buffers

Transformation buffer (TB): 10 mM Hepes, 250 mM KCl, 15 mM $CaCl_2$, 55 mM $MnCl_2.4H_2O$ (pH 6.7).

PBS: 137 mM NaCl, 2.7 mM KCl, 1.8 mM KH_2PO_4, 10 mM Na_2HPO_4.

Storage buffer: 50 mM Tris, 12.5 mM $MgCl_2.6H_2O$, pH 7.4, containing protease inhibitors EDTA (1 mM), benzamidine (10 μg/ml), trypsin inhibitor (20 μg/ml), and phenylmethylsulfonyl fluoride (PMSF, 0.2 mM).

Lysis buffer: 10 mM Tris-HCl (pH 7.4) containing protease inhibitors EDTA (1 mM), benzamidine (10 μg/ml), trypsin inhibitor (20 μg/ml), and PMSF (0.2 mM).

Acidified alcohol: 197 ml of 95% ethanol, 52 ml of ddH_2O, 1.5 ml concentrated HCl to make 250 ml.

3.7% *Paraformaldehyde* / 1×PBS: Dissolve 3.7 g paraformaldehyde in 100 ml 1×PBS by heating slowly to 60°C. Adjust pH to 7.2-7.4 upon cooling.

0.05% *Triton X-100* / 1×PBS: Mix 50 μl of Triton X-100 with 100 ml 1×PBS.

2% *BSA* / 1×PBS: Dissolve 0.02 g BSA in 1 ml 1×PBS.

1.5 M *Tris*, pH 6.8 and 8.8.

0.5 M *Tris-HCl* (pH 6.8), 8% SDS, 60% glycerol, 80 μg/ml bromophenol blue, 8% β-mercaptoethanol.

Transfer buffer: 25 mM Tris, 192 mM glycine, 20% methanol.

TAE buffer (Tris Acetate-EDTA): 4.84 g Tris, 2 ml 0.5 M Na_2EDTA (pH 8.0), 1.1 ml glacial acetic acid, and water to make 1 litre.

Agarose loading buffer: 25 mg bromophenol blue, 3.3 ml 150 mM Tris, pH 7.6, 6 ml glycerol, 0.7 ml water to make 10 ml.

3.2 Molecular Biology and Cell Culture

3.2.1 Human TAS2R1, TAS2R3 and TAS2R4 genes

The human synthetic FLAG-TAS2R1 (NCBI Accession ID # NM_019599), TAS2R3 (NM_16943) and TAS2R4 (NM_16944) genes comprise of 947 bp, 995 bp and 897 bp respectively. The salient features of the synthetic genes include a Kozak consensus (GCCACCATGG) 5' to the ATG start codon, an octa-peptide FLAG tag (DYKDDDDK) at the 5' end of the gene, and restriction sites for EcoRI at the 5' end and NotI at the 3'end to facilitate cloning. The sequences encoding the human TAS2R1, TAS2R3 and TAS2R4 genes were optimized for mammalian cell codon usage and synthesized commercially by GenScript, NJ, USA **(Figures 3.2.1, 3.2.2, 3.2.3)**. These synthetic codon-optomized genes were then inserted into the EcoRI and NotI sites of the mammalian expression vector pcDNA3.1 (Invitrogen). Amino acid substitutions introduced into the synthetic FLAG-TAS2R4 gene were synthesized commercially (GenScript Inc. USA). DNA sequences of all the mutated genes were verified by automated DNA sequencing (MICB DNA Sequencing Facility, Winnipeg). The wild type and mutant genes in pcDNA 3.1 were used for transfection.

3.2.2 Preparation of LB (Luria-Bertani)-ampicillin agar plates

Petri plates for growth of *E. coli* were prepared by dissolving 20 g of LB-agar in 500 ml of distilled water using a 1L flask and autoclaved for 45 min. Following autoclaving, it was allowed to cool for approximately 30 min at RT with constant stirring at a slow speed on a stirrer/hot plate (Corning PC-420D). 500 µl of 100 mg/ml stock solution of ampicillin was added, the LB-Agar was poured into sterile petri dishes (20-25 ml/plate), and allowed to solidify for 4-5 h at RT. The plates were then stored at 4°C until use.

EcoRI Kozak FLAG-Tag

```
GAATTCGCCACCATGGATTACAAAGACGACGACGATAAGCTGGAGTCACACCTGATCATCTACTTCCTGCTGGCTGTCA
TTCAGTTCCTGCTGGGCATCTTCACAAACGGGATCATTGTGGTCGTGAATGGAATCGACCTGATTAAGCACCGAAAAAT
GGCACCCCTGGATCTGCTGCTGTCCTGCCTGGCCGTGTCTAGGATCTTTCTGCAGCTGTTCATCTTCTACGTCAACGTG
ATCGTCATTTTCTTTATCGAGTTCATTATGTGCAGCGCCAACTGTGCTATCCTGCTGTTTATTAATGAGCTGGAACTGT
GGCTGGCCACCTGGCTGGGGGTGTTCTACTGCGCAAAGGTGGCCTCAGTCAGGCACCCTCTGTTTATCTGGCTGAAGAT
GCGCATTAGCAAACTGGTGCCATGGATGATCCTGGGAAGTCTGCTGTATGTGTCAATGATTTGTGTCTTCCATTCCAAA
TACGCTGGCTTCATGGTGCCCTATTTTCTGCGGAAGTTCTTTTCTCAGAACGCAACCATCCAGAAAGAGGACACACTGG
CCATCCAGATTTTCAGCTTTGTGGCTGAGTTCAGCGTCCCTCTGCTGATCTTCCTGTTTGCCGTGCTGCTGCTGATTTT
TAGTCTGGGCAGGCATACTCGCCAGATGCGAAATACCGTGGCTGGATCTCGAGTCCCAGGAAGAGGAGCTCCTATCAGT
GCACTGCTGTCTATCCTGAGTTTCCTGATTCTGTACTTTAGCCACTGTATGATCAAGGTGTTCCTGAGCTCCCTGAAAT
TTCATATCCGGAGATTCATTTTTCTGTTCTTTATCCTGGTCATCGGAATCTACCCATCAGGCCACAGCCTGATCCTGAT
TCTGGGCAACCCCAAGCTGAAACAGAATGCCAAGAAATTCCTGCTGCATTCCAAGTGCTGTCAGTGATAAGCGGCCGC
                                                                  Stop   NotI
```

```
GAATTCGCCACCATG GATTACAAAGACGAC GACGATAAGCTGGAG TCACACCTGATCATC TACTTCCTGCTGGCT
 E  F  A  T  M   D  Y  K  D  D   D  D  K  L  E   S  H  L  I  I   Y  F  L  L  A
GTCATTCAGTTCCTG CTGGGCATCTTCACA AACGGGATCATTGTG GTCGTGAATGGAATC GACCTGATTAAGCAC
 V  I  Q  F  L   L  G  I  F  T   N  G  I  I  V   V  V  N  G  I   D  L  I  K  H
CGAAAAATGGCACCC CTGGATCTGCTGCTG TCCTGCCTGGCCGTG TCTAGGATCTTTCTG CAGCTGTTCATCTTC
 R  K  M  A  P   L  D  L  L  L   S  C  L  A  V   S  R  I  F  L   Q  L  F  I  F
TACGTCAACGTGATC GTCATTTTCTTTATC GAGTTCATTATGTGC AGCGCCAACTGTGCT ATCCTGCTGTTTATT
 Y  V  N  V  I   V  I  F  F  I   E  F  I  M  C   S  A  N  C  A   I  L  L  F  I
AATGAGCTGGAACTG TGGCTGGCCACCTGG CTGGGGGTGTTCTAC TGCGCAAAGGTGGCC TCAGTCAGGCACCCT
 N  E  L  E  L   W  L  A  T  W   L  G  V  F  Y   C  A  K  V  A   S  V  R  H  P
CTGTTTATCTGGCTG AAGATGCGCATTAGC AAACTGGTGCCATGG ATGATCCTGGGAAGT CTGCTGTATGTGTCA
 L  F  I  W  L   K  M  R  I  S   K  L  V  P  W  M  I  L  G  S   L  L  Y  V  S
ATGATTTGTGTCTTC CATTCCAAATACGCT GGCTTCATGGTGCCC TATTTTCTGCGGAAG TTCTTTTCTCAGAAC
 M  I  C  V  F   H  S  K  Y  A   G  F  M  V  P   Y  F  L  R  K   F  F  S  Q  N
GCAACCATCCAGAAA GAGGACACACTGGCC ATCCAGATTTTCAGC TTTGTGGCTGAGTTC AGCGTCCCTCTGCTG
 A  T  I  Q  K   E  D  T  L  A   I  Q  I  F  S   F  V  A  E  F   S  V  P  L  L
ATCTTCCTGTTTGCC GTGCTGCTGCTGATT TTTAGTCTGGGCAGG CATACTCGCCAGATG CGAAATACCGTGGCT
 I  F  L  F  A   V  L  L  L  I   F  S  L  G  R   H  T  R  Q  M   R  N  T  V  A
GGATCTCGAGTCCCA GGAAGAGGAGCTCCT ATCAGTGCACTGCTG TCTATCCTGAGTTTC CTGATTCTGTACTTT
 G  S  R  V  P   G  R  G  A  P   I  S  A  L  L   S  I  L  S  F   L  I  L  Y  F
AGCCACTGTATGATC AAGGTGTTCCTGAGC TCCCTGAAATTTCAT ATCCGGAGATTCATT TTTCTGTTCTTTATC
 S  H  C  M  I   K  V  F  L  S   S  L  K  F  H   I  R  R  F  I   F  L  F  F  I
CTGGTCATCGGAATC TACCCATCAGGCCAC AGCCTGATCCTGATT CTGGGCAACCCCAAG CTGAAACAGAATGCC
 L  V  I  G  I   Y  P  S  G  H   S  L  I  L  I   L  G  N  P  K   L  K  Q  N  A
AAGAAATTCCTGCTG CATTCCAAGTGCTGT CAGTGATAAGCGGCC GC
 K  K  F  L  L   H  S  K  C  C   Q  *  *  *  *
```

Figure 3.2.1. Nucleotide and amino acid sequence of codon-optimized T2R1. The locations of *EcoRI* and *NotI* restriction sites introduced at the 5' and 3' of the gene are shown in blue color. Kozak sequence (shown in green) was introduced before the start codon and a FLAG tag nucleotide sequence (red color) was introduced between start codon and T2R1 sequence. The sequence was obtained from Pubmed (Accession ID # NM_019599).

EcoRI Kozak FLAG-Tag

```
GAATTCGCCACCATGGATTACAAGGACGACGATGATAAGATGGGGCTGACCGAGGGGGTGTTTCTGATTCTGAGCGGGA
CACAGTTTACTCTGGGGATTCTGGTGAACTGCTTTATCGAGCTGGTCAATGGCAGCTCCTGGTTCAAGACCAAAAGGAT
GTCACTGAGCGACTTTATCATTACCACACTGGCCCTGCTGCGCATCATTCTGCTGTGTATCATTCTGACAGATAGTTTT
CTGATTGAGTTCAGCCCCAACACTCACGACAGCGGGATCATTATGCAGATCATTGATGTCAGTTGGACATTCACTAATC
ATCTGTCAATCTGGCTGGCCACTTGCCTGGGAGTGCTGTACTGTCTGAAGATTGCTTCCTTTTCTCACCCTACCTTCCT
GTGGCTGAAATGGCGGGTGTCCAGAGTGATGGTCTGGATGCTGCTGGGAGCTCTGCTGCTGAGCTGCGGCTCCACAGCA
TCTCTGATCAACGAGTTTAAGCTGTATTCTGTGTTCCGCGGCATTGAGGCTACCCGAAATGTCACAGAACACTTCAGGA
AGAAACGCAGCGAATACTATCTGATCCATGTGCTGGGGACTCTGTGGTACCTGCCCCCTCTGATCGTCTCTCTGGCCAG
TTATTCACTGCTGATTTTTAGTCTGGGCCGACACACTCGGCAGATGCTGCAGAACGGGACCTCTAGTCGGGACCCCACT
ACCGAGGCCCATAAGAGAGCTATCAGGATCATTCTGAGCTTCTTTTTCCTGTTCCTGCTGTACTTTCTGGCATTCCTGA
TCGCCTCCTTTGGAAACTTCCTGCCTAAGACCAAAATGGCAAAAATGATTGGCGAAGTGATGACAATGTTTTATCCAGC
CGGGCACAGCTTCATCCTGATTCTGGGAAATTCCAAGCTGAAACAGACATTCGTGGTCATGCTGAGATGTGAAAGCGGC
CATCTGAAGCCAGGCTCCAAAGGGCCCATCTTTTCTTGAGCGGCCGC
                                          Stop  NotI

GAATTCGCCACCATG GATTACAAGGACGAC GATGATAAGATGGGG CTGACCGAGGGGGTG TTTCTGATTCTGAGC
 E  F  A  T  M   D  Y  K  D  D   D  D  K  M  G   L  T  E  G  V   F  L  I  L  S
GGGACACAGTTTACT CTGGGGATTCTGGTG AACTGCTTTATCGAG CTGGTCAATGGCAGC TCCTGGTTCAAGACC
 G  T  Q  F  T   L  G  I  L  V   N  C  F  I  E   L  V  N  G  S   S  W  F  K  T
AAAAGGATGTCACTG AGCGACTTTATCATT ACCACACTGGCCCTG CTGCGCATCATTCTG CTGTGTATCATTCTG
 K  R  M  S  L   S  D  F  I  I   T  T  L  A  L   L  R  I  I  L   L  C  I  I  L
ACAGATAGTTTTCTG ATTGAGTTCAGCCCC AACACTCACGACAGC GGGATCATTATGCAG ATCATTGATGTCAGT
 T  D  S  F  L   I  E  F  S  P   N  T  H  D  S   G  I  I  M  Q   I  I  D  V  S
TGGACATTCACTAAT CATCTGTCAATCTGG CTGGCCACTTGCCTG GGAGTGCTGTACTGT CTGAAGATTGCTTCC
 W  T  F  T  N   H  L  S  I  W   L  A  T  C  L   G  V  L  Y  C   L  K  I  A  S
TTTTCTCACCCTACC TTCCTGTGGCTGAAA TGGCGGGTGTCCAGA GTGATGGTCTGGATG CTGCTGGGAGCTCTG
 F  S  H  P  T   F  L  W  L  K   W  R  V  S  R   V  M  V  W  M   L  L  G  A  L
CTGCTGAGCTGCGGC TCCACAGCATCTCTG ATCAACGAGTTTAAG CTGTATTCTGTGTTC CGCGGCATTGAGGCT
 L  L  S  C  G   S  T  A  S  L   I  N  E  F  K   L  Y  S  V  F   R  G  I  E  A
ACCCGAAATGTCACA GAACACTTCAGGAAG AAACGCAGCGAATAC TATCTGATCCATGTG CTGGGGACTCTGTGG
 T  R  N  V  T   E  H  F  R  K   K  R  S  E  Y   Y  L  I  H  V   L  G  T  L  W
TACCTGCCCCCTCTG ATCGTCTCTCTGGCC AGTTATTCACTGCTG ATTTTTAGTCTGGGC CGACACACTCGGCAG
 Y  L  P  P  L   I  V  S  L  A   S  Y  S  L  L   I  F  S  L  G   R  H  T  R  Q
ATGCTGCAGAACGGG ACCTCTAGTCGGGAC CCCACTACCGAGGCC CATAAGAGAGCTATC AGGATCATTCTGAGC
 M  L  Q  N  G   T  S  S  R  D   P  T  T  E  A   H  K  R  A  I   R  I  I  L  S
TTCTTTTTCCTGTTC CTGCTGTACTTTCTG GCATTCCTGATCGCC TCCTTTGGAAACTTC CTGCCTAAGACCAAA
 F  F  F  L  F   L  L  Y  F  L   A  F  L  I  A   S  F  G  N  F   L  P  K  T  K
ATGGCAAAAATGATT GGCGAAGTGATGACA ATGTTTTATCCAGCC GGGCACAGCTTCATC CTGATTCTGGGAAAT
 M  A  K  M  I   G  E  V  M  T   M  F  Y  P  A   G  H  S  F  I   L  I  L  G  N
TCCAAGCTGAAACAG ACATTCGTGGTCATG CTGAGATGTGAAAGC GGCCATCTGAAGCCA GGCTCCAAAGGGCCC
 S  K  L  K  Q   T  F  V  V  M   L  R  C  E  S   G  H  L  K  P   G  S  K  G  P
ATCTTTTCTTGAGCG GCCGC
 I  F  S  *  *   *
```

Figure 3.2.2. Nucleotide and amino acid sequence of codon-optimized T2R3. The locations of *EcoRI* and *NotI* restriction sites introduced at the 5' and 3' of the gene are shown in blue color. Kozak sequence (shown in green) was introduced before the start codon and a FLAG tag nucleotide sequence (red color) was introduced between start codon and T2R3 sequence. Gene sequence was obtained from Pubmed (Accession ID # NM_016943).

EcoR1 Kozak FLAG Tag

```
GAATTCGCCACCATGGACTACAAGGACGACGATGACAAACTTCGGTTATTCTATTTCTCTGCTATTATTGCCTCAGTTA
TTTTAAATTTTGTAGGAATCATTATGAATCTGTTTATTACAGTGGTCAATTGCAAAACTTGGGTCAAAAGCCATAGAAT
CTCCTCTTCTGATAGGATTCTGTTCAGCCTGGGCATCACCAGGTTTCTTATGCTGGGACTATTTCTGGTGAACACCATC
TACTTCGTCTCTTCAAATACGGAAAGGTCAGTCTACCTGTCTGCTTTTTTTGTGTTGTGTTTCATGTTTTTGGACTCGA
GCAGTGTCTGGTTTGTGACCTTGCTCAATATCTTGTACTGTGTGAAGATTACTAACTTCCAACACTCAGTGTTTCTCCT
GCTGAAGCGGAATATCTCCCCAAAGATCCCCAGGCTGCTGCTGGCCTGTGTGCTGATTTCTGCTTTCACCACTTGCCTG
TACATCACGCTTAGCCAGGCATCACCTTTTCCTGAACTTGTGACTACGAGAAATAACACATCATTTAATATCAGTGAGG
GCATCTTGTCTTTAGTGGTTTCTTTGGTCTTGAGCTCATCTCTCCAGTTCATCATTAATGTGACTTCTGCTTCCTTGCT
AATACACTCCTTGAGGAGACATATACAGAAGATGCAGAAAAATGCCACTGGTTTCTGGAATCCCCAGACGGAAGCTCAT
GTAGGTGCTATGAAGCTGATGGTCTATTTCCTCATCCTCTACATTCCATATTCAGTTGCTACCCTGGTCCAGTATCTCC
CCTTTTATGCAGGGATGGATATGGGGACCAAATCCATTTGTCTGATTTTTGCCACCCTTTACTCTCCAGGACATTCTGT
TCTCATTATTATCACACATCCTAAACTGAAAACAACAGCAAAGAAGATTCTTTGTTTCAAAAAATGAGCGGCCGCAATC
T
```

Stop Not1

```
GAATTCGCCACCATG GACTACAAGGACGAC GATGACAAACTTCGG TTATTCTATTTCTCT GCTATTATTGCCTCA
 E  F  A  T  M   D  Y  K  D  D   D  D  K  L  R   L  F  Y  F  S   A  I  I  A  S
GTTATTTTAAATTTT GTAGGAATCATTATG AATCTGTTTATTACA GTGGTCAATTGCAAA ACTTGGGTCAAAAGC
 V  I  L  N  F   V  G  I  I  M   N  L  F  I  T   V  V  N  C  K   T  W  V  K  S
CATAGAATCTCCTCT TCTGATAGGATTCTG TTCAGCCTGGGCATC ACCAGGTTTCTTATG CTGGGACTATTTCTG
 H  R  I  S  S   S  D  R  I  L   F  S  L  G  I   T  R  F  L  M   L  G  L  F  L
GTGAACACCATCTAC TTCGTCTCTTCAAAT ACGGAAAGGTCAGTC TACCTGTCTGCTTTT TTTGTGTTGTGTTTC
 V  N  T  I  Y   F  V  S  S  N   T  E  R  S  V   Y  L  S  A  F   F  V  L  C  F
ATGTTTTTGGACTCG AGCAGTGTCTGGTTT GTGACCTTGCTCAAT ATCTTGTACTGTGTG AAGATTACTAACTTC
 M  F  L  D  S   S  S  V  W  F   V  T  L  L  N   I  L  Y  C  V   K  I  T  N  F
CAACACTCAGTGTTT CTCCTGCTGAAGCGG AATATCTCCCCAAAG ATCCCCAGGCTGCTG CTGGCCTGTGTGCTG
 Q  H  S  V  F   L  L  L  K  R   N  I  S  P  K   I  P  R  L  L   L  A  C  V  L
ATTTCTGCTTTCACC ACTTGCCTGTACATC ACGCTTAGCCAGGCA TCACCTTTTCCTGAA CTTGTGACTACGAGA
 I  S  A  F  T   T  C  L  Y  I   T  L  S  Q  A   S  P  F  P  E   L  V  T  T  R
AATAACACATCATTT AATATCAGTGAGGGC ATCTTGTCTTTAGTG GTTTCTTTGGTCTTG AGCTCATCTCTCCAG
 N  N  T  S  F   N  I  S  E  G   I  L  S  L  V   V  S  L  V  L   S  S  S  L  Q
TTCATCATTAATGTG ACTTCTGCTTCCTTG CTAATACACTCCTTG AGGAGACATATACAG AAGATGCAGAAAAAT
 F  I  I  N  V   T  S  A  S  L   L  I  H  S  L   R  R  H  I  Q   K  M  Q  K  N
GCCACTGGTTTCTGG AATCCCCAGACGGAA GCTCATGTAGGTGCT ATGAAGCTGATGGTC TATTTCCTCATCCTC
 A  T  G  F  W   N  P  Q  T  E   A  H  V  G  A   M  K  L  M  V   Y  F  L  I  L
TACATTCCATATTCA GTTGCTACCCTGGTC CAGTATCTCCCCTTT TATGCAGGGATGGAT ATGGGGACCAAATCC
 Y  I  P  Y  S   V  A  T  L  V   Q  Y  L  P  F   Y  A  G  M  D   M  G  T  K  S
ATTTGTCTGATTTTT GCCACCCTTTACTCT CCAGGACATTCTGTT CTCATTATTATCACA CATCCTAAACTGAAA
 I  C  L  I  F   A  T  L  Y  S   P  G  H  S  V   L  I  I  I  T   H  P  K  L  K
ACAACAGCAAAGAAG ATTCTTTGTTTCAAA AAATGAGCGGCCGCA ATC
 T  T  A  K  K   I  L  C  F  K   K  *  A  A  A   I
```

Figure 3.2.3. Nucleotide and amino acid sequence of codon-optimized T2R4. The locations of *EcoRI* and *NotI* restriction sites introduced at the 5' and 3' of the gene are shown in blue color. Kozak sequence (shown in green) was introduced before the start codon and a FLAG tag nucleotide sequence (red color) was introduced between start codon and T2R4 sequence. Gene sequence was obtained from Pubmed (Accession ID NM_016944).

3.2.3 Preparation of competent *E. coli* cells

Competent *E. coli* cells were made following the Inoue method (Inoue et al., 1990). Briefly, DH5α cells from frozen stock (in LB/50% glycerol) were grown overnight (ON) in tubes containing 5 ml of LB media at 37°C. 100 µl of the saturated *E.coli* DH5α culture was inoculated in 100 ml SOB media in a 1L flask, and grown to an A_{600} of 0.6 at 22°C for 18 h with vigorous shaking (200-250 rpm). The flask was removed from the shaker and placed on ice for 10 min. The culture was transferred to 50 ml falcon tubes and the cells harvested by centrifugation at 2500 × g (4100 rpm) for 10 min at 4°C using SLA 1500 rotor in Sorvall RC-6 Centrifuge. The cell pellet was resuspended gently in 32 ml of ice-cold transformation buffer, incubated on ice for 10 min, and again centrifuged as above. The cell pellet was resuspended gently in 8 ml of ice-cold transformation buffer. DMSO was added with gentle swirling to a final concentration of 7% (0.6 ml for 8 ml transformation buffer). After incubating on ice for 10 min, the cell suspension was aliquoted into 200 µl per eppendorf tube and stored at -80° C.

3.2.4 Transformation of competent *E. coli*

For transformation with different plasmids, a vial of frozen competent *E. coli* cells was thawed on ice. 50 µl of the cells were transferred to a 1.5 ml eppendorf tube and 0.1 µg (1-5 µl) of the plasmid was added to the tube. The mixture was incubated on ice for 35 min. The cells were then incubated at 42°C for 30 sec, cooled on ice for 2 min and supplemented with 1 ml of LB media. The tube was placed in a 37°C incubator and shaken gently for 1 h. A momentary spin was given and 100 µl of the mixture was spread-plated on LB plates containing 100 µg/ml ampicillin and colonies allowed to form ON at 37°C. For plasmid

miniprep, a select few colonies were inoculated in 5 ml LB media containing 5 µl of 100 mg/ml ampicillin stock solution and allowed to grow ON at 37°C with vigorous shaking (240 rpm) in an Orbital shaker, Forma Scientific.

3.2.5 Transformation of unstable plasmids

The T2R4 mutants T291A, H292A and K296R plasmids were unstable in common *E. coli* strains including DH5α, therefore, their plasmid DNAs were transformed into the low copy number CopyCutter^{TM} EPI400^{TM} Electro competent *E. coli* cells (Epicenter Biotechnologies). To induce these clones to high copy numbers, the EPI400 *E. coli* cultures expressing these plasmids were grown ON, and their optical density was measured at OD_{600}. The cultures were then diluted in LB media to obtain a final culture density with OD_{600} of 0.2. These cultures were then induced with 1 x Copy Cutter induction solution for 4 h at 37°C with vigorous shaking. This solution raises the copy number to improve plasmid yields. DNA purification using the Qiagen maxi-preparation kit was carried out after 4 h.

3.2.6 DNA purification and Restriction digest

After growth at 37°C for 16-18 h, DNA was purified from the ON cultures using Qiagen DNA purification miniprep kit. The DNA was eluted in 30 µl sterile water and restriction digest was done by incubating the following reaction mixture at 37°C for 1.5 h : 1 µg DNA, 1 µl BSA (10X), 1 µl EcoRI buffer (NEB), 1 µl *EcoRI* (20,000U/ml), 1 µl *NotI*, and water added upto 10 µl. The samples were analyzed by gel electrophoresis on a 1% agarose gel. The isolates showing the correct banding pattern were sequence confirmed by automated DNA sequencing (MICB DNA Sequencing Facility, Winnipeg). The correct size isolates

were grown ON in 100 ml LB-Ampicillin media and DNA from these was purified in larger amounts using Qiagen Maxiprep kit. This plasmid DNA was used for molecular and cell biology experiments.

3.2.7 Isolation and culture of porcine ASMCs and PASMCs

4^{th}-6^{th} generation pulmonary arteries and airways were dissected from newborn piglet (< 24 h old) into ice cold Ca^{2+} free Krebs-Henseleit buffer containing (in mM) 25 $NaHCO_3$, 112.6 NaCl, 4.7 KCl, 1.38 NaH_2PO_4, 2.46 $MgSO_4.7H_2O$, 5.56 Dextrose; pH 7.4. The arteries and airways were allowed to recover in cold HEPES-buffered saline solution (HBS); composed of (in mM) 130 NaCl, 5 KCl, 1.2 $MgCl_2$, 1.5 $CaCl_2$, 10 Hepes, 10 glucose; pH 7.4. Pulmonary arterial and airway smooth muscle cells were obtained using a dispersed cell culture method as described previously (Shimoda et al., 2000). Briefly, pulmonary arteries and airways were washed twice with a 20 mM $CaCl_2$ (reduced-Ca^{2+}) HBS solution, finely minced, then transferred to a digestion medium containing reduced-Ca^{2+} HBS, type I collagenase (1,750 U/mL), dithiothreitol (1 mM), bovine serum albumin (2 mg/ml), and papain (9.5 U/mL) for 15 min at 37°C with gentle agitation. The dispersed cells were collected by centrifugation at 1,200 rpm for 5 min, washed in Ca^{2+}-free HBS to remove digestion solution, then resuspended in Ham's F-12 medium supplemented with 10% FBS, 1% penicillin and 1% streptomycin and seeded at a density of $4.4x10^4$ cells/cm^2. Experiments were performed when cells reached 80% confluence.

3.2.8 Generation of GRK-KD stable cell lines

The GRK2, GRK3, GRK5 and GRK6 shRNA constructs were previously used in mast cells for knockdown of endogenous GRKs (Guo et al., 2011). Of the five different shRNA constructs used for knockdown (KD) of GRKs 2, 3, 5 and 6, the constructs which gave the most efficient KD were selected for use in this study. HEK293T cells were transfected with GRK2, GRK3, GRK5 and GRK6 shRNA constructs (3 μg/10^6 cells) using lipofectamine-2000. A scrambled shRNA construct was used as control. Following 24 h of transfection, the medium was changed and the cells were replenished with fresh media. After another 24 h, the transfected cells were split in three dilutions (1:20, 1:100 and 1:500). Next day, puromycin (3 μg/ml) was added to select stable integration into the genome. Colony formation was observed in 7-10 days. A few isolated colonies were selected and analyzed for GRK-KD using quantitative (q)-PCR.

3.3 RNA extraction and Polymerase Chain Reaction (PCR)

3.3.1 RNA isolation and cDNA synthesis

Total RNA was isolated from untransfected cells (used as control) and transfected HEK293T cells or human/porcine PASMCs and ASMCs using RNeasy mini kit (Qiagen) according to the manufacturer's instructions. The concentration and purity of the extracted total RNA was determined by using a Nanodrop 2000 (Thermo Scientific, Canada). Genomic DNA was removed by treating 10 μg of the extracted RNA with 8 units of DNase I (New England Biolabs) for 75 mins at 37°C. About 1 μg of purified RNA was reverse transcribed using SSIII RT (superscript III reverse transcriptase, Invitrogen), dNTPs, Oligo-dT primer and first strand buffer. The synthesized cDNA was used as template for amplification by PCR.

3.3.2 Reverse-transcriptase (RT)-PCR

The primer sequences used for PCR analysis and their expected amplicon sizes are listed in **Table 3.1.1**. PCR was performed in a total volume of 20 µl containing 1 µl reverse transcribed cDNA, 400 nM of each primer in hot start buffer, 0.4 U hot start enzyme and 50 µM dNTPs. An initial denaturation step of 94ºC for 10 min was followed by 55 cycles of denaturation at 94ºC for 30 sec, annealing at 62°C, extension at 72ºC for 30 sec and finished with a final extension at 72ºC for 5 min on a thermocycler (MJ mini cycler, Bio rad). The housekeeping gene GAPDH was used as a positive control in the PCR reactions. – RT reaction was used as an internal control and a no template control (water only) was used as a negative control. All PCR products were separated on 2% agarose gel stained with ethidium bromide. Gel images were recorded and photographed under UV light. PCR reaction was performed at least three times.

3.3.3 Quantitative (q)-PCR

Reaction mixtures with a final volume of 10 µl consisted of reverse transcribed cDNA, primers, 1x SYBR Green containing dNTP mix and Taq polymerase. The short-length primer sequences used for detection are shown in **Table 3.1.2**. The reaction consisted of the following steps; an initial denaturation step of 1 min at 95ºC, then 50 cycles of 94ºC for 30 sec, annealing at 66ºC for GRK2, GRK3 and GRK5, 69ºC for GRK6, and extension at 72ºC for 30 sec and a final extension at 72ºC for 2 min. This was followed by melt curve analysis from 72ºC to 95ºC at every 1ºC increase in temperature for about 1 sec for 23 cycles. Melt curve analysis confirmed the presence of a single PCR product in each reaction. Analysis was performed by $2^{-\Delta Ct}$ method. Reactions were performed in triplicates. An Eco Real-time PCR

System (Illumina, Inc., USA) was used for these experiments and Eco-Study software was used for data analysis.

3.3.4 shRNA knockdown, hPASMC transfection by electroporation method

hPASMCs ($1x10^5$ cells) were suspended in 100 µl nucleofector solution. Following this, 2 µg of T2R1-specific shRNA, scrambled shRNA and 100 µl nucleofector solution were combined in separate tubes. A cell specific type nucleofector program was selected and applied to the cell/DNA mixture. The cells were taken out and resuspended in 500 µl prewarmed cell culture media and seeded in 6 well plate for further quantitative PCR (qPCR) and calcium mobilization experiments. Receptor activation was determined in untransfected cells and/or after 48 h of transfection.

3.3.5 Nanostring nCounter® gene expression analysis

nCounter® system is a time and cost-effective technique that offers a multiplexed measurement of gene transcripts in a single reaction. The system utilizes molecular barcodes that enables digital detection of hundreds of individual gene targets. We established the set of interested genes with RefSeq accession numbers of mRNA from NCBI database, and ordered the TAS2R codesets from NanoString Technologies. The nCounter® Gene Expression method is accurate and more reliable than q-PCR and micro-array techniques. Unlike the other methods, the protocol does not include any amplification steps that can introduce bias to the results. The NanoString nCounter® system available at Farncombe Metagenomics Facility, McMaster University at a fee-for-service was utilized to screen the TAS2R genes. Total RNA was extracted from HEK293T cells, hASMCs and hPASMCs using RNeasy Mini kit (Qiagen). These samples were analyzed by Nanostring nCounter® system to quantify the

mRNA expression levels of endogenous genes in these cells. This was done using Nanostring nCounter gene expression system technology which captures and counts individual mRNA transcripts with just 100 ng of total RNA sample. Appropriate positive and negative controls were included in the reaction (Geiss et al., 2008).

3.4 Protein Detection

3.4.1 Preparation of Cell membranes

Following 48 h of transfection, T2R4-expressing HEK293T cells were incubated with 1 mM quinine for 15 min. The cells were immediately suspended in lysis buffer containing protease and phosphatase inhibitors, poured into a 15 ml dounce homogenizer and homogenized with 20-25 strokes on ice. Mock-transfected cells and unstimulated T2R4-transfected HEK cells were used as controls. The suspension was centrifuged at 700 g for 10 min to remove large cell debris. The supernatant was again centrifuged at 50,000 g for 20 min at 4°C using Sorvall MTX150 Micro-Ultracentrifuge (Thermo Scientific). The prepared membranes were resuspended in storage buffer containing protease and phosphatase inhibitors. For determining the protein concentration, the prepared membranes were solubilized in 1% DM by nutating for 1 h at 4°C. The solubilized protein was then centrifuged at 50,000 rpm for 20 min and protein concentration was measured using DC protein assay.

3.4.2 Immuno Blot Analysis

Following 48 h of transfection with T2R1-specific shRNA or scrambled shRNA, hPASMCs were lysed using lysis buffer (Pierce Scientific, Canada) containing protease

inhibitors. For GRK-KD studies in HEK293T cells, the cells were pelleted and lysed for 1 h on ice using lysis buffer (Pierce Scientific). The total cell lysate was then centrifuged at 5,000 rpm for 5 min at 4°C in Sorvall Legend Micro 21R centrifuge (Thermo Scientific). Protein (10 μg/lane) was resolved on 12% polyacrylamide gel. The nitrocellulose membranes were blocked in 3% BSA for 90 min, incubated with rabbit polyclonal anti-T2R1, rabbit polyclonal anti-GRK, or anti-β actin ON with gentle shaking at 4°C. Following four washes of 15 min each with PBS containing 0.3% BSA and 0.1% Triton X-100, the blot was incubated with secondary antibody (goat anti-rabbit HRP) for 1 h. After 4 washes (15 min each), enhanced chemiluminescence (ThermoFisher Scientific, Canada) was used for detection of proteins on Kodak film.

3.4.3 MLC phosphorylation in ASMCs and PASMCs

Human and porcine PASMCs and ASMCs were treated with 500 μM DXM or 1 μM U46619, or buffer alone for 20 minutes. The cells were lysed with ice-cold lysis buffer (Pierce Scientific) containing protease inhibitors. The cell lysate was then separated by 10% SDS-PAGE and Western blot was performed. Membranes were incubated with primary antibody, either a 1:500 dilution of phospho-MLC-Ser19 monoclonal antibody or 1:200 dilution of MLC polyclonal antibody, ON at 4°C. Blots were washed and then probed with a 1:4000 dilution of peroxidase conjugated secondary antibody and visualized using ECL detection reagents.

3.5 Cell Surface Expression Studies

3.5.1 Flow cytometry

Cell surface expression of wild type T2R1, T2R3, T2R4, TPα, and mutants of T2R4 was determined using a BD FACS Canto flow cytometer. HEK293T cells, in 6-well tissue culture plate, were transfected with 3 μg DNA/1×10^6 cells. Following 24 h of transfection, 1×10^6 /ml viable cells were collected and washed with cold PBS buffer and incubated with mouse monoclonal anti-FLAG M2 primary antibody (1:500 dilution in PBS) for 1 h on ice. The serine and threonine mutants of T2R4 were treated with quinine for 15 min before incubating them with anti-FLAG antibody. After 2 to 3 washings, cells were incubated with Alexa 488 goat anti-mouse secondary antibody (1:1000 dilution). For determination of surface expression of endogenous T2R4 in hASMCs, cells were collected and incubated with polyclonal rabbit anti-T2R4 (1:300). This was visualized using goat anti-rabbit 488 antibody (1:1000 dilution). Following washing, cells were resuspended in 300 μl PBS buffer. The fluorescence signals of 10,000 cells/tube were measured by the BD FACS Canto using single-color analysis. The results were analyzed using the FACS Diva and FlowJo software programs. The cell surface expression was calculated in terms of Mean Fluorescence Intensity (MFI) as percentage increase over control which was set at 100%. Cells treated with isotype-specific IgG antisera were used as control. For agonist treatment assays, the untreated receptor was used as control.

3.5.2 Brefeldin A treatment

BFA, an antifungal metabolite, is an inhibitor of protein transport from the endoplasmic reticulum (ER) to the Golgi, and therefore affects trafficking of the protein to the plasma membrane. T2R4-expressing HEK293T cells were pretreated with 5 μg/ml BFA for 4 h at 37°C and then incubated with 1 mM quinine for 15 min or 1 h. The reactions were

stopped by keeping the cells on ice and then processed for cell surface expression analysis of T2R4 by flow cytometry as described in section 3.5.1.

3.6 Sub-Cellular Localization Studies

3.6.1 Immunofluorescence

To determine the subcellular localization of WT-T2R4 or select mutants transiently expressed in HEK293T cells, or of endogenous T2R1 and T2R38 in hPASMCs, immunofluorescence (IF) microscopy was performed. Briefly, HEK293T cells or hPASMCs were seeded on sterilized poly-L-lysine-coated glass coverslips in 6-well tissue culture plates. Next day the HEK293T cells were transiently transfected with WT-T2R4 or mutant constructs using lipofectamine 2000 according to published procedures. Following 24 h of transfection, T2R4 and mutant expressing cells, or hPASMCs, were washed with 1xPBS and fixed with 3.7% paraformaldehyde for 15 min, then permeabilized using 0.05% Triton X 100 for 20 min at room temperature. After washing with PBS, the cells were blocked using 2% bovine serum albumin (IgG- and protease-free) for 90 min. HEK293T cells were then labeled for 90 min using a 1:500 dilution of the monoclonal mouse-anti-FLAG antibody (N-terminal tagged T2R4) and a 1:100 dilution of rabbit anti-calnexin polyclonal antibody (endoplasmic reticulum marker). hPASMCs were labeled with 1:100 dilution of rabbit polyclonal anti-T2R1 or anti-T2R38. The cells were washed and incubated with fluorophore-conjugated secondary antibodies using a 1:1000 dilution of goat anti-mouse Alexa fluor 488 and a 1:300 dilution of goat anti-rabbit Alexafluor 594 for HEK293T cells or with 1:300 dilution of goat anti-rabbit Alexa 488 for hPASMCs for 60 min. Following washing, the nuclei were stained with a 1:1000 dilution of Hoechst-33342 stain for 10 sec, washed and the coverslips were air

dried for 30-45 min. Prolong-antifade gold was used to mount the coverslips on slides, and the edges were sealed with nail polish. Representative cells were selected and visualized using an Olympus BX81 microscope.

3.7 Second-Messenger Assays

3.7.1 Measurement of Inositol triphosphate (IP_3) mobilization in HEK293T cells

Activated T2R couples to the heterotrimeric G-protein, βγ-subunits of the G-protein activate phospholipase C-β2 (PLC-β2). The PLC-β2 cleaves PIP_2 into DAG and IP_3. Thus, IP_3 was measured to characterize the signaling efficacy of WT-T2R4 and mutants. Briefly, an IP_3 standard graph was generated using known concentrations of IP_3 (20 pM - 20 μM) and the fluorescence was measured according to manufacturer's protocol (HitHunter IP_3 Fluorescence Polarization assay kit, DiscoveRx, CA, USA). This standard graph was used to measure the agonist-dependent or agonist-independent IP_3 produced by cells. FLAG-T2R4 or the mutants were expressed in HEK293T cells using 3μg DNA per 1×10^6 cells in six-well tissue culture plates. Cells expressing WT-T2R4 or the mutants were stimulated with quinine and IP_3 mobilization was measured. The amount of IP_3 produced was reported in terms of picomoles. Results were normalized to IP_3 mobilized by cell surface expression of the receptor as determined by flow cytometry.

3.7.2 Measurement of Inositol triphosphate (IP_3) mobilization in ASMCs and PASMCs

IP_3 assays were carried out in human and porcine PASMCs and ASMCs using a commercially available IP_3 assay kit (HitHunter IP_3 fluorescence polarization [FP] assay, DiscoveRx, Fremont, CA) according to the instructions supplied by the manufacturer. Human

and porcine PASMCs and ASMCs were treated with 500 μM DXM or 1 μM U46619, or buffer alone for 20 minutes. An IP_3 standard graph was generated using known concentrations of IP_3 (20 pM - 20 μM) and the fluorescence was measured according to manufacturer's protocol. This standard graph was used to measure the agonist-dependent or agonist-independent IP_3 produced by cells. The amount of IP_3 produced was reported in terms of picomoles.

3.7.3 Measurement of Intracellular Calcium $(Ca^{2+})_i$

FLAG-T2R4 was expressed in HEK293T cells using 3μg of DNA per 1×10^6 cells in six-well tissue culture plates. For GRK-KD assays, FLAG-T2R4 was transiently expressed in HEK293T cells stably expressing GRK2, GRK3, GRK5 and GRK6-specific shRNA. T2R4 expressed in stably-transfected scrambled shRNA construct in HEK293T cells was used as control. For experiments involving T2R4-mutants, HEK293T cells were transiently co-transfected with Gα16/gust44 and T2R4 in a 1:1 ratio. After 6-8 h of transfection, 1×10^5 cells/well were plated in 96-well black-wall clear bottom plates. After another 14-16 h, the cells were loaded with 100 μl/well calcium-sensitive Fluo-4 NW dye (Invitrogen) for 40 min at 37°C and another 30 min at room temperature. For PKC experiments, the cells were incubated with 0.1 μM PMA or 10 μM Bis1 during the final 15 min of dye incubation. Changes in intracellular calcium were measured after addition of quinine by FlexStation-3 microplate reader (Molecular devices), at 525 nm emission following excitation at 494 nm. Dose-response curves were generated and EC_{50} values were calculated using Graph Pad Prism software.

3.7.4 Desensitization assays

FLAG-T2R4-expressing HEK293T cells (1×10^5 cells/well) were plated in poly-L-lysine coated 96-well black-wall clear bottom plates. The cells were loaded with Fluo-4 NW dye for 40 min at 37°C followed by 30 min at room temperature. During the final 15 min, the cells were exposed either to 1 mM quinine, 1mM yohimbine, or to PMA and Bis1 in the presence of dye. This is represented as a pre-treatment, whereas, T2R4-expressing cells without any quinine pre-treatment and treated with assay buffer only are denoted as untreated cells. The cells were washed twice with assay buffer after 15 min of pre-treatment and loaded again with 100 µl of dye. Changes in intracellular calcium were measured for the next 3 min after 1 mM quinine or yohimbine was added by the FlexStation 3 microplate reader. Quinine-mediated Ca^{2+} responses of untreated cells, used as control, were considered as 100% and Ca^{2+} responses of pre-treated cells were normalized to this value.

3.8 *Ex vivo* Studies

3.8.1 Isometric Myography

Isometric myograph experiments were pursued in the laboratory of Dr. Shyamala Dakshinamurti, Children's Hospital Research Institute of Manitoba. Pulmonary arteries and airways (100-300 µm luminal diameter, 4^{th} - 6^{th} generation) from day 0 piglet were gently cut into 2-3 mm rings. The diameter was determined by using micrometer slide and an eyepiece reticule. Rings were optimally equilibrated at a median resting tension of 1.5 mN on mounting pins attached to a force transducer on a multi-chamber isometric wire myograph (Danish Myo Systems) in Krebs-Henseleit buffer at 37°C, continuously bubbled with a 95% O_2, 5% CO_2 gas mixture to give a pH of 7.40 to 7.45. Pulmonary artery ring normalization

was modified from Mulvany and Halpern (Mulvany and Halpern, 1977) for isometric myography of small resistance arteries, by stepwise addition of resting tension until a small accrual of passive tension was observed; resting tension was then decreased by one step below that level, to set the vessel at optimal resting tension for isometric study (Angus and Wright, 2000). After equilibration, maximum active tension to KCl stimulation was determined for each ring. Thromboxane A2 receptor (TP) mimetic U46619 (30 nM), a potent vasoconstrictor for vascular smooth muscle, was used for pre-contracting the arterial rings. In selected rings, endothelium was removed by gentle rotation of the ring on fine steel rod in cold Krebs-Henseleit buffer; rings were considered endothelium-denuded when artery rings pre-contracted by challenge with TP receptor mimetic U46619 (10^{-6} M), exhibited an acetylcholine (10^{-5} M) mediated relaxation of no greater than 5% of pre-existing tone, compared to control rings. Isometric tension in response to agonists was recorded by computer using Powerlab data collection and Chart 5 software; contraction was expressed relative to maximal KCl-induced force. A minimum of n =15 rings from 5 piglets were used for each experiment.

3.9 Detection of superoxide by Dihydroxyethidium (DHE) fluorescence method

Superoxide was measured in hPASMCs by DHE fluorescence method. hPASMCs ($1x10^5$ cells) were cultured in serum deprived condition for 72 h in 5% CO_2 and 21% O_2. The cells were then treated with 0.5 mM DXM for 4 h. DHE stock (31.7 μM) was prepared in 10 mg/ml DMSO and then diluted in PBS. Cells were washed twice in PBS and then loaded with DHE for 45 min at 37°C. The excess dye was washed off, and the intracellular fluorescence intensity was detected using a FlexStation 3 microplate reader with the following settings,

excitation at 500 nm and emission at 610 nm (Gong et al., 2010; Munzel et al., 2002).

3.10 Statistical analysis

Statistical analysis was performed using one-way analysis of variance (ANOVA) with *Tukey's* post hoc test, *Dunnette's* post-test, or unpaired two-tailed Student's *t* test from a minimum of 3 independent experiments to determine the statistical significance wherever applicable. * $p<0.05$, ** $p<0.01$, *** $p<0.001$.

CHAPTER 4

4.0 RESULTS

4.1 Dextromethorphan mediated bitter taste receptor activation in the pulmonary circuit causes vasoconstriction

Jasbir D. Upadhyaya, Nisha Singh, Anurag S. Sikarwar, Raja Chakraborty, Sai P. Pydi, Rajinder P. Bhullar, Shyamala Dakshinamurti, Prashen Chelikani

PLoS One. 2014;9(10):e110373. doi: 10.1371 /journal.pone.0110373.t001

4.1.1 DXM-mediated bitter taste receptor activation

Expression of T2Rs has been reported in non-gustatory tissues, such as the respiratory circuit (Deshpande et al., 2010; Finger et al., 2003; Shah et al., 2009; Tizzano et al., 2010), gastrointestinal tissues (Rozengurt, 2006; Wu et al., 2002), reproductive tissues (Xu et al., 2013), mesenchymal stromal and vascular smooth muscle cells (Lund et al., 2013), brain (Singh et al., 2011b), heart (Foster et al., 2013), and normal mammary and breast cancer cells (Singh et al., 2014). In human airway epithelia, bitter compounds stimulate the ciliary activity to hasten the elimination of harmful substances and initiate protective airway reflexes (Shah et al., 2009). Activation of T2Rs in ASM leads to muscle relaxation and bronchodilation, that is three fold greater than that elicited by currently used beta-adrenergic receptor agonists (Deshpande et al., 2010). Previously the expression of TAS2R46 was reported in human aortic smooth muscle cells and rats injected with denatonium showed a significant drop in their blood pressure (Lund et al., 2013). However, the presence of all 25 human T2Rs in other vascular tissues like the PASM had not been established. These findings led to my hypothesis that T2Rs are expressed in hPASMCs and might be involved in regulating the vascular tone.

Thus, the expression of T2Rs in PASMCs was characterized by reverse-transcriptase (RT)-PCR. The effects of the bitter agonist DXM on pulmonary artery were also delineated by performing functional studies. Previously in site-directed mutational studies, the response of T2R1 to DXM was characterized by our lab, therefore, T2R1 was selected for further analysis in this study. Knockdown with T2R1 specific shRNA decreased mRNA levels, protein levels and DXM-induced calcium responses in PASMCs. To analyze if T2Rs are involved in regulating the pulmonary vascular tone, *ex vivo* studies using pulmonary arterial

and airway rings were pursued.

4.1.2 Expression analysis of TAS2R transcripts and functional characterization

To determine the expression of TAS2R transcripts in hPASMCs, all 25 TAS2Rs were selected for analysis by RT-PCR. Total RNA was isolated from hPASMCs, cDNA was synthesized and RT-PCR was performed. Transcripts of most of the TAS2Rs were detected in the hPASMCs, except for TAS2R16, TAS2R38, TAS2R40 and TAS2R41 (**Figure 4.1.1**). This could be due to the low copy number and/or expression of these TAS2R genes in hPASMCs. Having demonstrated that hPASMCs express TAS2R transcripts (**Figure 4.1.1**), we analyzed whether these T2Rs are functional, by stimulating the cells with several known bitter agonists (Meyerhof et al., 2010) (**Figure 4.1.2A**). The bitter compounds used for activating these cells were yohimbine (1 mM), quinine, DXM, nicotine (2 mM each), chloramphenicol, picrotoxinin (3 mM each), colchicine, thiamine, caffeine, PTC, PROP, sodium thiocyanate (5 mM each), salicin, chloroquine and denatonium benzoate (10 mM each). A list of the T2Rs activated by these compounds is provided in **Table 4.1.1**. The respective concentrations were selected based on their published E_{max} values, and keeping in view the low affinity of T2Rs for their ligands, usually in the higher micro to millimolar range (Clark et al., 2012; Meyerhof et al., 2010). The increased intracellular calcium levels upon stimulation indicated that T2Rs in cultured hPASMCs are functional (**Figure 4.1.2A**). Most of these compounds were able to activate multiple T2Rs. The maximum response was seen for DXM, currently known to activate only T2R1 (Born et al., 2013; Meyerhof et al., 2010). Previously, in a site directed mutational analysis of T2R1 we have shown that DXM

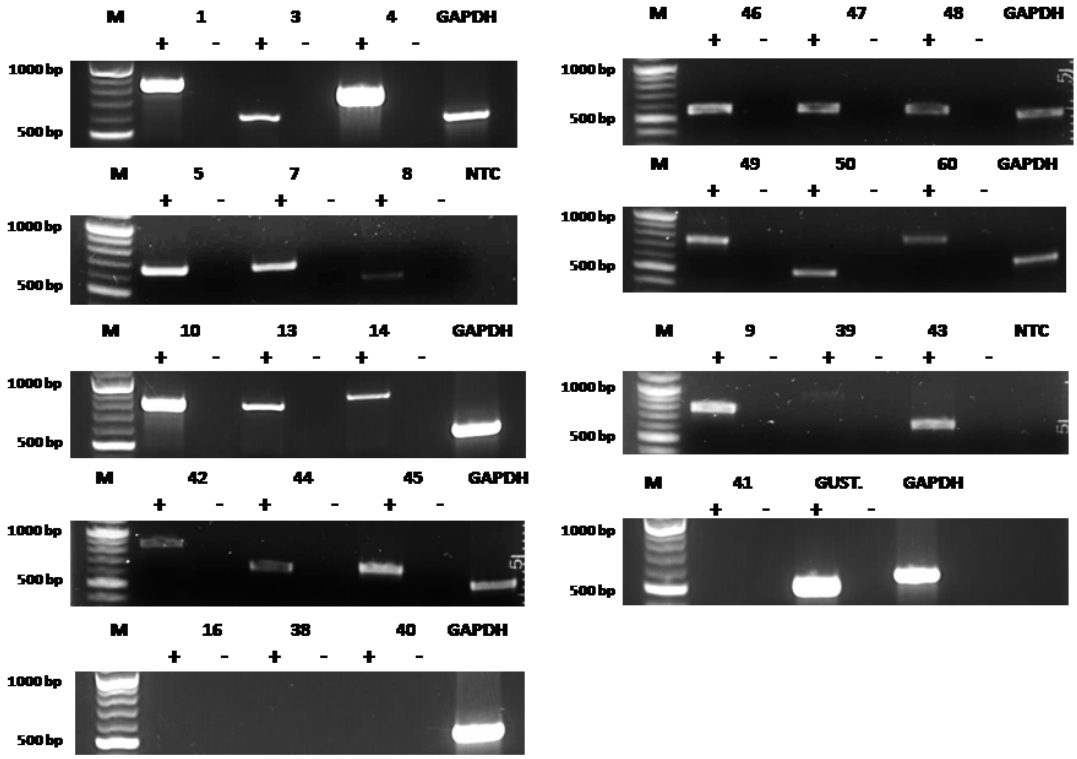

Figure 4.1.1. Reverse transcriptase (RT)-PCR analysis of the expression of bitter taste receptors (TAS2Rs) in hPASMCs. Agarose gel electrophoresis (1%) analysis of the RT-PCR products showed that 21 TAS2Rs were expressed in hPASMCs. GAPDH was used as an internal control for the PCR reactions. + and – represent the addition and omittance of reverse transcriptase in the reaction respectively. NTC represents a no template control in which the cDNA template was omitted. M represents 100 bp molecular weight standard (NEB). All transcripts were observed at the expected amplicon size. Each agarose gel electrophoresis is representative of 4-5 independent experiments.

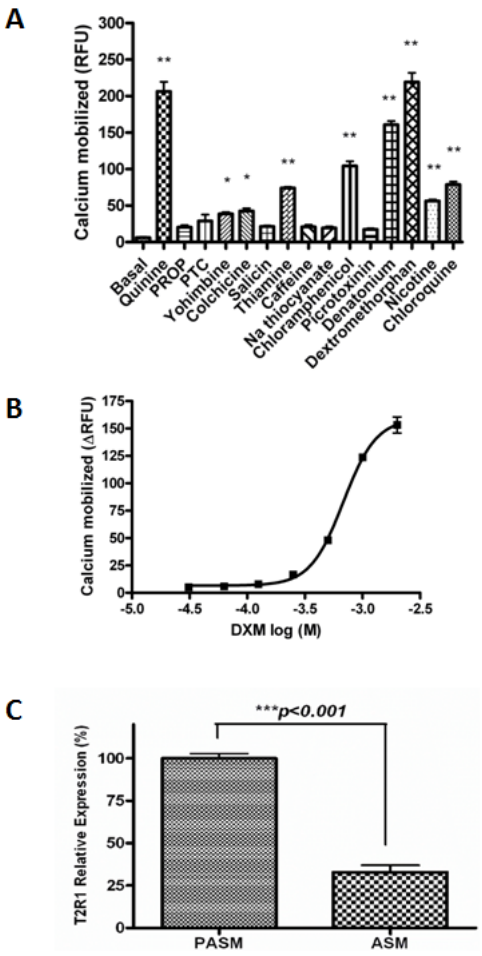

Figure 4.1.2. Functional response of hPASMCs to different bitter agonists. A. Bitter compounds of diverse structures cause increase in intracellular calcium $[Ca^{2+}]_i$ in primary cultures of hPASMCs. $[Ca^{2+}]_i$ responses to 1 mM yohimbine, 2 mM quinine, DXM and nicotine, 3 mM chloramphenicol and picrotoxinin, 5 mM colchicine, thiamine, caffeine, PTC, PROP and sodium thiocyanate, and 10 mM denatonium benzoate, salicin and chloroquine. Results are mean ± SEM from n = 5 done in triplicates. *p<0.05 vs control and **p<0.01 vs control. **B.** Concentration dependent changes in $[Ca^{2+}]_i$ of hPASMCs expressing endogenous T2R1 induced by exogenous bitter agonist DXM (log M). Data were collected from five independent experiments. Dose response curve was generated and an EC_{50} value of 676 ± 90 μM for DXM in hPASMCs was calculated using Graph Pad Prism software. **C.** Relative expression levels of T2R1 in hPASMCs and hASMCs as determined by quantitative (q)-PCR. Relative expression of T2R1 in hASMCs was normalized to that in hPASMCs which was considered as 100%. Data presented are from five independent experiments. Results are normalized to the expression of GAPDH. Values are plotted as mean ± SEM. Relative expressions were computed using $2^{-\Delta CT}$ method. Statistical significance of T2R1 expression in hPASMCs was determined by student t-test, ***p<0.001 vs T2R1in hASMCs.

Table 4.1.1 A list of bitter taste receptors activated by the compounds used in Fig. 4.1.2

Bitter Compound	Bitter taste receptor (T2R)
Quinine	T2R4, T2R7, T2R10, T2R14, T2R39, T2R40, T2R43, T2R44, T2R46
PROP, PTC	T2R38
Yohimbine	T2R1, T2R4, T2R10, T2R38, T2R46
Colchicine	T2R4, T2R39, T2R46
Salicin	T2R16
Thiamine	T2R1, T2R39
Caffeine	T2R7, T2R10, T2R14, T2R43, T2R46
Sodium thiocyanate	T2R1, T2R38
Chloramphenicol	T2R1, T2R8, T2R10, T2R39, T2R43, T2R46
Picrotoxinin	T2R1, T2R10, T2R14, T2R46, T2R47
Denatonium benzoate	T2R4, T2R8, T2R10, T2R13, T2R39, T2R43, T2R46, T2R47
Dextromethorphan	T2R1
Chloroquine	T2R3, T2R10, T2R39

causes a concentration-dependent increase in intracellular calcium in cells expressing T2R1, and were able to map the DXM binding pocket on T2R1 (Singh et al., 2011a). Next, cultured hPASMCs were treated with different concentrations of DXM (**Figure 4.1.3**). As shown in **Figure 4.1.2B**, the addition of DXM induced a concentration dependent increase in intracellular calcium in hPASMCs, with an EC_{50} value of 676 ± 90 μM. The effect of DXM on intracellular calcium release in hASMCs was also analyzed and significantly low calcium was released with 2 mM DXM in hASMCs when compared to hPASMCs (**Figure 4.1.4**).

Differences in the expression of TAS2R1 among hPASMCs and hASMCs were analyzed by performing qPCR in both cell types. The data demonstrated that expression of TAS2R1 in hPASMCs was three fold higher than that in hASMCs (**Figure 4.1.2C**). Further, qPCR analysis was done to analyze the expression pattern of TAS2R1 in porcine PASMCs and ASMCs (**Figure 4.1.5**). Expression pattern of TAS2R1 in porcine PASMCs and ASMCs was similar to its expression pattern observed in human PASMCs and ASMCs, i.e. TAS2R1 expression in PASMCs was 3-fold higher than that observed in ASMCs.

4.1.3 T2R1 knockdown in hPASMCs

To analyze if the increase in intracellular calcium level after DXM incubation was T2R1 specific, knockdown of T2R1 in hPASMCs was pursued. Transfection of hPASMCs with T2R1-specific shRNA decreased T2R1 mRNA by 50 ± 12% compared to the scrambled shRNA control (**Figure 4.1.6A)**. Agarose gel analysis of the PCR products followed by densitometric analysis revealed around ~ 40% knockdown (**Figure 4.1.6B**). Immunoblot analysis revealed a decrease of ~ 50% in T2R1 protein expression (**Figure 4.1.6C**). This was accompanied by ~ 50% decrease in the intracellular calcium level stimulated by the T2R1

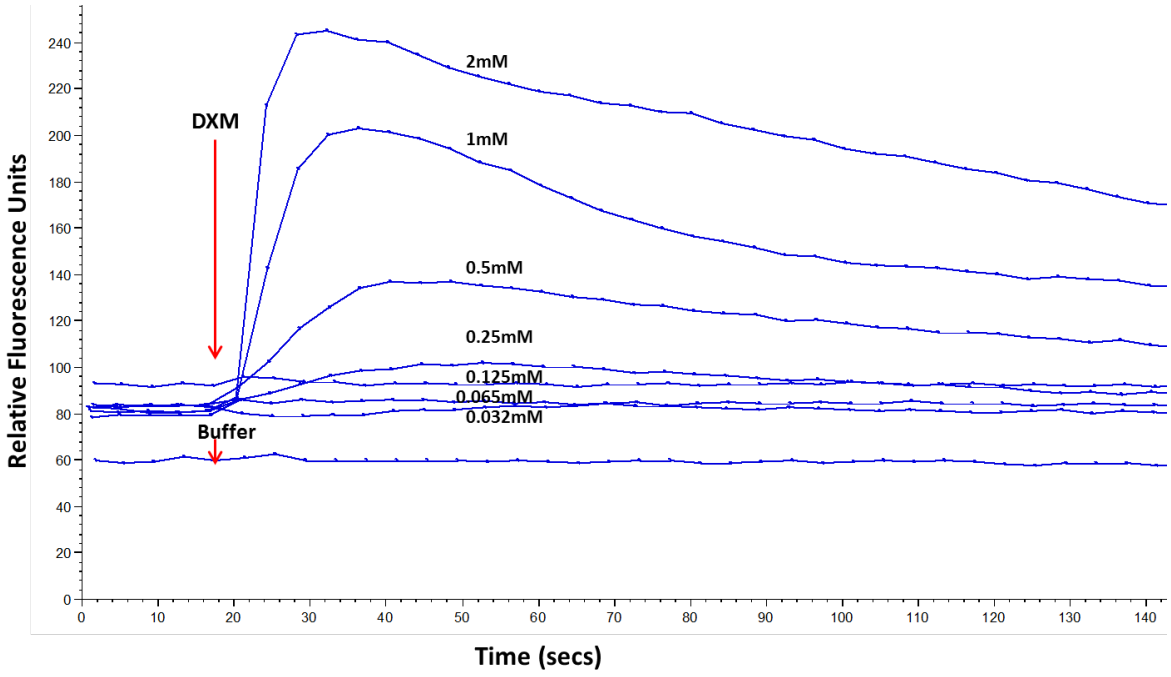

Figure 4.1.3. Representative calcium traces of hPASMCs stimulated with different concentrations of DXM or assay buffer (bottom trace). The calcium mobilized (Relative Fluorescence Units or RFUs) was detected using the calcium sensitive dye Fluo-4 NW (Invitrogen), and fluorescence measured using the automated Flex Station 3 microplate reader. In brief, the basal calcium mobilized was measured for the first 20 sec in all the 8 wells (one column) of a 96 well plate, followed by the simultaneous addition of different concentrations of the test compound, shown by arrows in the figure, to all the 8 wells by the in-built automated dispenser in Flex Station 3. Then calcium traces were recorded for the next 180 sec.

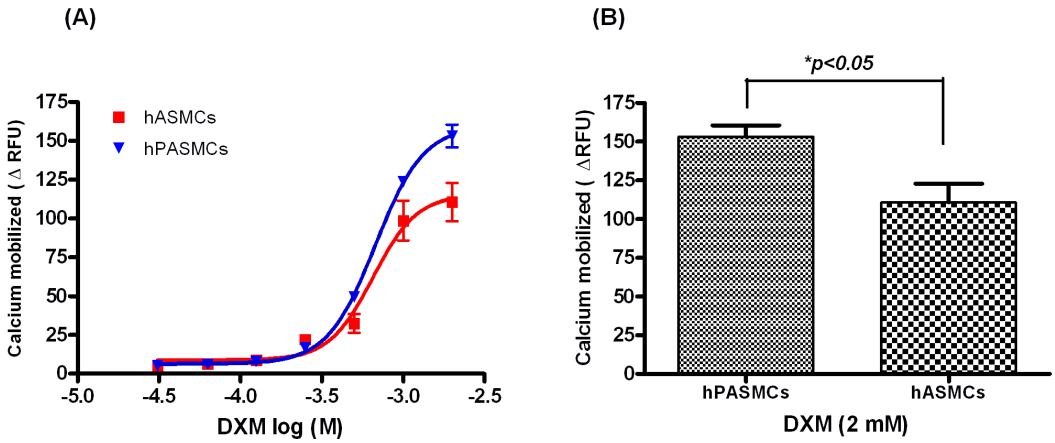

Figure 4.1.4. Comparison of intracellular calcium release in hPASMCs and hASMCs in response to different concentrations of DXM. A. Concentration-dependent changes in $[Ca^{2+}]_i$ of hPASMCs and hASMCs induced by different concentrations of bitter agonist DXM (log M). Data were collected from 3-5 independent experiments carried out in triplicates. Dose response curves were generated using Graph Pad Prism software. **B.** Bar graph showing difference in intracellular calcium release in hPASMCs and hASMCs in response to 2 mM DXM (E_{max} concentration). Significant difference in calcium release was observed between hPASMCs and hASMCs with significance level of *p<0.05.

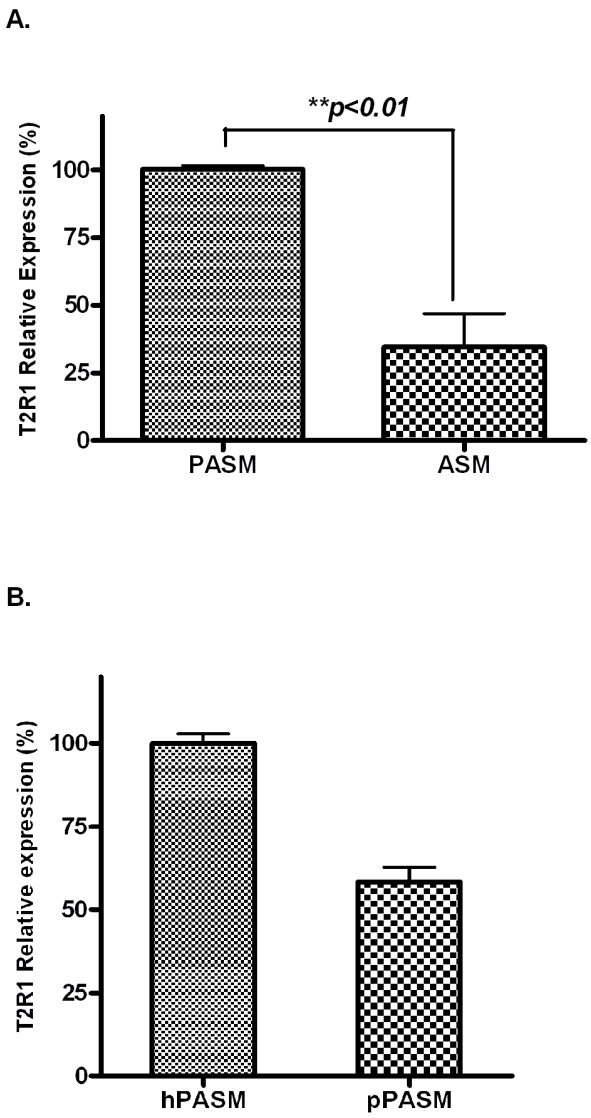

Figure 4.1.5. Quantification of T2R1 expression in human and porcine cells. A. Relative expression level of T2R1 in porcine PASMCs and ASMCs as determined by quantitative (q)-PCR. T2R1 expression in porcine PASMCs was considered as 100% and relative expression of T2R1 in ASMCs was normalized to it. **B.** Relative expression of T2R1 in human and porcine PASMCs. The relative expression of T2R1 in porcine PASMCs was normalized to that of hPASMCs, which was considered as 100%. Data presented are from five independent experiments done in triplicates. Results are normalized to the expression of GAPDH. Values are plotted as mean ± SEM. Relative expressions were computed using $2^{-\Delta CT}$ method. Student's t-test was used to check the significance.

agonist DXM (**Figure 4.1.6D**). Further, immunofluorescence microscopy of hPASMCs with polyclonal antisera directed against T2R1 revealed that the receptor was partly localized on the cell surface. However, no staining was observed for the negative controls, isotype specific IgG antisera and T2R38 (**Figure 4.1.7**).

4.1.4 DXM mediated differential responses of piglet pulmonary arterial and airway rings

Pulmonary arterial rings were optimally equilibrated at a median resting tension of 1.5 mN. To examine the DXM mediated physiological response in pulmonary arterial rings, with and without U46619 pre-contraction, rings were exposed to serial concentrations of DXM (10^{-5} to 10^{-3} M). Treatment of the resting arterial rings with 300 μM DXM caused noticeable force generation, which increased slowly and took 15-20 min to reach a plateau. This was followed by a slight increase in force at 650 μM of DXM, which remained stable even after adding up to 1 mM of DXM (**Figure 4.1.8A**). Next, a DXM dose response curve was constructed by normalizing the force generation to maximal KCl stimulation, and the EC_{50} was calculated to be 211 ± 2 μM (**Figure 4.1.8B**). To confirm this vasoconstrictor response of DXM, the arterial rings were pre-contracted with U46619 (30 nM). DXM exposure caused contraction of pre-contracted rings starting from 100 μM concentration which increased till 650 μM, and then reached a plateau (**Figure 4.1.9**). In contrast, chloroquine induced relaxation of U46619 pre-contracted arterial rings (30–35%, **Figure 4.1.9B**). The levels of pre-contraction to U46619 (30 nM) in pulmonary arteries was ~ 140% of KCl (50 mM)-induced contractions. We also explored the role of endothelium in this DXM-mediated functional response by using endothelium-denuded pulmonary arterial rings. DXM

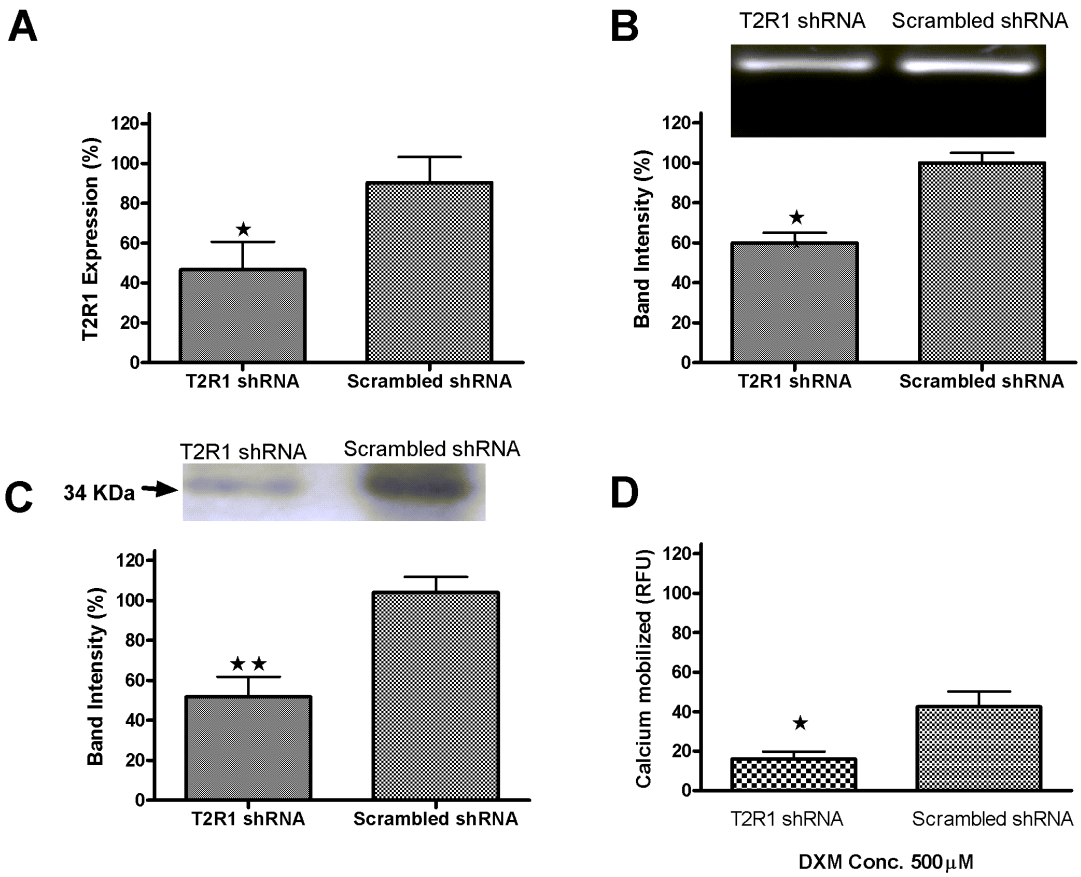

Figure 4.1.6. Knockdown of T2R1 in hPASMCs. A. Primary cultures of hPASMCs were transfected with scrambled shRNA (control) or T2R1-specific shRNA. 48 h post-transfection, cells were used for RNA extraction and real-time PCR. Results are normalized to GAPDH expression. Percentage (%) knockdown efficiency was computed using $2^{-\Delta\Delta CT}$ method. Values are mean ± SEM, n = 5. Statistical significance was determined by student t-test,*p<0.05 vs scrambled shRNA (control). **B.** Representative agarose gel analysis of figure A. Lane 1 represents T2R1-shRNA and lane 2 scrambled shRNA. Quantification of T2R1 knockdown is represented via bar graph using the densitometric analysis. Statistical significance was determined by student t-test, *p<0.05 vs scrambled shRNA. **C.** Western blot analysis showing T2R1 knockdown at the protein level in hPASMCs. Band intensity was normalized to expression of β-actin. Bar graph shows the quantitative analysis of receptor knockdown in the blot. Statistical significance was determined by student t-test, **p<0.01 vs scrambled shRNA (control). **D.** Functional effects of T2R1 knockdown in hPASMCs. hPASMCs were transfected with scrambled shRNA (control) and T2R1-specific shRNA. 48 h post-transfection, cells were used for calcium mobilization experiment, and stimulated with 500 μM DXM. Data were collected from five independent experiments carried out in triplicates. Values are mean ± SEM, n = 5. Statistical significance was determined by student t-test, *p<0.05 vs scrambled shRNA (control).

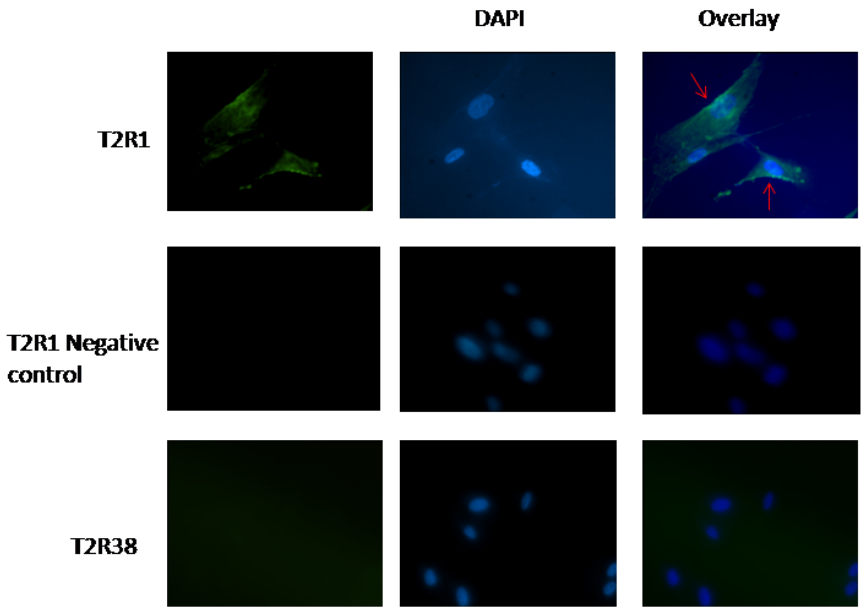

Figure 4.1.7. Immunofluorescence showing expression of T2R1 in hPASMCs. hPASMCs were processed by standard immunofluorescence microscopy as described in the methods. T2R1 antisera was utilized to identify the indicated protein (first row). The negative control (second row) utilized an isotype-matched non-specific IgG as the primary antibody, and T2R38 antisera (third row) showed no signals. Rabbit anti-human T2R1 was visualized with goat anti-rabbit Alexa 488 antibody (green) and nuclei were stained with DAPI (blue). Merged images show that T2R1 localized partly on the cell surface of hPASMCs cells as indicated by arrows.

stimulated endothelium denuded pulmonary artery rings acted in a similar manner with EC_{50} of 238 ± 1 μM (**Figure 4.1.10**). In contrast to pulmonary arterial rings, DXM completely relaxed the 10 μM acetylcholine (ACh) pre-contracted airway rings in a dose-dependent manner with an EC_{50} of 74 ± 1 μM, and reaching baseline at $3x10^{-4}$ M (**Figure 4.1.8C and D**). Further, when ACh (10 μM) pre-contracted airway rings were exposed to different concentrations of chloroquine (10^{-5} to $3x10^{-4}$ M), it was found that chloroquine caused relaxation in a dose dependent manner (**Figure 4.1.11**). Relaxant effects of DXM on airway rings and of chloroquine on airway and arterial rings are consistent with previous studies done in mouse airways, guinea pig aorta and tracheal rings and human pulmonary arteries (Deshpande et al., 2010; Manson et al., 2014).

4.1.5 IP_3 measurement and analysis of MLC and phospho MLC

Activation of the canonical bitter taste signaling involves: T2R-gustducin-PLCβ and IP_3, which in turn causes an increase in global intracellular calcium levels (Zhang et al., 2013). Therefore, to investigate the contrasting mechanisms involved in DXM-mediated responses in pulmonary artery and airways, IP_3 production was measured in human and porcine cells. In human cells, there was no effect of DXM-treatment on IP_3 production in ASMCs as compared to untreated cells. However, significantly higher IP_3 production was observed in DXM-treated hPASMCs, which was two-fold of DXM-treated hASMCs (**Figure 4.1.12**). Similarly, significantly higher IP_3 was obtained in DXM-treated PASMCs of porcine origin as compared to DXM-treated ASMCs (**Figure 4.1.13A**). DXM-treatment led to a small increase in IP_3 production in porcine ASMCs, which was not significant when compared to the basal IP_3 levels.

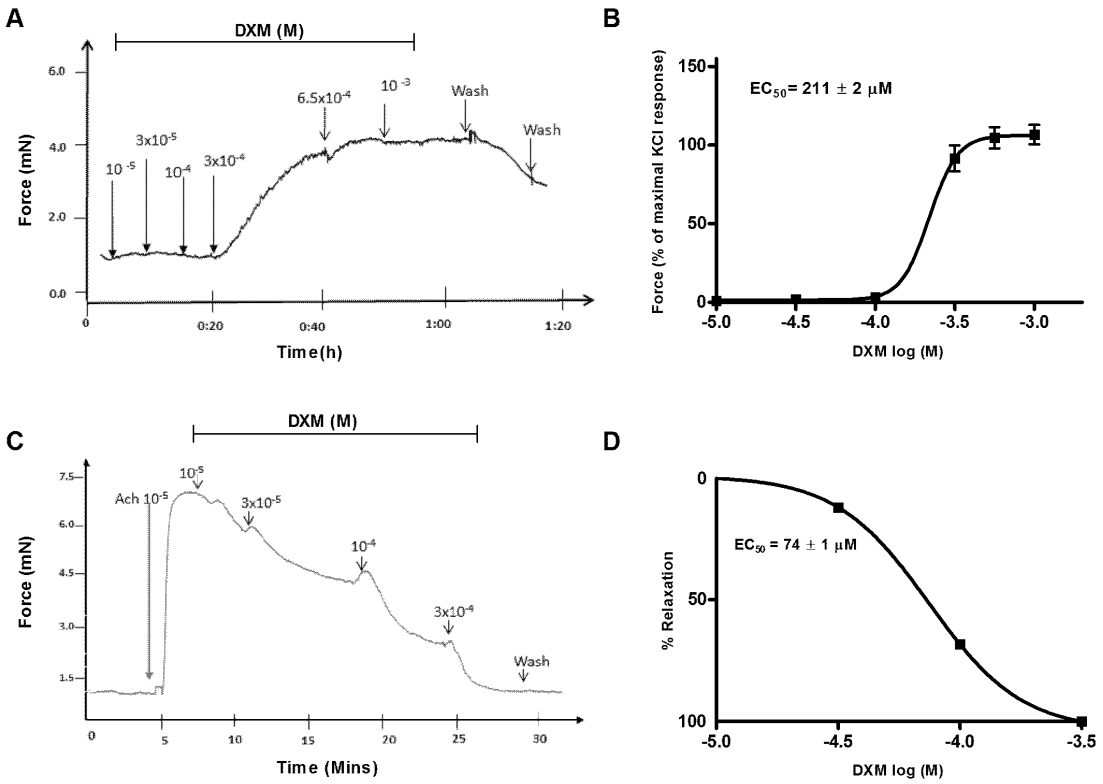

Figure 4.1.8. Myograph analysis of the effects of DXM on porcine pulmonary arterial and airway rings. A. The figure represents the raw trace showing the effect of DXM (10^{-5} to 10^{-3} M) stimulation on resting tension of pulmonary artery rings. Force generation started from 300 µM, increasing slowly to plateau after 15-20 min; followed by a slight increase in force at 650 µM DXM. There was no further increase in tension even with up to 1 mM DXM. Force returned to baseline 20-30 min after 3-4 washings of pulmonary artery rings with Krebs solution. **B.** Dose response curve of DXM normalized to maximal KCl stimulation in pulmonary arterial rings. Cumulative dose response curve of DXM with highest concentration being $3x10^{-4}$ M and lowest 10^{-5} M on isometric tension of pulmonary artery rings. The DXM responses were normalized to maximal KCl stimulation and the EC_{50} was calculated to be 211 ± 2 µM. The results are presented as mean ± SEM and are from a minimum of n = 15 rings from 5 piglets. **C.** Representation of raw trace of the DXM doses added to piglet airway rings pre-contracted with 10^{-5} M ACh. DXM completely relaxed the Pre-contracted airways in a dose dependent manner reaching baseline at $3x10^{-4}$ M. **D.** Dose response curve of DXM normalized to maximal KCl stimulation in airway rings. The figure shows the effect of DXM dose response on porcine airway rings pre-contracted with 10^{-5} M ACh. DXM mediated relaxation is expressed as percentage of the maximum force due to KCl stimulation and the EC_{50} calculated was found to be 74 ± 1 µM. The results are presented as mean ± SEM and are from a minimum of n = 15 rings from 5 piglets.

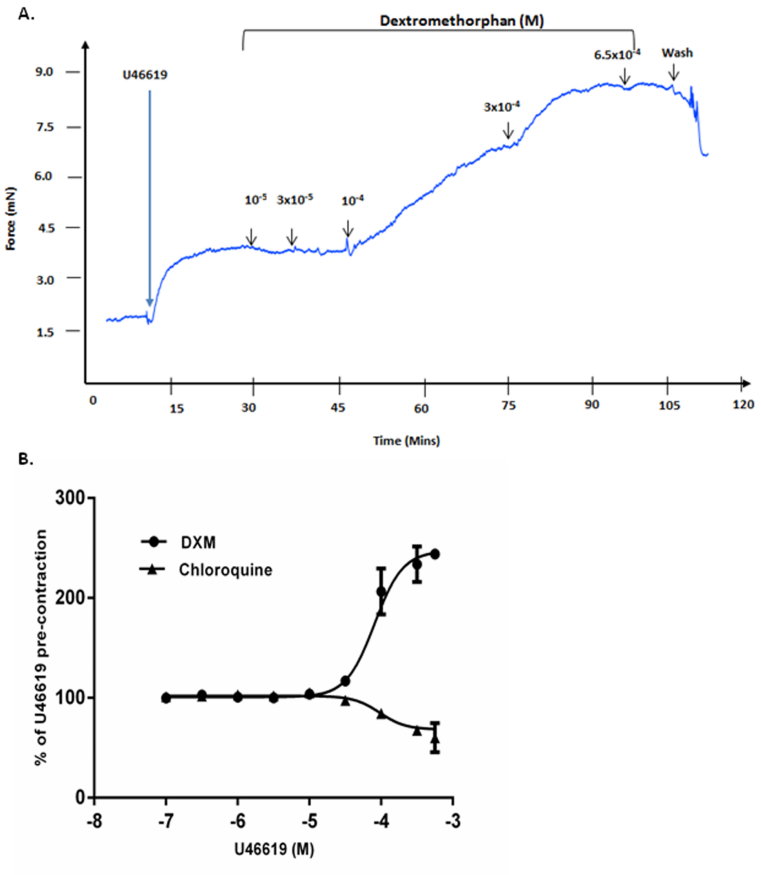

Figure 4.1.9. Myograph analysis of the effects of DXM and chloroquine on U46619 pre-contracted porcine pulmonary arterial rings. A. Raw traces showing effect of DXM (10^{-5} to $6.5x10^{-5}$ M) stimulation on resting tension of U46619 (30 nM) pre-contracted pulmonary artery rings. Force generation started from 100 µM and reached a plateau after 650 µM DXM. **B.** Effects of DXM and chloroquine on pre-contracted porcine arterial rings. Data are representative of n =6 rings and presented as mean ± S.E.M. The levels of pre-contraction to U46619 (30 nM) in pulmonary arteries was ~ 140% of KCl (50 mM)-induced contractions.

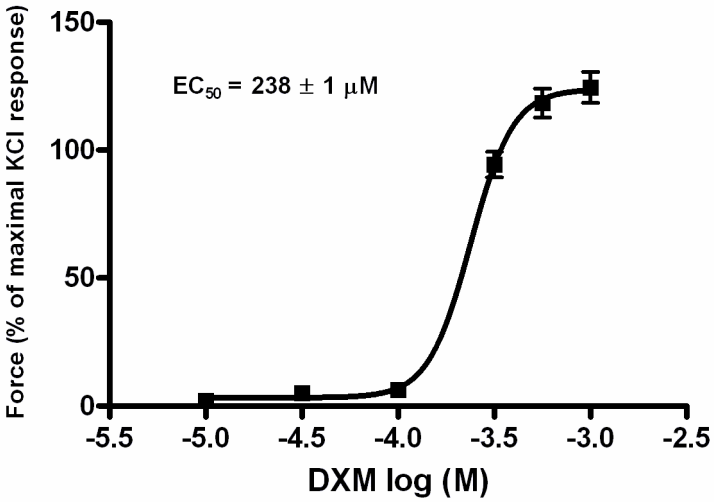

Figure 4.1.10. Myograph analysis of the effects of DXM on endothelium-denuded porcine pulmonary arterial rings. Dose response curve of DXM normalized to maximal KCl stimulation in pulmonary arterial rings. The figure represents a cumulative dose response curve of DXM with highest concentration being 10^{-3} M and lowest 10^{-5} M on isometric tension of pulmonary artery rings. The DXM responses were normalized to maximal KCl stimulation and the EC_{50} was calculated to be 238 ± 1 μM. The results are presented as mean ± SEM and are from a minimum of n= 15 rings from 5 piglets.

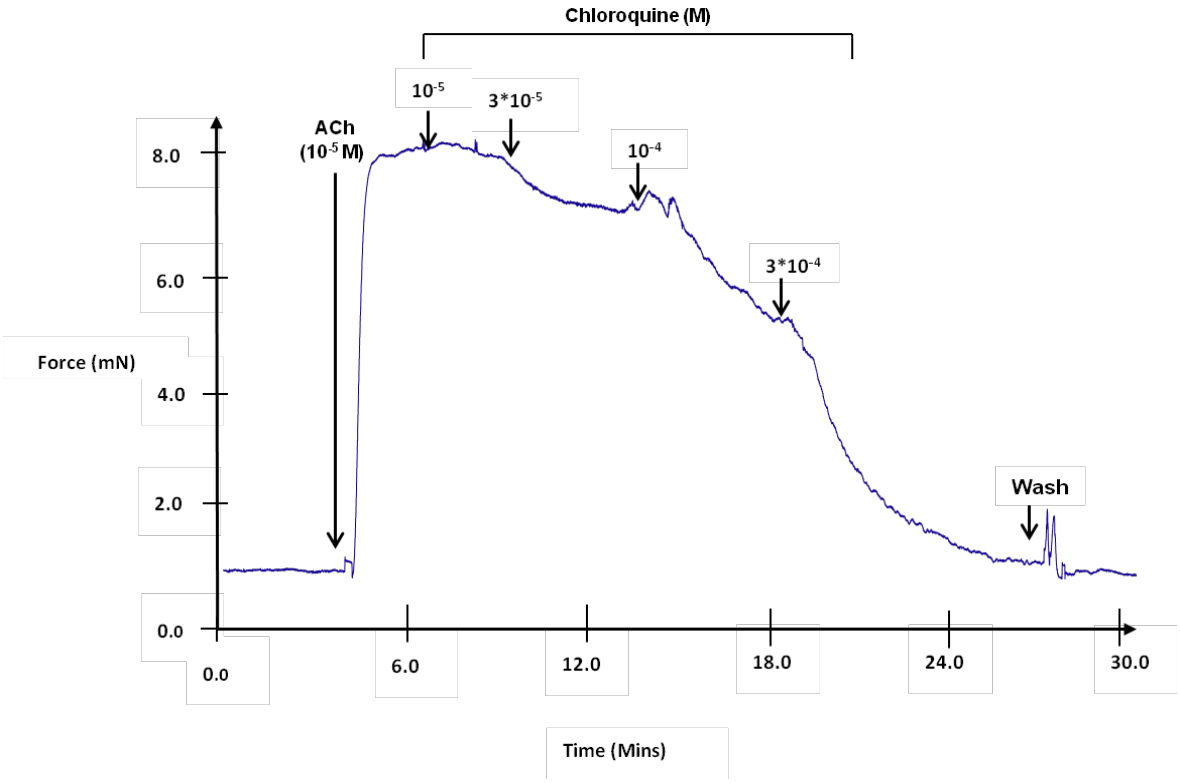

Figure 4.1.11. Effects of bitter compound chloroquine on porcine airway rings. Piglet airway rings were contracted with 10 µM of acetylcholine (ACh) and then chloroquine (10 µM-300 µM) was added to the bath as shown, resulting in relaxation in a dose dependent manner. Results are representative of five independent experiments and are from a minimum of n= 15 rings from 5 piglets.

One of the key intracellular signaling mechanisms underlying vascular smooth muscle cell contraction is the phosphorylation status of the 20 kDa MLC (Carrillo-Sepulveda and Barreto-Chaves, 2010; Silver, 1986). Contraction is induced by the increased phosphorylation of MLC. Therefore, the phosphorylation status of MLC in DXM treated and untreated porcine PASMCs and ASMCs was measured. U46619, a potent vasoconstrictor, was used as a positive control. DXM treatment of PASMCs led to an increase in phosphorylation of MLC compared to the untreated PASMCs (**Figure 4.1.13B**). However, DXM-treatment of porcine ASMCs did not cause any significant change in the MLC phosphorylation status (**Figure 4.1.13C**).

4.1.6 Effect of DXM on superoxide production

In vivo studies in rat models, and *in vitro* studies using human aortic endothelial cells (Wu et al., 2012) and neuron-glial cell cultures (Zhang et al., 2005) showed that DXM acts as a NADPH oxidase inhibitor causing a decrease in superoxide production. Studies in rats show that superoxide production by NADPH oxidase has a role in the development of hypertension and generation of vasoconstrictor responses in aorta (Alvarez et al., 2008). To investigate the inhibitory role of DXM on NADPH oxidase activity in hPASMCs, superoxide production in hPASMCs was measured. DXM (500 μM) treatment of hPASMCs did not cause any significant modification in superoxide production compared to the untreated group (**Figure 4.1.14**).

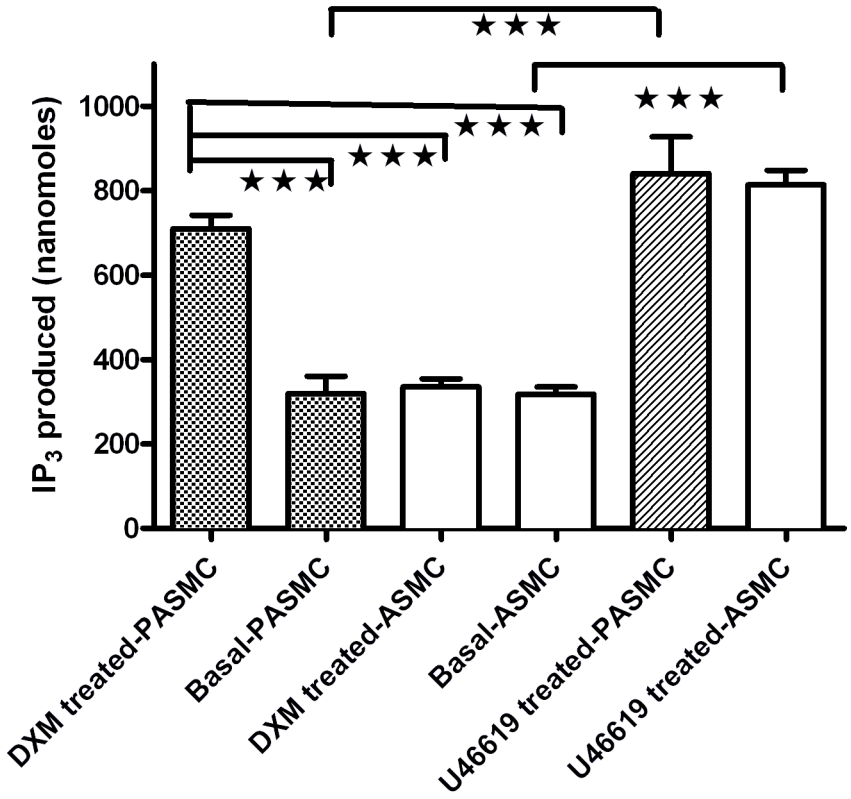

Figure 4.1.12. IP_3 produced in human PASMCs and ASMCs. Bar plot representation of total IP_3 produced (nanomoles) in hPASMCs and hASMCs upon treatment with DXM. hASMCs and hPASMCs were stimulated with T2R1 agonist DXM (500 μM) and the vasoconstrictor U46619 (TP agonist, 1 μM),which was used as a positive control. Shown are the agonist-independent or basal activity (-), and activity after stimulation (+) with agonist. Results are from a minimum of four independent experiments performed in triplicates. A one way ANOVA with *Tukey's* post hoc test was used to check the significance level of the amount of IP_3 produced. DXM treatment caused no change in IP_3 level in hASMCs, whereas, a significantly increased IP_3 was observed in DXM-treated hPASMCs, as compared to hASMCs, at significance level of ***$p<0.001$. Error bars represent mean ± SEM.

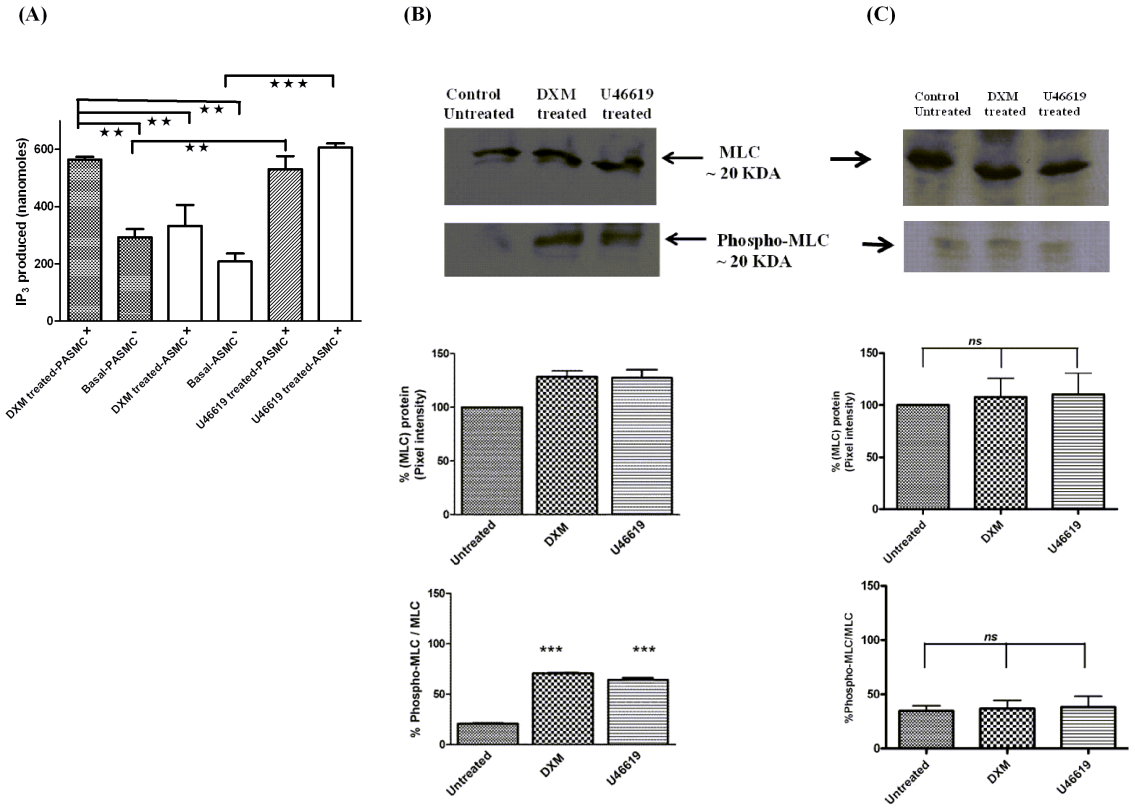

Figure 4.1.13. IP_3 measurement in porcine PASMCs and ASMCs, and analysis of MLC and phospho MLC in porcine PASMCs. A. Bar plot representation of total IP_3 produced (nanomoles) in pPASMCs and pASMCs upon treatment with DXM. pASMCs and pPASMCs were stimulated with DXM (500 µM) or U46619 (1 µM) which was used as a positive control. Shown are the agonist-independent or basal activity (-), and activity after stimulation (+) with agonist. Results are from a minimum of 4 independent experiments performed in triplicates. A one way ANOVA with *Tukey's* post hoc test was used to check the significance. The double asterisk indicate a significant difference in the amount of IP_3 produced after stimulation with 500 µM DXM in pPASMCs with respect to DXM response in pASMCs at significance level of **p<0.01. Error bars represent mean ± SEM. **B.** Representative western blot image and the respective densitometry analysis of three blots showing total MLC and phospho MLC in pPASMCs after DXM-treatment (500 µM). PASMCs treated with buffer alone or U46619 (1 µM) treated cells were used as controls. Both DXM and U46619 stimulated MLC phosphorylation. Significant results were obtained between untreated vs DXM treated and untreated vs U46619 treated at significance level ***p<0.001 for phospho-MLC. **C.** Representative western blot image and the respective densitometry analysis of three blots showing total MLC and phospho MLC in pASMCs after DXM-treatment (500 µM). No significant change in total MLC expression or phospho MLC was found between untreated sample and U46619 treated or DXM treated sample. The results are from a minimum of three independent experiments (n = 3) and shown as mean ± SEM.

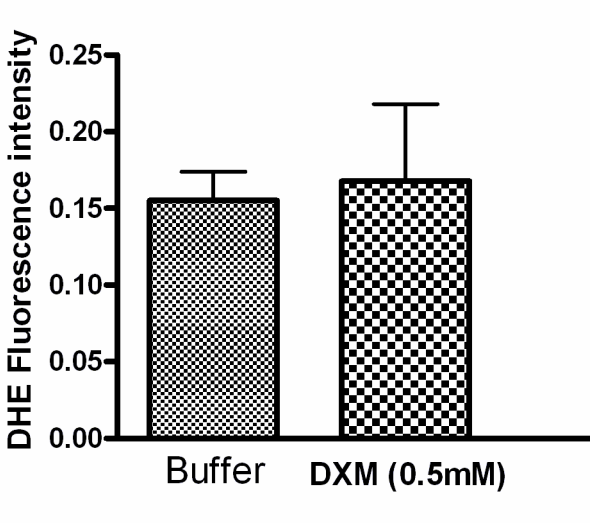

Figure 4.1.14. Effect of DXM on superoxide production in hPASMCs. hPASMCs were treated with 0.5 mM DXM or media alone for 4 h. DHE fluorescence assay was done to measure the superoxide production as described in methods. Superoxide production was expressed as fluorescence intensity and as the mean ± SEM of three independent experiments performed in triplicates.

4.2 Structure-function role of C-terminus in human bitter taste receptor T2R4 signaling

Jasbir Upadhyaya, Nisha Singh, Rajinder P. Bhullar, Prashen Chelikani

Biochim Biophysica Acta 2015; 1848(7):1502-1508. doi: 10.1016/j.bbamem.2015.03.035,

PMID: 25858111

4.2.1 Structure-function role of C-terminus in T2R4 signaling

The highly conserved amino acid residues and motifs found in most GPCRs generally have critical roles in the mechanism of receptor activation. For example, class A GPCRs have highly conserved motifs, the LxxxD motif in TM2, D/ERY motif in TM3, CWxP motif in TM6, and NPxxY motif in TM7 (Arakawa et al., 2011), which are absent in T2Rs. Previously 13 highly conserved residues and two conserved motifs in T2Rs, LxxxR in TM2 and LxxSL in TM5 (Pydi et al., 2014a; Singh et al., 2011a) have been revealed by our lab. These conserved residues and motifs bear no similarity to class A GPCR motifs, suggesting that T2Rs have a unique activation mechanism. Most of the structure-function studies in T2Rs are focused on determining the role of TM and loop region residues involved in T2R activation and ligand binding. The role of the C-terminus in T2R structure and function, however, remains poorly understood.

Previous studies have shown that the cytoplasmic C-terminal region of GPCRs plays an important role in receptor trafficking (Bermak et al., 2001; Pankevych et al., 2003; VanLeeuwen et al., 2003; Venkatesan et al., 2001), intracellular signaling (Lyu et al., 2000; Namba et al., 1993; Pankevych et al., 2003) and agonist-induced receptor internalization (Bohm et al., 1997). GPCRs export from the endoplasmic reticulum (ER) represents the first step in intracellular trafficking of receptors and influences their cell-surface expression and function (Dong and Wu, 2007; Petaja-Repo et al., 2000). However, the definitive sequences involved in trafficking and/or signal transduction remain unclear. Sequence analysis of human GPCRs showed that basic residues are frequent in membrane-proximal region of the C-terminus. Mutation of the C-terminal membrane-proximal basic residues (MPBRs) results in a marked reduction in the cell surface expression of multiple GPCRs (Dong et al., 2012;

Giraudo and Maccioni, 2003; Okamoto et al., 2013; Tetsuka et al., 2004; Venkatesan et al., 2001), thus, suggesting that these residues are critically involved in mediating the anterograde trafficking of a broad range of membrane proteins, including GPCRs.

In this study, the residues in the C-terminus of T2R4 which are required for optimal cell surface expression and receptor function have been examined. Sequence analysis identified a conserved KLK/R motif in the C-terminus of T2Rs. Alanine scanning mutagenesis of the entire C-terminus of T2R4 (except for Ala299) was pursued. A number of residues which were responsible for proper targeting of T2R4 to the cell surface were identified. Alanine mutations of Lys294, Leu295 and Lys296 residues of the KLK motif showed a significant reduction in maximal Ca^{2+} responses (E_{max}). Interestingly, the EC_{50} of quinine for K294A increased almost 3-fold in comparison to the WT-T2R4. A constitutively active mutant (CAM), K296A, which displayed five-fold basal activity over the wild type receptor was discovered. In addition to the alanine mutants, residues of the KLK motif were replaced by functionally similar arginine or valine. The conservative substitution mutants, K294R, L295V and K296R, displayed E_{max} and EC_{50} values similar to WT-T2R4. Data from this study, based on mutagenesis and pharmacological characterization of the mutants, revealed that the KLK motif in T2R4 performs a critical functional role, and the presence of basic and hydrophobic residues in the C-terminus is important for T2R4 trafficking and activation.

4.2.2 Role of C-terminus residues in cell surface expression

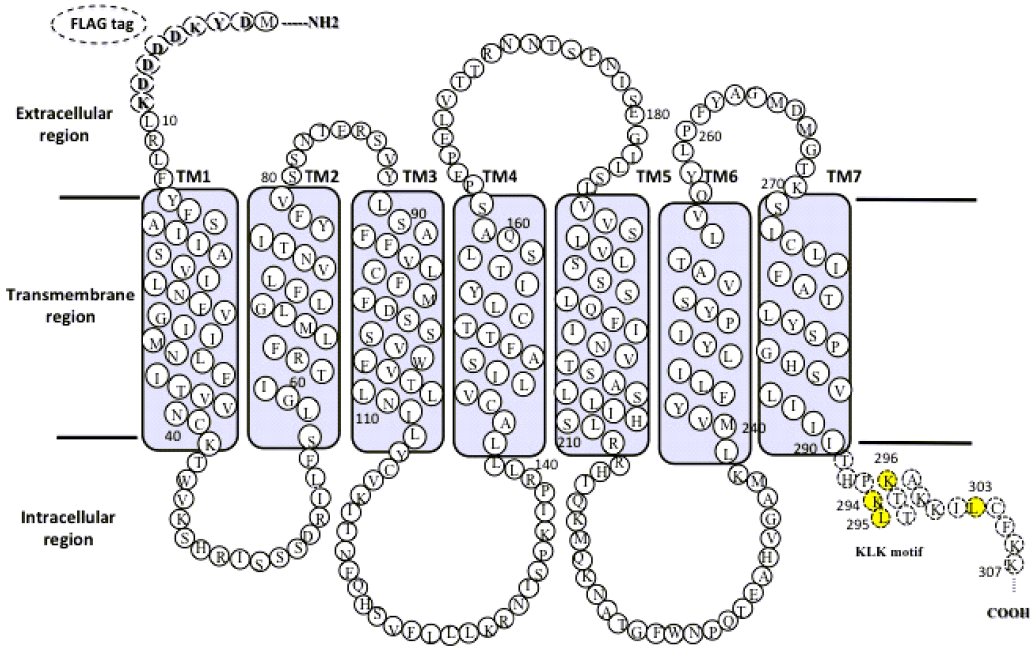

Figure 4.2.1. Amino acid sequence of the bitter taste receptor T2R4. Two-dimensional representation of the T2R4 amino acid sequence. It comprises a short extracellular N-terminus, seven transmembrane (TM) helices, three extracellular loops (ECLs), three intracellular loops (ICLs) and a short intracellular C-terminus. The C-terminus residues are shown in dashed circles. The conserved KLK motif and Leu303 are highlighted in yellow color. Also shown is the FLAG-epitope at the N-terminus.

A.

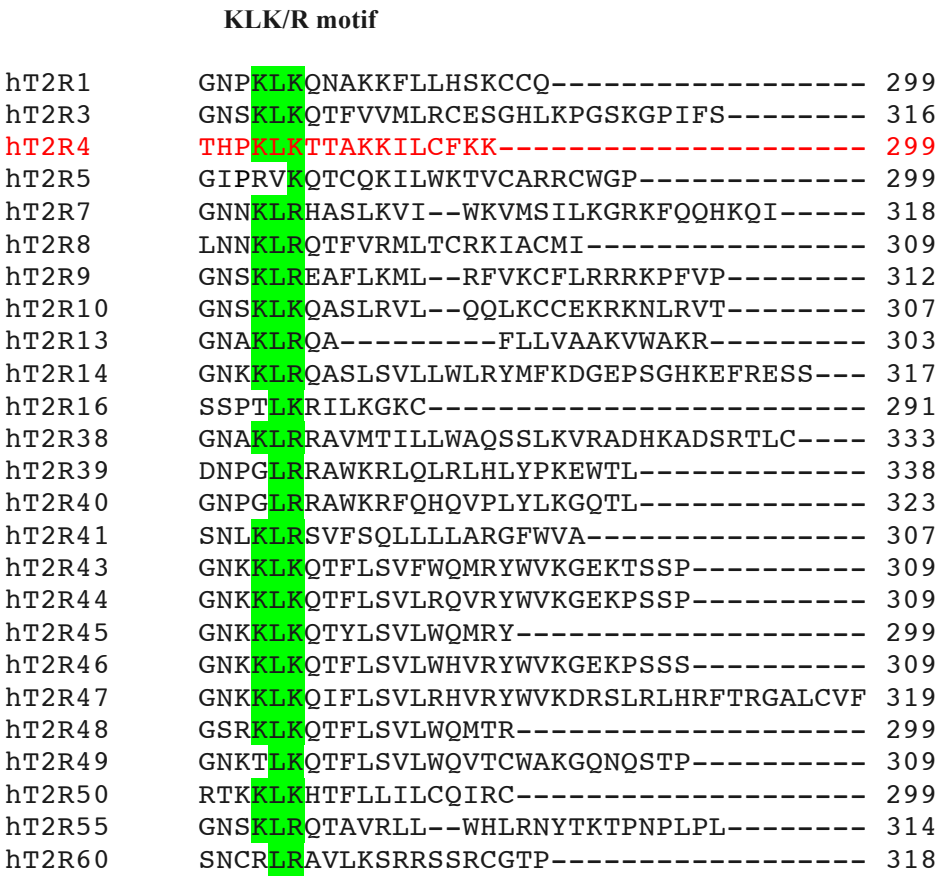

B.

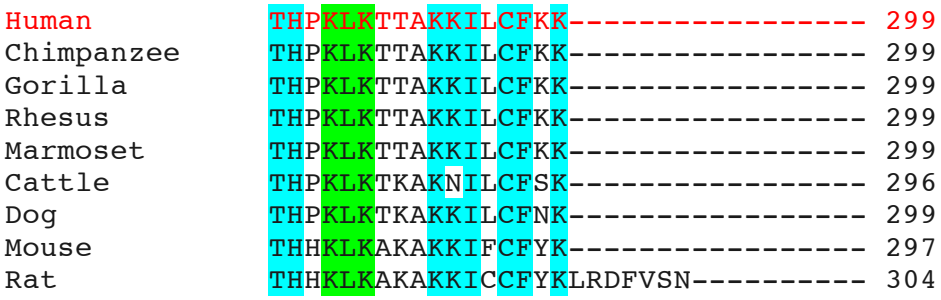

Figure 4.2.2. Multiple sequence alignment of C-terminus of T2Rs. A. Sequence alignment of the C-terminus of the 25 human T2Rs. T2R4 is shown in red, the conserved KLK/R motif is highlighted in green. **B.** Sequence alignment of C-terminus of T2R4 from different species. Human T2R4 is shown in red, the KLK motif is highlighted in green, and the highly conserved amino acids are in blue color. Sequence alignment was done using the ClustalW algorithm. These sequences do not include the FLAG-epitope at N-termini.

Studies have demonstrated the importance of C-terminal region of GPCRs for a variety of receptor functions, including cell surface expression, signaling pathways, dimerization, agonist-induced internalization, and desensitization. The role of the C-terminus of T2Rs in receptor function remains to be elucidated. Previously, using TM prediction algorithms a secondary structure for T2R4 was proposed (Pydi et al., 2012). T2R4 has a short C-terminus which consists of 17 amino acids, one of them being alanine (**Figure 4.2.1**). Six of these residues are lysines and one is histidine, indicating the polybasic nature of this cytoplasmic region. Human T2Rs have multiple basic residues in the C-terminus. The number of basic residues varies with length of the C-termini, ranging from 3 in T2R41 and T2R49 to 12 in T2R47 (**Figure 4.2.2A**). This indicates that these residues might have a role of functional importance in regulating receptor signaling, trafficking, ubiquitination or endosomal sorting. Thus, an alanine scan mutagenesis of all C-terminus residues (except Ala299) of T2R4 was performed, and the role of these mutations on cell surface expression and receptor function was characterized. The residues were mutated to an alanine, with the expectation that this substitution will have a minimal effect on receptor folding and ligand binding. In addition to the alanine mutations, conservative substitutions such as lysine to arginine, and leucine to valine for the residues of the KLK motif and for Leu303 which is conserved in 18 of the 25 T2Rs were made (**Figure 4.2.2A**). The KLK motif is highly conserved, while Leu303 is conserved in 7 of the 9 species analyzed or 78% conserved (**Figure 4.2.2B**).

Having the relatively conserved C-terminal MPBRs in GPCRs, it was investigated whether these MPBRs are also required for cell surface trafficking of T2Rs. For this, amino-terminal FLAG-tagged WT-T2R4 or the mutants were transiently expressed in HEK293T cells and cell surface expression, of the non-permeabilized cells, was measured by flow

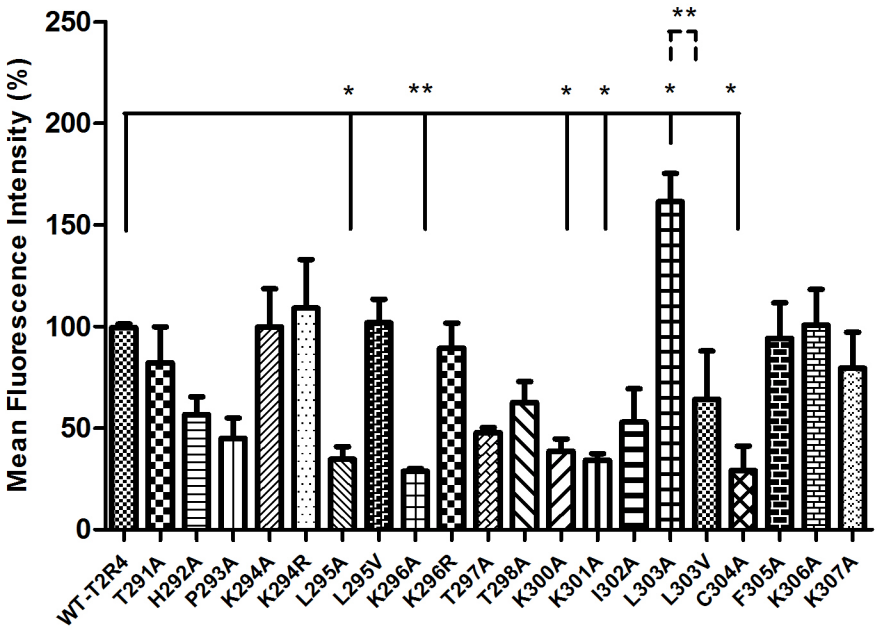

Figure 4.2.3. Cell surface expression of T2R4 and C-terminus mutants. Analysis of cell surface expression was performed by flow cytometry using the monoclonal mouse anti-FLAG antibody (1:500 dilution), which detects the FLAG-sequence at N-terminus of T2R4 and mutant receptors. The primary antibody was detected by goat anti-mouse Alexa 488 antibody (1:1000 dilution). The mean fluorescence intensities of mutants were normalized to that of WT-T2R4 and expressed in percentage. Some of the mutants showed statistically significant reduced surface expression, whereas, L303A showed significantly increased expression compared to wild type. Data is representative of 5-7 independent experiments. Significance was analyzed using one way ANOVA with *Dunnette's* post hoc test, *$p<0.05$ and **$p<0.01$.

cytometry. The data revealed that alanine mutations of many C-terminus residues resulted in reduced surface expression when compared to WT-T2R4 (**Figure 4.2.3**). Mutants L295A, K296A, K300A, K301A and C304A showed significantly reduced surface expression levels amounting to a reduction of 60%-70% (**Figure 4.2.3**). Of these residues, Leu295 and Lys296 form part of the conserved KLK motif, at positions 294 to 296, towards the amino end of the C-terminus in T2Rs. Lys294 in the KLK motif is the least conserved residue in this triplet at 76%, Leu295 is at 96% and Lys296 or Arg is 100% conserved among T2Rs. Leucine at position 295 is replaced by a valine in 4% or one T2R. The K294A mutant showed cell surface expression similar to WT-T2R4, indicating that Leu295 and Lys296 residues of this conserved motif are critical for proper targeting of T2R4 to the cell surface. These residues were further mutated to functionally similar valine or arginine to mimic the T2Rs that contain these residues at the indicated positions. Mutants K294R, L295V and K296R behaved similar to the wild type receptor in terms of cell surface expression (**Figure 4.2.3**). For other residues replaced with alanine, the cell surface expression was comparable to that of WT-T2R4 as no statistically significant results were obtained. In contrast, Leu303, which is conserved in 18 T2Rs (72%), after substitution with alanine showed an increase of 61 ± 14% in surface expression (**Figure 4.2.3**). Interestingly the conservative substitution, L303V, displayed expression comparable to WT-T2R4. The surface expression was significantly different between the two mutants with $^{**}p<0.01$.

4.2.3 Functional characterization

After assessing the involvement of C-terminus in optimizing the cell surface expression of T2R4, it was next examined whether these residues have a role in stimulating

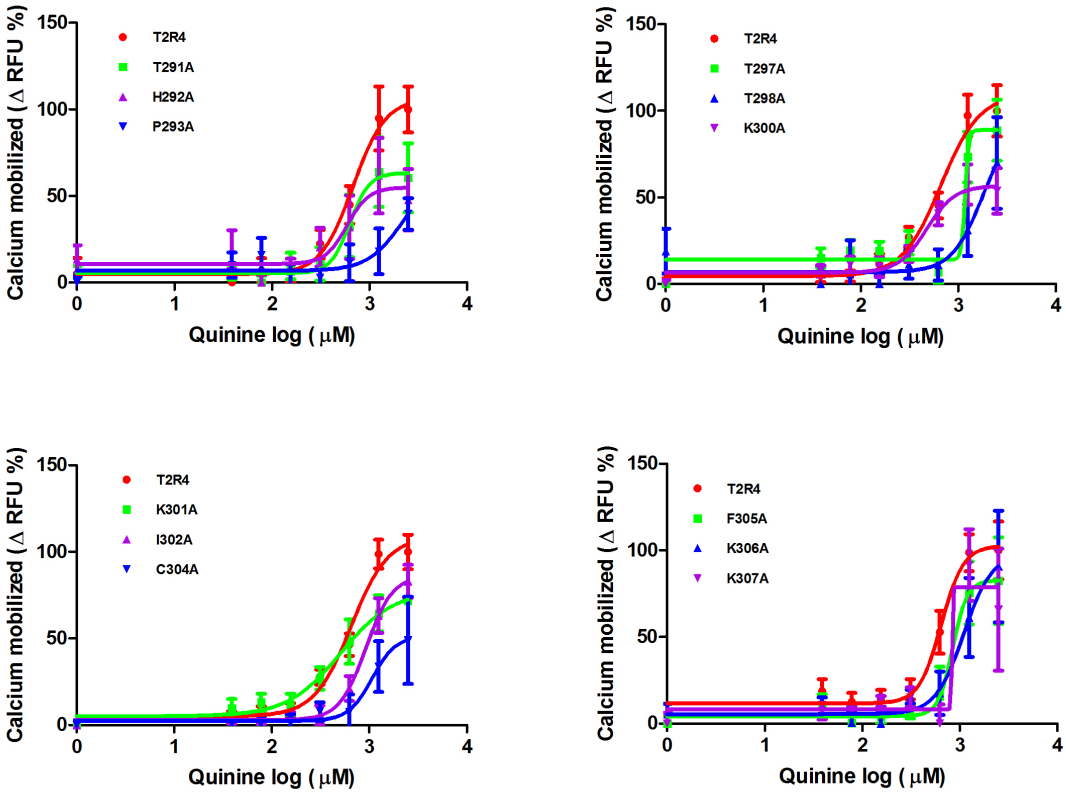

Figure 4.2.4. Functional characterization of T2R4 C-terminus mutants. Concentration-dependent changes in intracellular calcium $[Ca^{2+}]_i$ induced by the bitter compound quinine in HEK293T cells co-transfected with Gα16/gust44 and T2R4 or mutants. Data is representative of 3-4 independent experiments performed in triplicates. After subtracting the responses of quinine-induced mock-transfected cells, dose-response curves were generated and EC_{50} values were calculated by non-linear regression analysis using Graph Pad Prism software. RFU, relative fluorescence units.

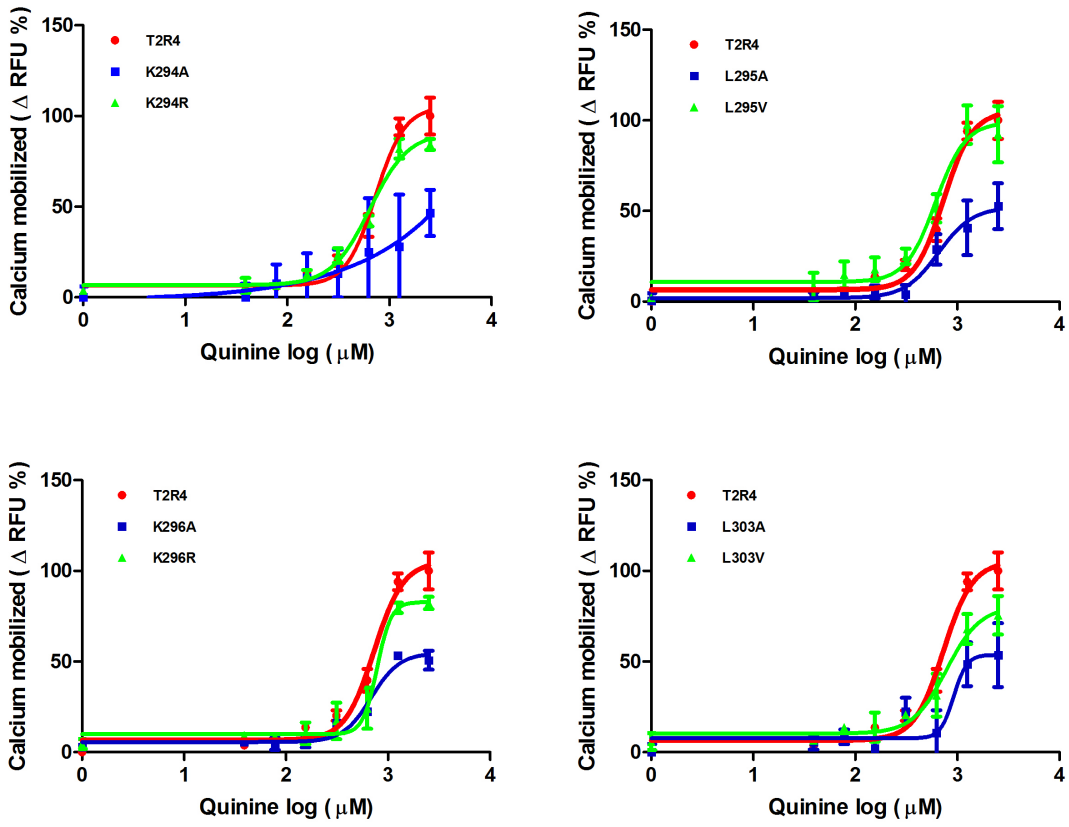

Figure 4.2.5. Functional characterization of T2R4 C-terminus mutants of the KLK motif. Concentration-dependent relationship of quinine-mediated changes in $[Ca^{2+}]_i$ in HEK293T cells co-transfected with Gα16/gust44 and WT-T2R4 or mutants of KLK/R motif and Leu303. Data is representative of 3-4 independent experiments performed in triplicates. After subtracting the responses of quinine-induced mock-transfected cells, dose-response curves were generated and EC_{50} values were calculated by non-linear regression analysis using Graph Pad Prism software. RFU, relative fluorescence units.

Table 4.2.1. Pharmacological characterization of WT-T2R4 and C-terminus mutants. Functional characterization was performed by measuring changes in intracellular calcium after application of different concentrations of quinine. Cell surface expression was determined by flow cytometry.

Receptor	EC_{50} (μM)	Emax (%)	Cell surface expression (%)
WT-T2R4	715 ± 264	100 ± 14	100 ± 2
T291A	647 ± 141	61 ± 20	82 ± 17
H292A	758 ± 477	48 ± 17**	56 ± 8
P293A	NS	42 ± 9**	45 ± 10
K294A	2132 ± 700**	53 ± 17*	100 ± 20
K294R	693 ± 249	84 ± 3	109 ± 19
L295A	712 ± 277	52 ± 12*	30 ± 6*
L295V	680 ± 304	92 ± 15	102 ± 10
K296A	776 ± 341	50 ± 5**	29 ± 1**
K296R	817 ± 245	82 ± 3	89 ± 11
T297A	NS	89 ± 17	48 ± 2
T298A	NS	60 ± 26	63 ± 10
K300A	513 ± 195	54 ± 13*	39 ± 6*
K301A	591 ± 299	69 ± 2	34 ± 4*
I302A	935 ± 102	82 ± 4	53 ± 16
L303A	1281 ± 891	53 ± 4*	161 ± 14*
L303V	853 ± 343	75 ± 10	52 ± 21
C304A	1209 ± 100	50 ± 14**	29 ± 10*
F305A	874 ± 212	82 ± 25	94 ± 17
K306A	1194 ± 454	91 ± 32	101 ± 18
K307A	NS	65 ± 30	80 ± 17

The data represents the mean ± SEM of 3-5 independent experiments performed in triplicates. NS – not saturated, concentration-dependent increase in calcium not observed with quinine, E_{max} – the maximum possible effect of quinine. Significance was checked with one-way ANOVA using *Dunnett's* post hoc test, with *$p<0.05$, **$p<0.01$.

calcium mobilization and receptor function. HEK293T cells transiently transfected with WT-T2R4 or the mutants were stimulated with the agonist quinine, and calcium mobilization was measured as reported previously (Meyerhof et al., 2010; Pydi et al., 2012). All mutants displayed varied levels of calcium mobilization upon quinine stimulation (**Figure 4.2.4 and 4.2.5**). Alanine mutations of Lys294, Leu295 and Lys296 residues of the KLK motif showed a reduction in maximal Ca^{2+} responses (E_{max}, 53 ± 17%, 52 ± 12% and 50 ± 5% respectively, (**Figure 4.2.5 and Table 4.2.1**). Interestingly, the EC_{50} of quinine for K294A increased almost 3-fold in comparison to the WT-T2R4 (**Figure 4.2.5, Table 4.2.1**). There was not a remarkable change in the EC_{50} values of L295A and K296A compared to WT-T2R4, despite their reduced E_{max} values. In contrast, the conservative substitution mutants, K294R, L295V and K296R, displayed E_{max} and EC_{50} values similar to WT-T2R4. **Figure 4.2.6** shows representative calcium traces for select mutants and mock-transfected cells stimulated with a saturating concentration of 2.5 mM quinine or with buffer (control). The calcium signal of mutants P293A, T297A, T298A and K307A did not saturate even at the highest concentration of quinine (2.5 mM). A right-shift was observed in the dose-response curves of T297A and T298A, but despite of low surface expression, the E_{max} of T297A was similar to the WT-T2R4. The EC_{50} values of the K300A and K301A were within normal range and the reduced E_{max} corresponded well with their reduced surface expression. There was a right-shift in the dose-response curves of I302A, L303A, C304A, F305A, K306A and K307A with increased EC_{50} values. L303A, showed a 45% reduction in E_{max} despite of an increase in surface expression (**Figure 4.2.3, Figure 4.2.5, Table 4.2.1**). However, the L303V phenotype behaved similar to WT-T2R4. C304A showed reduced maximal calcium responses and a marginal increase in EC_{50}, which corresponded with its reduced surface

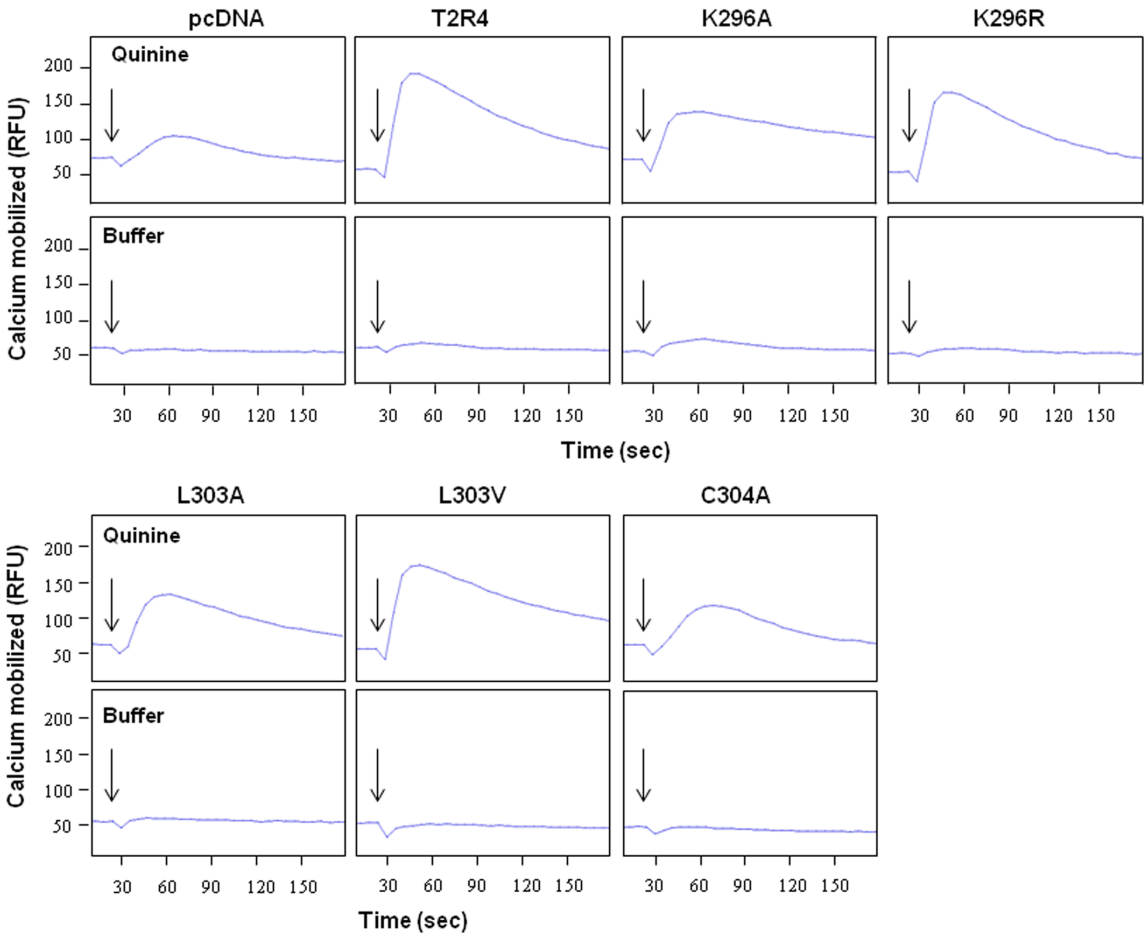

Figure 4.2.6. Representative calcium traces of T2R4 and select mutants transfected in HEK293T cells and induced with 2.5 mM quinine or buffer. The upper panel in each row represents calcium traces of transfected cells stimulated with 2.5 mM quinine, whereas, lower panel in each row shows calcium response of cells exposed to assay buffer. Quinine was added to the cells by the automated microplate reader at time point of 20 sec, which is denoted by arrows. The calcium mobilized, which was represented as relative fluorescence units (RFU), was detected by the calcium-sensitive Fluo-4 NW dye after application of a saturating concentration of quinine or buffer and measured by the Flex Station III microplate reader.

expression.

4.2.4 Characterization of basal signaling

Recently, several CAMs in T2R4 were characterized by our lab (Pydi et al., 2012; Pydi et al., 2014a). Constitutive activity locks a receptor in an active conformation and allows it to signal even in the absence of an agonist (Cerione et al., 1984; Costa and Herz, 1989). This activity, which has been observed for more than 60 GPCRs, is known to have important pathophysiological roles in human disease (Seifert & Wenzel-Seifert, 2002). To characterize the agonist-independent (or basal) signaling of the C-terminal mutants, changes in intracellular calcium with assay buffer alone (basal activity) were measured. This response was then normalized to receptor cell surface expression. Of the 20 mutants analyzed, K296A and C304A displayed more than 2-fold increase over WT-T2R4 basal activity (**Figure 4.2.7**).

Next, to assess the constitutive activity of K296A and C304A in detail, the effect of receptor density on basal calcium mobilization was analyzed (**Figure 4.2.8**). HEK293T cells were transiently transfected with increasing amounts of WT-T2R4 or mutant DNA (2 µg, 4 µg and 6 µg DNA per 10^6 cells). The rationale was that an increase in DNA concentration would increase the surface expression of receptors and as a result their activity. This method of identifying CAMs has been validated in our previous publications (Chakraborty et al., 2014; Pydi et al., 2014a). The effect of receptor density on Ca^{2+} mobilization was calculated from slope of expression vs. basal activity of K296A and C304A, which was compared to that of WT-T2R4. The slope of WT-T2R4 was 0.17 ± 0.01, whereas, that of K296A and C304A was 0.86 ± 0.03 and 0.25 ± 0.07 respectively (**Figure 4.2.8**). This data shows that K296A exhibits true constitutive activity, which is five-fold higher than that of WT-T2R4.

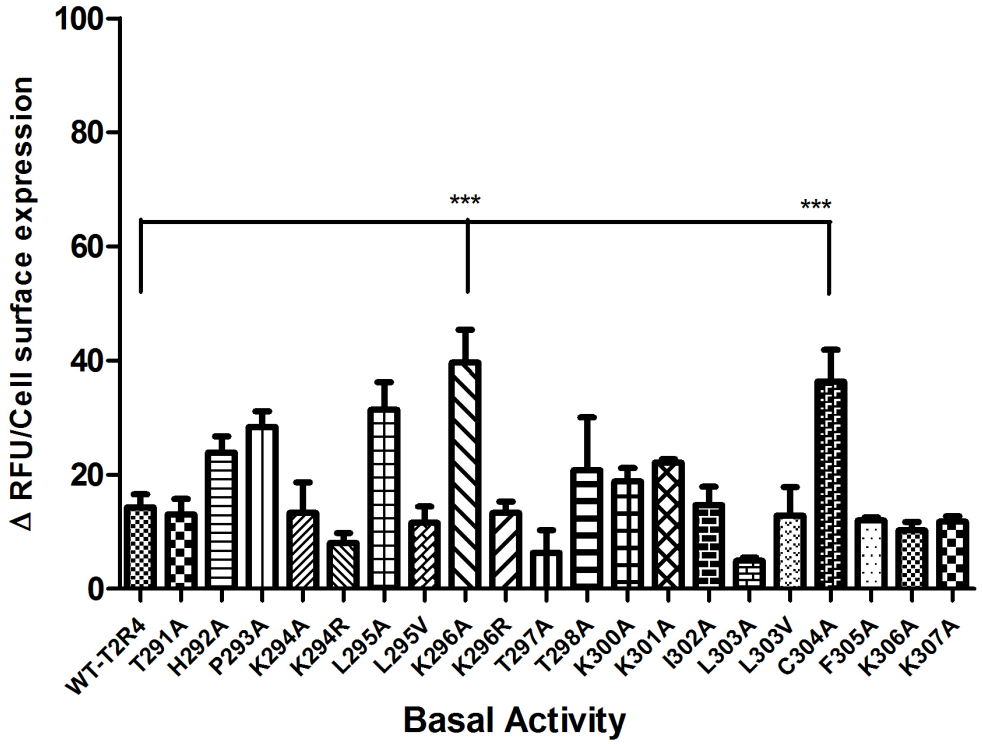

Figure 4.2.7. Pharmacological characterization of the basal activity of WT-T2R4 and C-terminus mutants. Shown is the receptor activity after stimulation with assay buffer alone to assess the agonist-independent or basal activity. Changes in calcium mobilized, represented by ΔRFU, were normalized to their cell surface expression as analyzed by flow cytometry. Significance was determined using one way ANOVA with *Dunnette's* post hoc test, *p<0.05, **p<0.01, ***p<0.001. Mutants K296A and C304A showed increased basal activity in comparison to wild type receptor. Data is representative of 3-4 independent experiments.

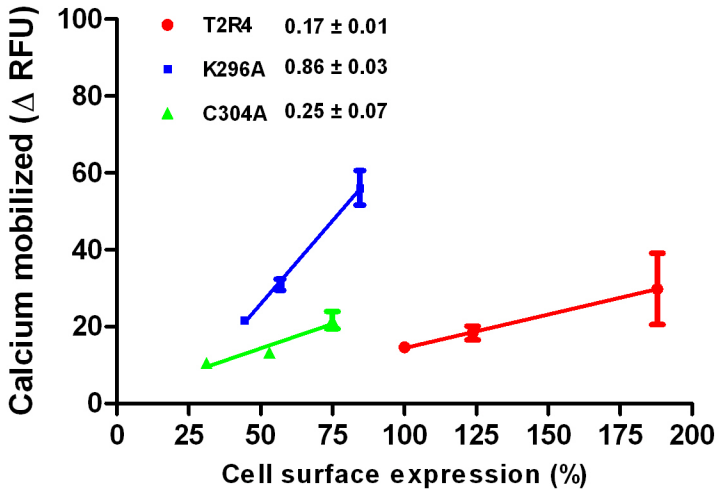

Figure 4.2.8. Effect of receptor density on basal calcium mobilization. WT-T2R4 (red line), K296A (blue line) and C304A (green line) constructs were transiently expressed in HEK293T cells at different receptor densities by varying amounts of DNA used in each transfection (2 µg, 4 µg, and 6 µg DNA per 10^6 cells). Receptor expression levels were determined by flow cytometry and normalized to WT-T2R4 transfected with 2 µg DNA per 10^6 cells, which was taken as 100%. The slope of WT-T2R4, which was calculated by linear regression analysis, was 0.17 ± 0.01, whereas that of K296A and C304A was 0.86 ± 0.03 and 0.25 ± 0.07, respectively. This shows that K296A displays five-fold increase over basal WT-T2R4 activity.

4.3 Quinine mediates desensitization but not internalization of human bitter taste receptor T2R4

Jasbir D. Upadhyaya, Raja Chakraborty, Rajinder P. Bhullar, Prashen Chelikani

4.3.1 Desensitization mechanism of T2Rs

It is now clear that bitter taste signaling is not limited to taste buds, and T2Rs are expressed in many extraoral tissues (Clark et al., 2012). They mediate protective reflexes by performing different physiological roles, including bronchodilation, in extraoral tissues and are implicated as potential therapeutic drug targets in the treatment of asthma (Deshpande et al., 2010; Zhang et al., 2013). Thus, it becomes important to understand how T2R signaling is regulated. GPCRs regulate the strength and duration of signal transduction to adapt to changing external conditions and to avoid damage from sustained signaling. The earliest event in GPCR desensitization is receptor phosphorylation (Pitcher et al., 1998). Two families of kinases are currently known to contribute to the desensitization of GPCRs; second messenger-dependent protein kinase A (PKA) or protein kinase C (PKC), and GPCR-specific G protein-coupled receptor kinases (GRKs) (Lefkowitz et al., 1998).

There is very limited information about the desensitization mechanisms of T2Rs and the regulatory proteins involved in the process are poorly defined. A recent study showed that like most GPCRs, endogenous T2Rs in human airway smooth muscle (ASM), undergo rapid homologous desensitization upon exposure to quinine and proposed the involvement of GRKs in the process (Robinett et al., 2011). Previously a hypothesis proposed that amphipathic tastants, like quinine, can enter the cell and interact with GRKs and delay signal termination, explaining their lingering after-taste (Zubare-Samuelov et al., 2005). The GRK family consists of seven different genes. Of the seven known GRKs, four GRKs (GRK2, GRK3, GRK5 and GRK6) are ubiquitously expressed in mammalian tissues (Reiter and Lefkowitz, 2006).

This study was designed to characterize the desensitization and internalization of T2R4 upon agonist-stimulation. Recently, extensive structure-function studies, including mapping of the agonist quinine-binding pocket on T2R4 (Pydi et al., 2012; Pydi et al., 2014a; Pydi et al., 2014b) were pursued by our lab. Thus, the well-characterized bitter taste receptor, T2R4 was selected for this study. Using quinine, the desensitization of T2R4 transiently-expressed in HEK293T cells was examined. Quinine is an alkaloid isolated from the bark of cinchona tree and is the most intense bitter tasting compound. To assess the potential role of GRKs in T2R4 desensitization, changes in quinine-induced functional response of T2R4 were measured by knocking down endogenous GRKs 2, 3, 5 and 6. To monitor the potential non-specific (or heterologous) forms of desensitization, the calcium responses of mock-transfected cells were subtracted from the receptor-specific responses. The observed functional responses of T2R4 in GRK knockdown cells, thus, represented a homologous form of receptor desensitization. The role of protein kinase C (PKC) in quinine-mediated T2R4 desensitization was explored by using phorbol 12-myristate-13- acetate (PMA) and Bisindolylameide 1 (Bis1), PKC activator and inhibitor respectively. Studies involving quinine-specific responses have reported no evidence for the involvement of a PKA-mediated desensitization mechanism (Robinett et al., 2011; Zubare-Samuelov et al., 2005). Thus, the role of PKA in quinine-induced T2R4 desensitization was not investigated. To analyze agonist-induced receptor internalization, cell surface expression of T2R4, upon exposure to different bitter compounds, was examined. Surprisingly, quinine caused upregulation of T2R4 surface expression which was both receptor and agonist-specific. Results from this study suggest that T2R desensitization primarily involves GRKs 3 and 6.

Interestingly, unlike most other GPCRs, T2R4 does not undergo internalization upon agonist treatment, and quinine acts as a pharmacological chaperone for T2R4.

4.3.2 nCounter® analysis of mRNA expression of TAS2Rs and other genes in HEK293T cells and hASMCs

The electropherogram summary of the quality of RNA used for the nCounter® analysis of select endogenous genes in HEK293T and hASMCs is shown in **Figure 4.3.1**. The RNA integrity number (RIN) depicts the quality of the isolated RNA, whereas, the 28S/18S ratios represent the presence of intact RNA. A ratio of 2.0 is considered a benchmark for 28S/18S which indicates the presence of intact RNA. The ratios of 1.5 and 1.2 for hASMCs and HEK293T cells respectively and the discrete bands of 28S and 18S rRNA at the indicated sizes shown by the bioanalyzer scan indicate that the samples have intact RNA **(Figure 4.3.1)**. The RIN values for hASMCs and HEK293T cells were 6.3 and 4.7 respectively, depicting that the total RNA used for the bioanalyzer scan was intact and of good quality.

The absolute mRNA expression levels of select endogenous genes in hASMCs and HEK293T cells are shown in **Figure 4.3.2.** The mRNA expression of house-keeping gene GAPDH is similar in both cell types. In contrast, expression of β-actin is ~ 4-fold higher in ASMCs than in HEK cells, which is in agreement with the contractile function of smooth muscle cells **(Figure 4.3.2A)**. In HEK cells, expression of GRK6 is the highest followed by GRKs 2, 3, 5 and 4. Whereas, GRK5 is the predominant GRK in ASMCs followed by GRKs 2, 6 and 3 **(Figure 4.3.2B)**. Heterotrimeric G-proteins are important downstream effectors

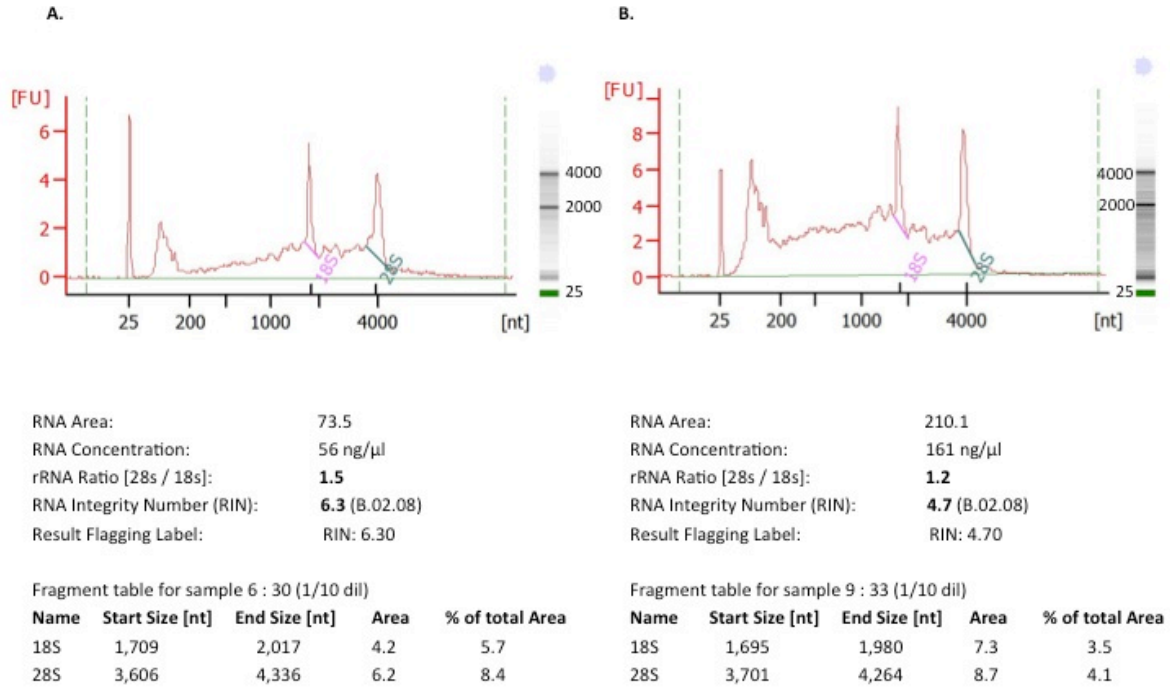

Fragment table for sample 6 : 30 (1/10 dil)

Name	Start Size [nt]	End Size [nt]	Area	% of total Area
18S	1,709	2,017	4.2	5.7
28S	3,606	4,336	6.2	8.4

Fragment table for sample 9 : 33 (1/10 dil)

Name	Start Size [nt]	End Size [nt]	Area	% of total Area
18S	1,695	1,980	7.3	3.5
28S	3,701	4,264	8.7	4.1

Figure 4.3.1. Electropherogram summary of total RNA of hASMCs and HEK293T cells. Bioanalyzer scan and agarose gel for the total RNA extracted from **A.** hASMCs and **B.** HEK293T cells. The 28S/18S ratios represent the presence of intact RNA. The RNA integrity number (RIN) indicates the good quality of RNA with no degradation.

which predominantly couple to GPCRs and initiate receptor signaling (Oldham and Hamm, 2008). Gα-subunits are categorized into four subfamilies, Gαs, Gαi, Gαq and Gα12 (Aittaleb et al., 2010). The expression of α-subunit of G-proteins GNA12, GNAI, GNAQ, GNAS, GNAT3 was analyzed. GNAT3 is an α-subunit of the heterotrimeric protein gustducin which is responsible for mediating taste perception. Gustducin is predominantly expressed in the taste tissue (Spielman, 1998). The most abundant Gα-protein in both ASMCs and HEK293T cells is GNAS, whereas, expression of other G-proteins was significantly lower in these cells **(Figure 4.3.2C)**. The expression of endogenous TAS2Rs was also assessed in both cells types. Similar pattern of T2R expression was observed in both cell types **(Figure 4.3.2D)**. Few T2Rs like TAS2R43-47, TAS2R50, TAS2R14, TAS2R19, TAS2R20, TAS2R3, TAS2R4 were expressed at higher levels than other TAS2Rs. However, the expression of TAS2Rs in HEK293T cells was much higher than in hASMCs **(Figure 4.3.2D)**.

4.3.3 Desensitization of T2R4

GPCRs that undergo desensitization display reduced responsiveness to a second stimulation with the same agonist (Tomhave et al., 1994). To examine T2R4 desensitization, T2R4 expressing HEK293T cells were pretreated with the agonist quinine for 15 min, after which they were washed with calcium-free assay buffer before re-exposure to the same concentration (1 mM) of quinine. Changes in intracellular calcium were measured for the next 3 min. Quinine pretreatment led to a decrease in subsequent quinine-mediated calcium responses to 35 ± 5% (equivalent to 60% ± 5.2% desensitization) compared to the control or untreated cells (**Figure 4.3.4A and 4.3.4C**).

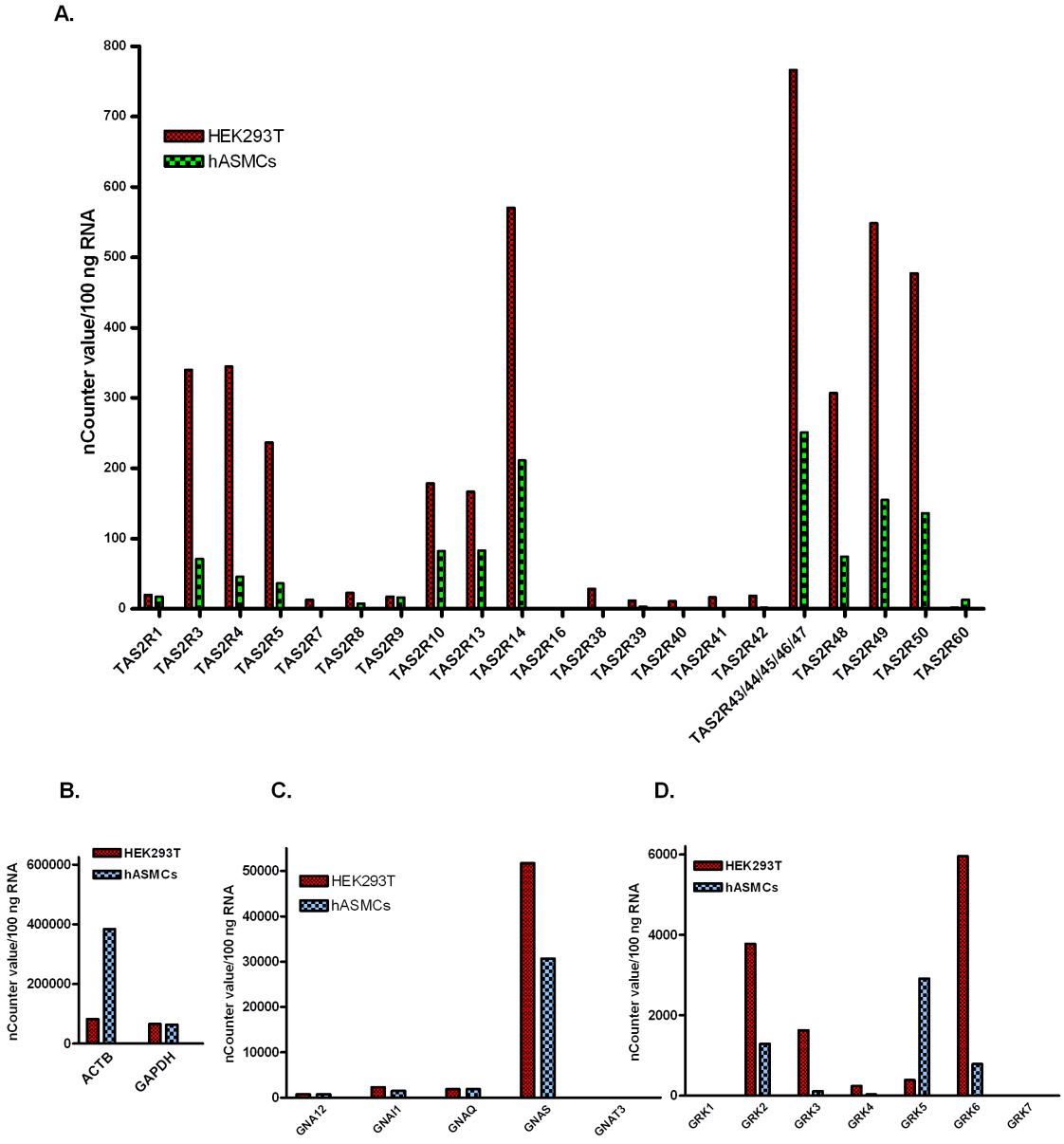

Figure 4.3.2. Nanostring analysis of mRNA expression of few endogenous genes in HEK293T cells and hASMCs. A. mRNA expression of the 25 T2Rs in HEK293T cells and hASMCs. **B.** mRNA expression of house-keeping genes β-actin (ACTB) and GAPDH in HEK293T cells and hASMCs. **C.** mRNA expression of G-proteins. **D.** mRNA expression of GRKs in HEK293T cells and hASMCs. The total RNA was extracted using RNeasy mini kit (Qiagen). The nCounter analysis was performed using 100 ng of total RNA. One count of the nCounter value can be interpreted as one mRNA transcript in 100 ng of total RNA from hASMCs and HEK293T cells.

Quinine induced desensitization of endogenous T2Rs was examined in human ASMCs previously (Robinett et al., 2011), so this was used as an external control in our study. In our experimental conditions, quinine pretreatment of ASMCs resulted in reduction of calcium response to 55% of the control (equivalent to 45% ± 2.8% desensitization of T2Rs, **Figure 4.3.4B and 4.3.4C**).

Additional studies for T2R4 desensitization were performed by using another T2R4 agonist, yohimbine (Meyerhof et al., 2010). Cross-compound desensitization was checked and it was noticed that quinine pretreatment evoked desensitization of the subsequent yohimbine induced calcium responses amounting to 17 ± 3% (**Figure 4.3.5A and 4.3.5C**). However, T2R4-expressing cells pretreated with yohimbine and subsequently exposed to quinine displayed calcium responses amounting to 65 ± 7 % (**Figure 4.3.5A and 4.3.5C**). Pretreatment with 1 mM yohimbine evoked only a marginal desensitization of the subsequent yohimbine-induced calcium responses (**Figure 4.3.5B and 4.3.5C**).

4.3.4 Role of endogenous GRKs in T2R4 desensitization

Having demonstrated that T2R4 gets desensitized in response to quinine, the role of GRKs in the regulation of T2R4 signaling was determined. Therefore, shRNAs were used to stably KD the expression of four ubiquitously expressed endogenous GRKs in HEK293T cells. GRK 2, 3, 5 and GRK6 specific shRNA expressing HEK293T cells were analyzed for their KD by quantitative-PCR and immunoblot (**Figure 4.3.6**). GRK2-KD and GRK3-KD cells displayed a reduction of 40% and 70% respectively in their mRNA levels compared to the scrambled shRNA control (**Figure 4.3.6A and 4.3.6B**). However, mRNA levels of GRK5 and GRK6 were reduced by 80% each in comparison to the scrambled shRNA control cells

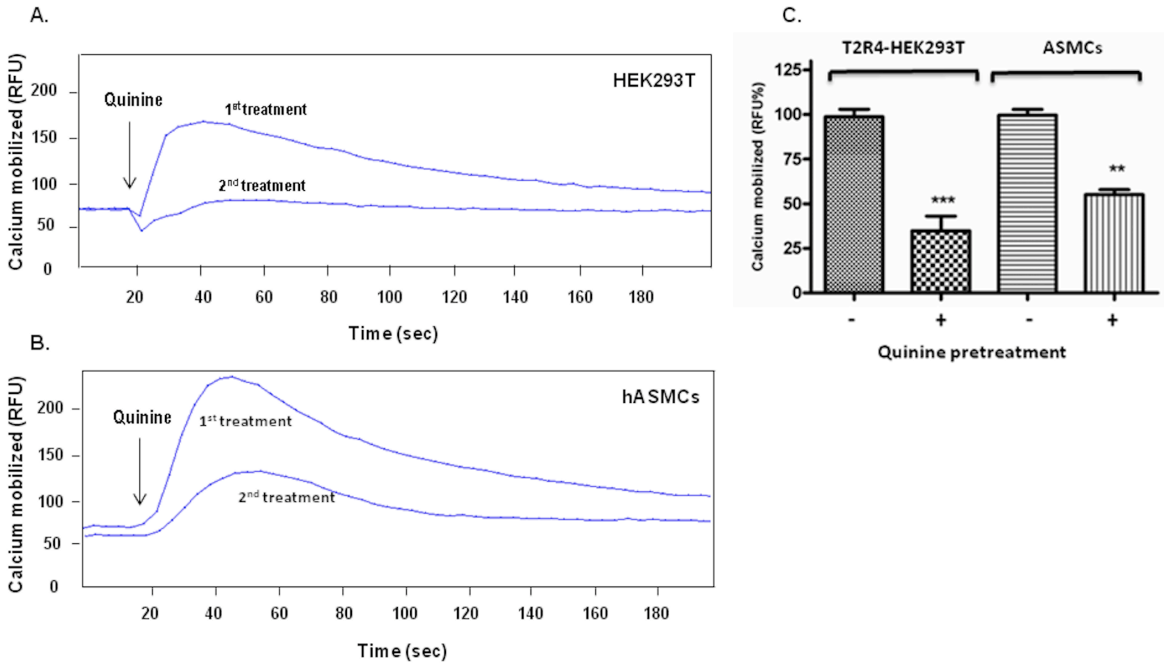

Figure 4.3.3. Quinine induced desensitization of T2Rs. Representative calcium traces showing desensitization of the quinine response to quinine pretreatment in HEK293T cells and hASMCs. **[A]**. Fluo-4 NW loaded T2R4 expressing HEK293T cells were pretreated with 1 mM quinine for 15 min, washed with calcium-free assay buffer and re-exposed to 1 mM quinine. The intracellular calcium mobilized was measured in terms of relative fluorescence units (RFU) at 525 nm following excitation at 494 nm, using a FlexStation 3 fluorescence microplate reader. **[B]**. Human ASM cells pretreated with quinine for 15 min, washed with calcium-free assay buffer and re-exposed to quinine were used as control. Cells pretreated with calcium-free assay buffer and then exposed to quinine represent first treatment. Cells pretreated with quinine and re-exposed to same concentration of quinine represent second treatment. **[C]**. Bar plot representation of the calcium responses in T2R4-HEK293T cells and hASMCs in response to quinine treatments. The results are represented with the calcium mobilized in untreated cells taken as 100%. Results are from a minimum of three independent experiments. Statistical significance was determined by student *t*-test.

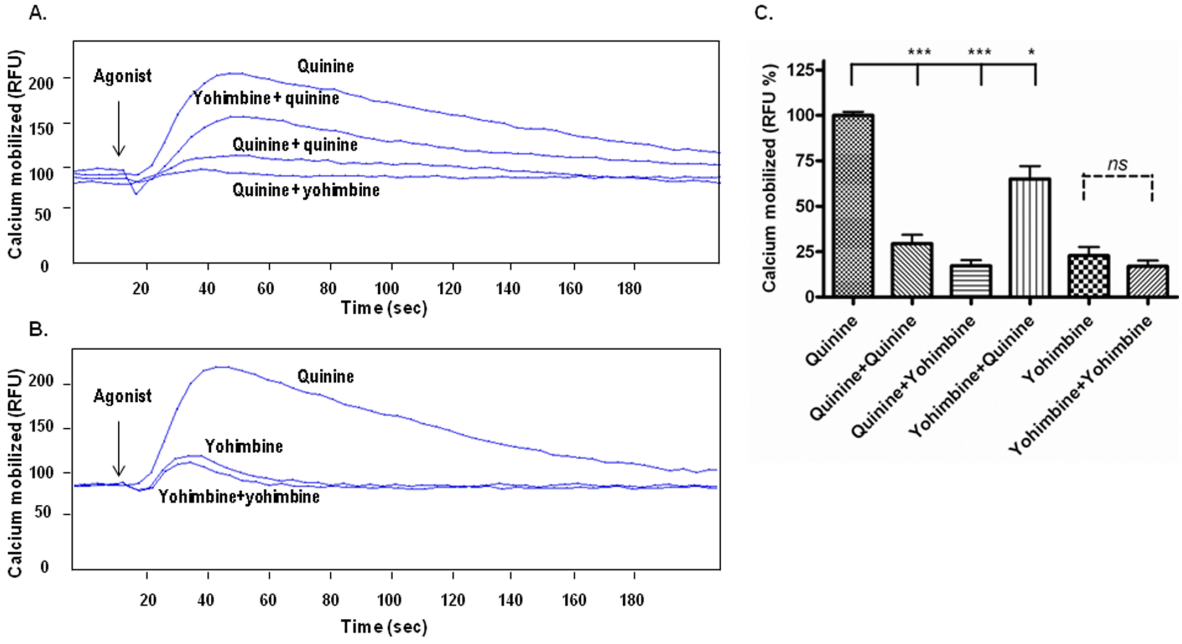

Figure 4.3.4. Agonist promoted desensitization of T2R4 expressed in HEK293T cells. **[A]**. Representative calcium traces of T2R4-expressing HEK293T cells pretreated with calcium-free assay buffer, quinine or yohimbine. **[B]**. Representative calcium traces of T2R4-expressing HEK293T cells pretreated with calcium-free assay buffer or yohimbine. Fluo-4 NW loaded cells were pretreated with buffer alone or 1 mM each of quinine or yohimbine for 15 min, washed with calcium-free assay buffer, and exposed to same concentrations of the agonist by the Flexstation 3 microplate reader. Changes in intracellular calcium were measured in terms of relative fluorescence units (RFU) at 525 nm following excitation at 494 nm. The arrow at 20 sec indicates the addition of agonist by Flexstation 3 microplate reader. **[C]**. Bar plot representation of the measured intracellular calcium. Buffer pretreated T2R4-expressing cells stimulated with quinine were represented as 100%, and calcium responses of other treatments were normalized to it. Data is representative of four independent experiments and expressed as mean ± SEM. Significance was checked by one-way ANOVA using *Dunnette's* post hoc test, *$p<0.05$, ***$p<0.001$.

(**Figure 4.3.6C and 4.3.6D**). Immunoblot analysis using GRK2, GRK3, GRK5 and GRK6 specific antibodies confirmed KD of the respective GRKs in HEK293T cells (**Figure 4.3.6E**).

GPCRs usually respond to agonist with an initial or transient Ca^{2+} spike, which decreases rapidly and reaches baseline. In contrast, phosphorylation-deficient receptors respond to agonist with a similar or an increased Ca^{2+} spike, which is followed by a sustained response that remains elevated for an extended period of time (Tomhave et al., 1994). T2R4 was expressed in GRK2, -3, -5 and -6 KD cells and after application of quinine, the effect of the KDs on T2R4 desensitization was determined by Ca^{2+} mobilization assay. The results revealed that Ca^{2+} mobilization in cells stimulated with quinine was more pronounced in GRK3-KD and GRK6-KD cells than in GRK2-KD or GRK5-KD cells, as compared to the scrambled control (**Figure 4.3.7A and 4.3.7B**). Quinine caused an increase in both the transient (peak) and sustained Ca^{2+} phases of GRK3-KD and GRK6-KD T2R4 expressing cells (**Figure 4.3.7A**). By contrast, GRK2-KD and GRK5-KD cells did not show any significant change in quinine-induced calcium response in comparison to the control cells (**Figure 4.3.7A and 4.3.7B**). To rule out the possibility that GRK2 and GRK5 could modulate calcium response to quinine at lower concentrations, T2R4-expressing GRK2-KD and GRK5-KD cells were stimulated with concentrations of quinine ranging from 500 μM to 60 μM (data not shown). No effect on quinine-induced calcium even at low quinine concentrations was observed in these cells.

To further test the effects of GRKs on T2R4 desensitization, T2R4-expressing scrambled shRNA control or GRK-KD HEK293T cells were exposed to quinine for 15 min and washed before re-exposure to the same concentration of quinine by the microplate

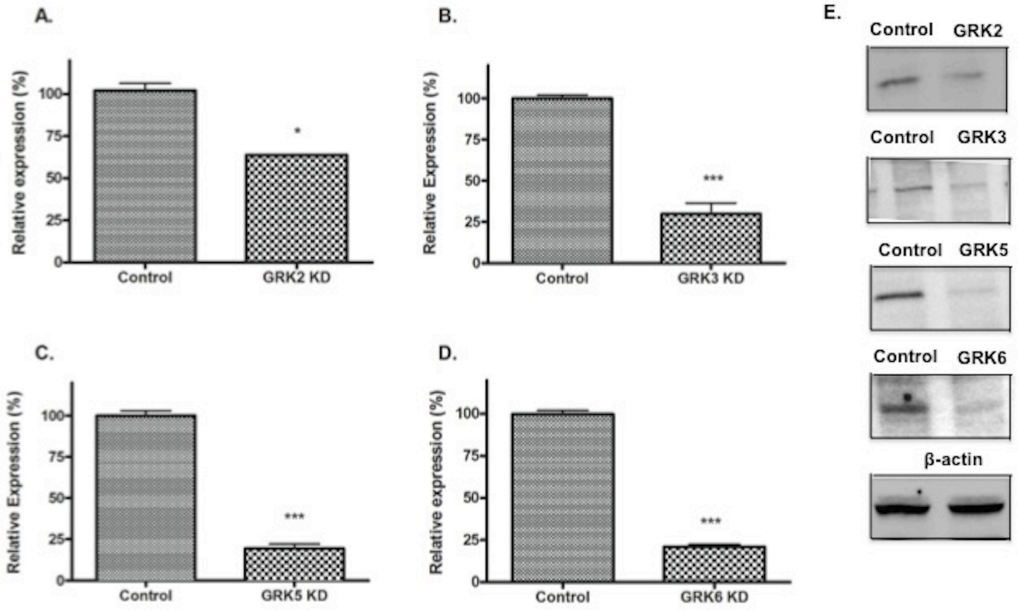

Figure 4.3.5. Stable knockdown of GRK2, GRK3, GRK5 and GRK6 in HEK293T cells. [A-D]. HEK293T cells were stably transfected with scrambled shRNA control or shRNA targeted against GRK2, GRK3, GRK5 and GRK6. After 2-3 weeks of antibiotic selection, the cells were analyzed for GRK KD. Quantitative PCR was performed to assess the GRK2, GRK3, GRK5, GRK6 mRNA levels in scrambled shRNA control and GRK knockdown cells. Relative expressions of the GRKs were normalized to GAPDH expression. Data represent mean ± SEM from three independent experiments done in triplicates. Relative expressions were computed using $2^{-\Delta Ct}$ method. Statistical significance was determined by unpaired two-tailed student's *t*-test, *p<0.05, ***p<0.001. **[E]**. Representative immunoblots of GRK-KD in HEK293T cells. Control represents HEK293T cells stably transfected with scrambled shRNA for the respective GRKs.

reader. Control cells displayed a reduction of ~ 65 ± 5 % in calcium response upon re-exposure to quinine (**Figure 4.3.8A**). By contrast, GRK3-KD and GRK6-KD cells showed calcium responses amounting to 50 ± 5% and 68 ± 4 % respectively after second exposure of quinine (**Figure 4.3.8A and 4.3.8B**). However, calcium response to quinine in GRK2-KD and GRK5-KD cells was very similar to that seen in control cells (**Figure 4.3.8A and 4.3.8B**). These data suggest that GRK3 and GRK6 participate in desensitization of T2R4 in HEK293T cells.

4.3.5 Role of PKC in T2R4 desensitization

To test the hypothesis that the canonical bitter taste signaling cascade (T2R-gustducin-PLCβ-IP_3R-Ca^{2+}) might cause activation of second messenger-dependent PKC, the involvement of PKC in T2R4 desensitization was analyzed. To assess the role of PKC, T2R4 expressing HEK293T cells were pretreated with the PKC activator, PMA, or inhibitor, Bis1. Pre-treatment of T2R4-expressing HEK293T cells with 0.1 μM PMA for 15 min resulted in a 40% reduction in Ca^{2+} responses compared to the control based on E_{max} value, i.e., 5 mM quinine (**Figure 4.3.9A and 4.3.9B**). Interestingly, addition of PKC inhibitor, Bis1, led to increased levels of intracellular Ca^{2+} release with an E_{max} of 130% compared to 100% for the control (**Figure 4.3.9A and 4.3.9B**). In this case, the E_{max} values clearly indicate a significant decrease or increase in the amount of Ca^{2+} mobilized upon PKC activation or inhibition respectively. PMA pretreatment was able to significantly reduce the quinine-mediated calcium responses even at lower concentrations of quinine (**Figure 4.3.9B**). A clear rightward shift on PKC activation was also observed. The effect of PKC activation and inhibition on T2R4 desensitization was also determined. PMA and Bis1 pretreatments did not

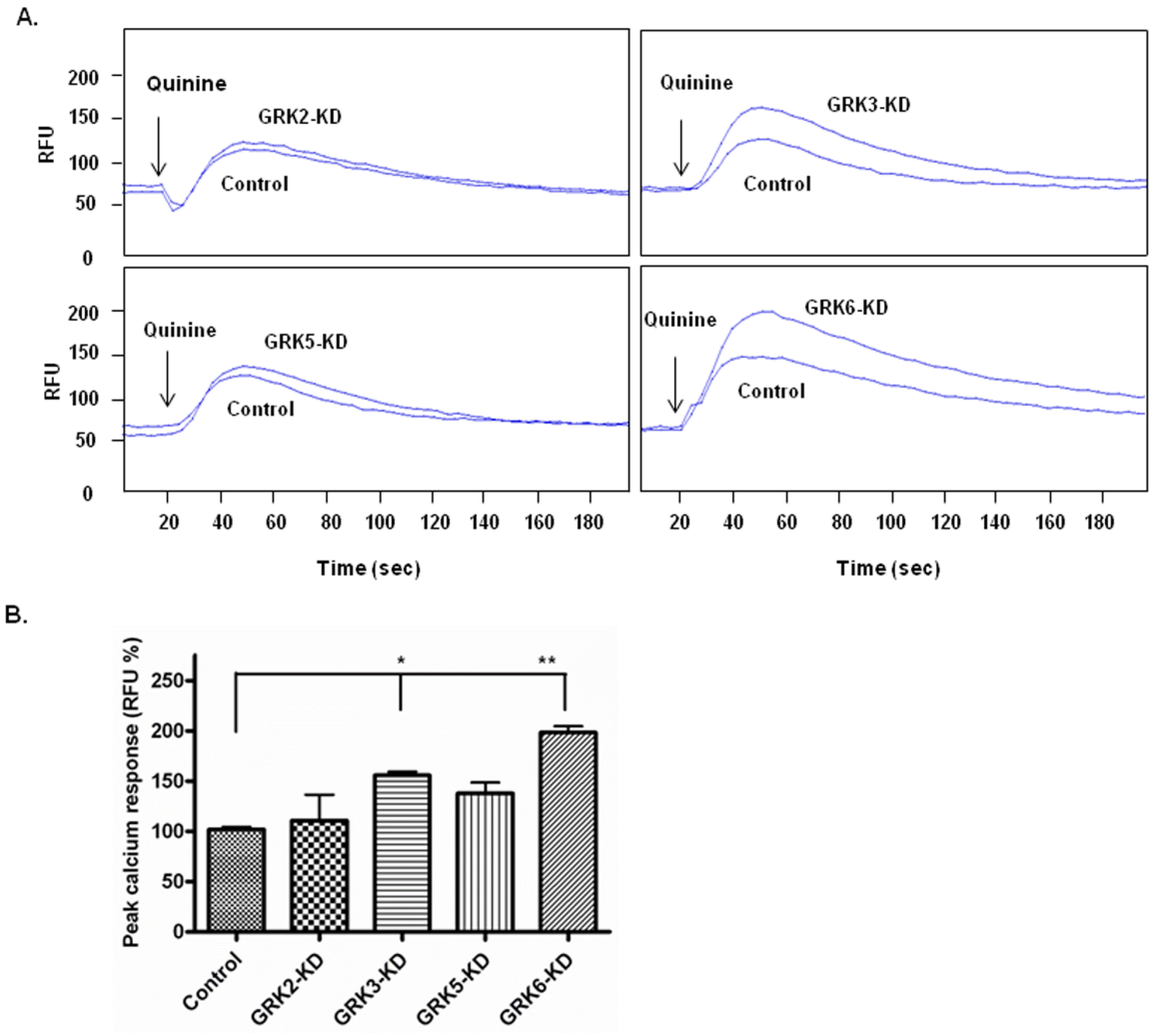

Figure 4.3.6. Characterization of GRK2, GRK3, GRK5 and GRK6 knockdown in HEK293T cells. [**A**]. Effects of knockdown of GRK2, GRK3, GRK5 KD and GRK6 KD on quinine induced calcium mobilization in T2R4 expressing HEK293T cells. The GRK stable KD cell lines or scrambled shRNA cells (control) were transiently transfected with FLAG-T2R4 and incubated with calcium-sensitive Fluo-4 NW dye. Changes in intracellular calcium were measured, after application of quinine by a FlexStation 3 microplate reader at 525 nm following excitation at 494 nm. The arrow at 20 sec indicates the addition of agonist by Flexstation 3 microplate reader. The image shows representative raw traces of calcium mobilized in terms of relative fluorescence units (RFU). The data is representative of at least 3-5 independent experiments. [**B**]. Peak calcium response (RFU%) in T2R4 expressing but GRK2, GRK3, GRK5 and GRK6 knockdown HEK293T cells in response to quinine incubation. The results were normalized to scrambled shRNA control which was taken as 100%. Significance was checked by one-way ANOVA using *Dunnette's* post hoc test, *p<0.05, **p<0.01.

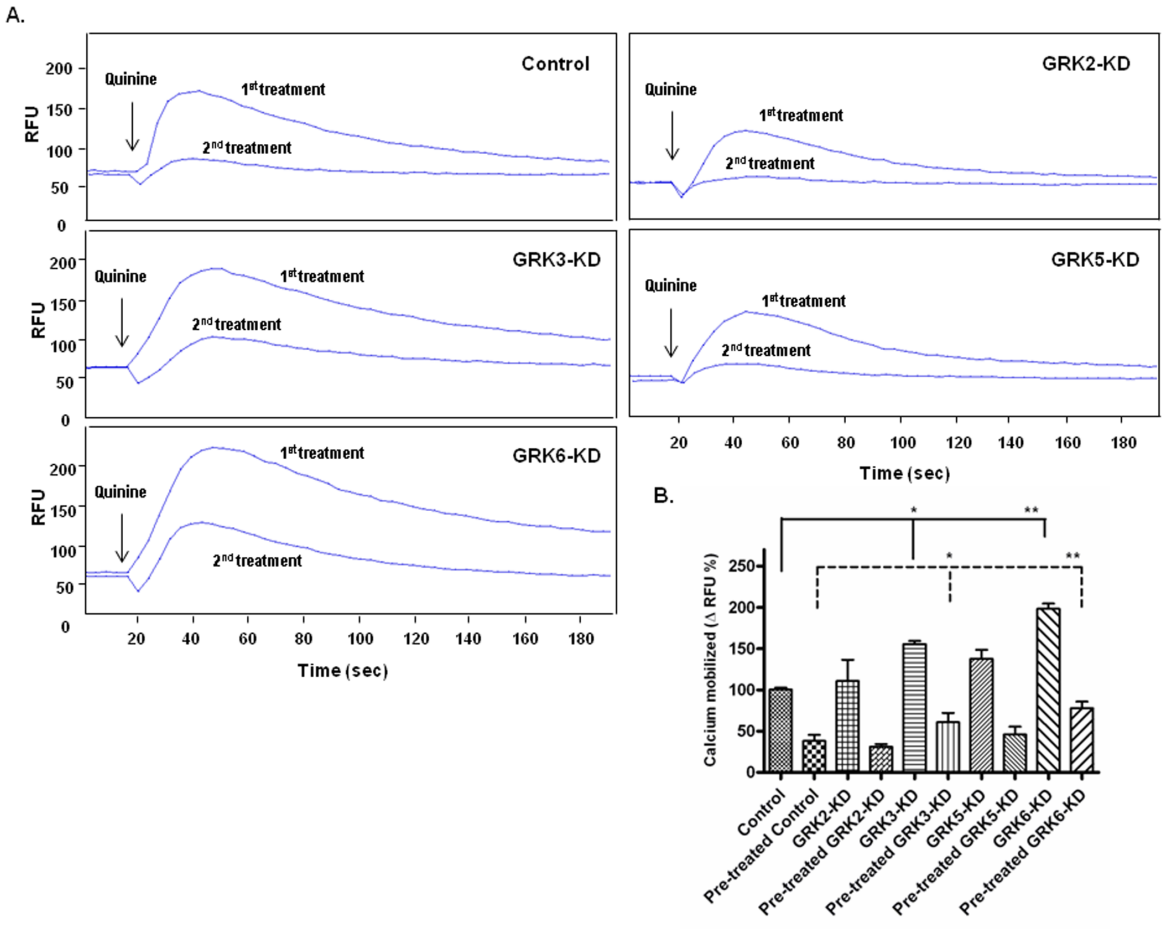

Figure 4.3.7. Effect of GRK knockdown on quinine induced T2R4 desensitization. [**A**]. Representative calcium traces of quinine induced desensitization in T2R4-expressing but GRK-KD HEK293T cells. The cells were loaded with Fluo-4 NW dye and exposed to quinine during the final 15 min of dye incubation. The arrow at 20 sec indicates the addition of agonist by Flexstation 3 microplate reader. The cells pretreated with calcium-free assay buffer and exposed to quinine represent first treatment, whereas, cells pretreated with quinine and re-exposed to same concentration of quinine represent second treatment. Changes in intracellular calcium were measured by Flexstation 3 microplate reader. [**B**]. Bar plot representation of the calcium mobilized (RFU%) in T2R4-expressing GRK-KD cells showing desensitization in response to quinine. Data shows mean ± SEM which is representative of three independent experiments. Significance was checked by one-way ANOVA using *Dunnette's* post test, *p<0.05, **p<0.01.

produce any significant change in quinine induced desensitization of T2R4 in HEK293T cells treated with 1 mM quinine (**Figure 4.3.9C**).

4.3.6 Agonist-mediated T2R4 trafficking

To examine whether agonist stimulation leads to T2R4 internalization, cell surface expression of T2R4 was examined by flow cytometry, with and without agonist treatment. We selected bitter compounds that were shown to activate T2R4; quinine, yohimbine, DB, dapsone and parthenolide (Meyerhof et al., 2010). The respective concentrations were selected based on their published threshold values, and keeping in view the low affinity of T2Rs for their ligands, usually in higher micromolar to millimolar concentrations (Clark et al., 2012; Meyerhof et al., 2010). T2R4 expressing cells were incubated with the compounds for 1 h at 37°C. N-terminal FLAG-tagged TPα, which does not internalize upon stimulation with its agonist, U46619, was used as a positive control. None of the compounds, except quinine, caused any significant change in T2R4 cell surface expression (**Figure 4.3.10A**). Interestingly, quinine upregulated the cell surface expression of T2R4 as demonstrated by flow cytometry analysis of the FLAG-tagged T2R4 (**Figure 4.3.10A**). DB, yohimbine, dapsone and parthenolide did not cause any statistically significant increase in T2R4 expression. Quinine caused a two-fold increase in T2R4 cell surface expression with a statistical significance of ***$p<0.001$.

To elucidate whether quinine-induced upregulation of T2R4 expression was a post-translational event, we used BFA which is an inhibitor of protein transport from the ER to the Golgi, and affects trafficking of the protein to plasma membrane. T2R4-expressing cells were treated with 5 μg/ml BFA for 4 h and then exposed to quinine or vehicle for 15 min or 60

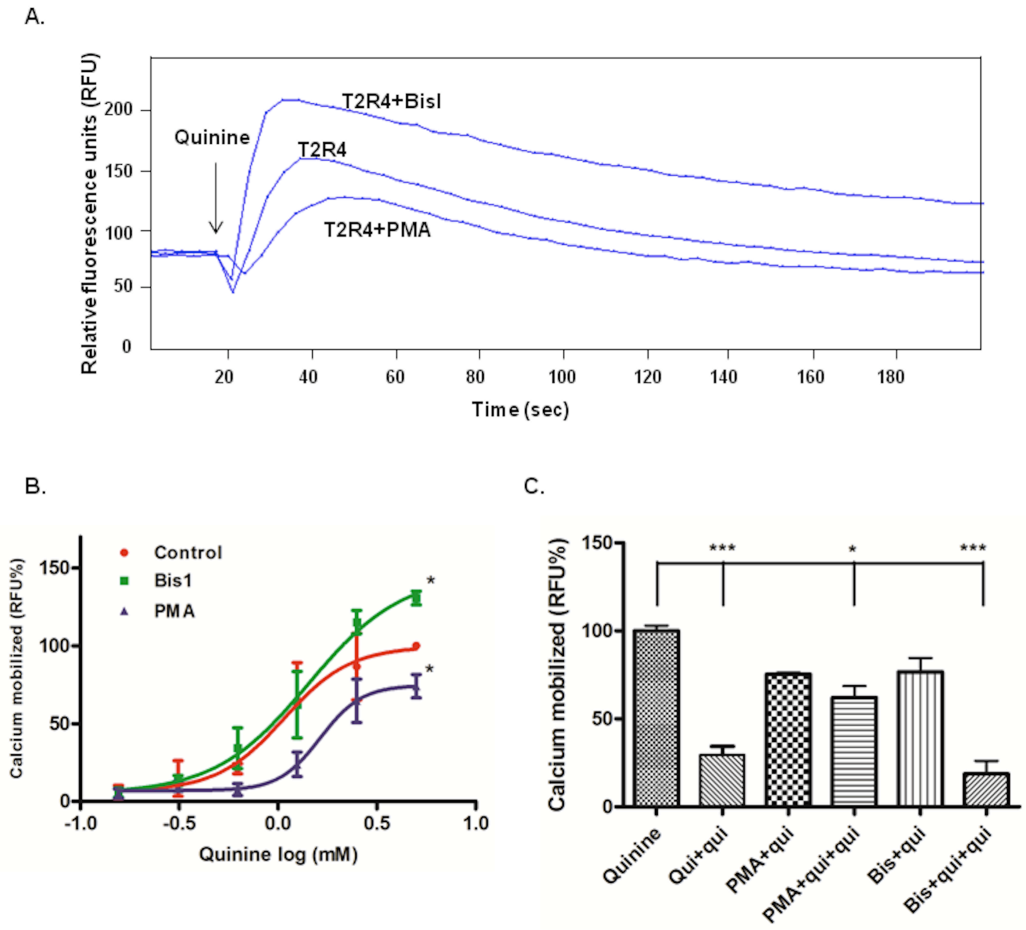

Figure 4.3.8. Effect of PKC activator and inhibitor on quinine mediated T2R4 calcium response. [**A**]. Representative calcium traces of T2R4-expressing HEK293T cells pretreated with 10 µM Bis-1, PKC inhibitor, or 0.1 µM PMA, PKC activator, and stimulated with 5 mM quinine. Untreated T2R4-expressing HEK293T cells stimulated with 5 mM quinine were used as control. [**B**]. Dose-response curves of T2R4-expressing HEK293T cells pretreated with PMA or Bis1 and stimulated with different concentrations of quinine. Responses of mock-transfected cells were subtracted and data is representative of three independent experiments. Dose-response curves were generated by nonlinear regression analysis using PRISM software version 5. [**C**]. Effect of PKC activation and inhibition on 1 mM quinine-induced T2R4 desensitization. FLAG-T2R4 expressing cells were plated in 96-well black-walled clear bottom tissue culture plates. The cells were incubated with calcium sensitive Fluo-4 NW dye. During the final 15 min, the cells were exposed to buffer, 1 mM quinine, bis1, bis1 with quinine, PMA, or PMA with quinine. The cells were washed with calcium-free assay buffer and changes in intracellular calcium mobilized were represented in terms of relative fluorescence units (RFU%) after application of 1 mM quinine at 525 nm following excitation at 494 nm, using a FlexStation 3 fluorescence microplate reader. Qui represents quinine. Significance was checked by one-way ANOVA using *Tukey's* post test, *p<0.05, ***p<0.001.

min, in the presence of BFA. This BFA treatment completely inhibited the trafficking of T2R4 by quinine and the expression levels were comparable to that of untreated control (**Figure 4.3.10B**).

4.3.7 Chaperone activity of quinine

Next, it was investigated if the observed chaperone action of quinine was T2R4-specific and/or agonist-specific. Therefore, three more GPCRs, T2R1, T2R3 and a Class A GPCR, TPα, were selected for further studies. A 15 min treatment of quinine did not produce any significant change in surface expression of T2R1, T2R3 and TPα (**Figure 4.3.10C**). In contrast, surface expression of T2R4 increased 1.5 fold in response to quinine. Quinine is a membrane-permeant molecule which can interact with other intracellular proteins (Zubare-Samuelov et al., 2005). To determine if other amphiphilic bitter compounds are capable of producing the same effect as quinine, we selected DXM, a membrane-permeable agonist of T2R1 (Singh et al., 2011a; Upadhyaya et al., 2010; Upadhyaya et al., 2014). Both T2R1 and T2R4 were exposed to DXM for 15 min before surface expression was analyzed by flow cytometry. DXM treatment caused no significant increase in surface expression of T2R1 or T2R4 (**Figure 4.3.10D**). The data thus suggests that the increased surface expression of T2R4 produced by quinine is both receptor and agonist-specific. It was then examined whether the effects of quinine on receptor expression varied with agonist incubation time. For this, T2R4 expressing cells were incubated with quinine for 15 min, 30 min, 60 min and 120 min at 37°C before receptor expression was analyzed. Untreated T2R4 was used as control. The cell surface expression of T2R4 increased in a time-dependent manner, reaching the peak at 60 min incubation and then stabilizing (**Figure 4.3.11A**). The expression

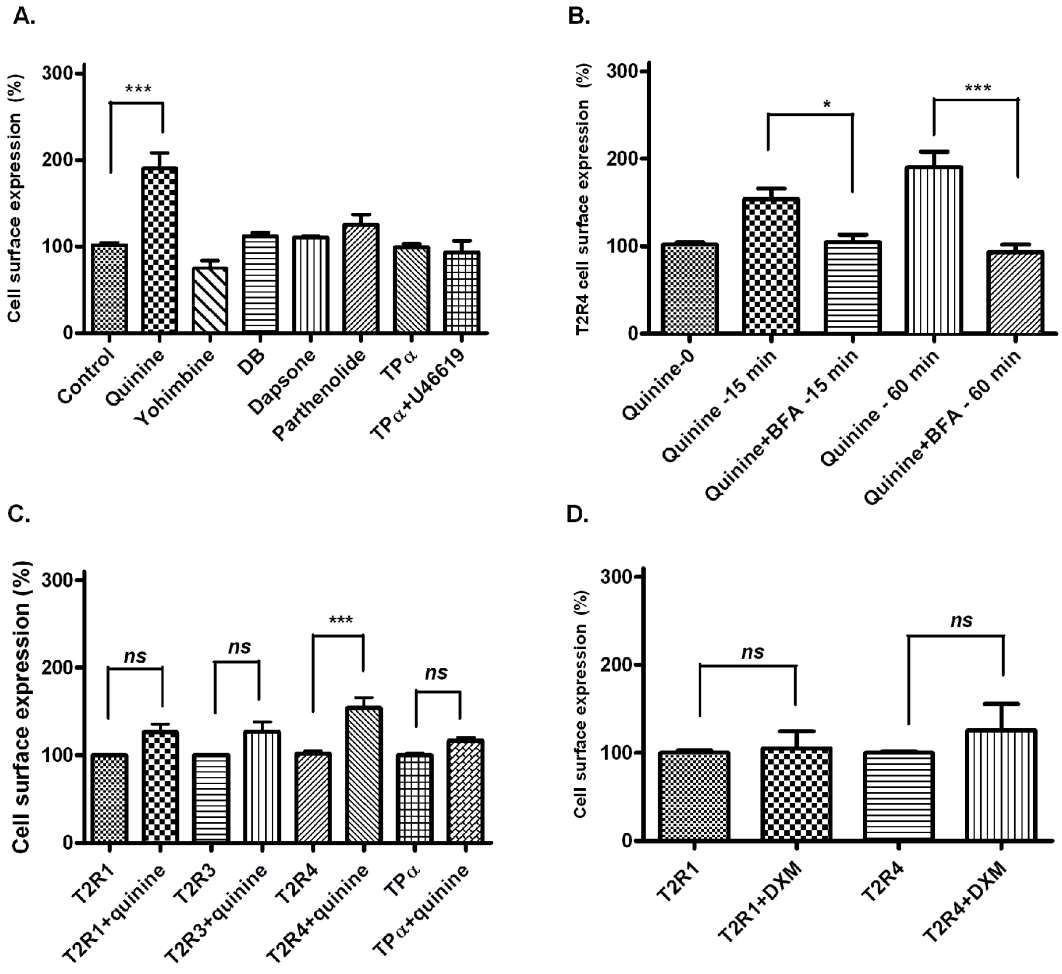

Figure 4.3.9. T2R trafficking and chaperone activity of quinine. [**A**]. Effect of agonist treatment on T2R4 cell surface expression. T2R4-HEK293T cells were treated with buffer (control) or 1 mM each of quinine, yohimbine, dapsone and parthenolide, or 2 mM denatonium benzoate (DB) for 1 h at 37ºC. TPα expressing HEK293T cells treated with its agonist, 1 µM U46619, were used as a positive control. [**B**]. Effect of BFA treatment on T2R4 trafficking. T2R4 expressing HEK293T cells were treated with vehicle or 5 µg/ml BFA for 4 h at 37ºC. The cells were incubated with 1 mM quinine, in the presence of BFA, for 15 min or 60 min at 37ºC. Cell surface expression of T2R4 was determined by flow cytometry and expressed as percentage increase over FLAG-T2R4 without quinine stimulation (basal), which was considered as 100%. Values represent the mean ± SEM of 3-7 independent experiments. [**C**]. Effect of quinine treatment on cell surface expression of FLAG-tagged T2R1, T2R3, T2R4 and TPα transiently expressed in HEK293T cells. [**D**]. Effect of DXM treatment on surface expression of transiently expressed T2R1 and T2R4 in HEK293T cells. Receptor-expressing cells were incubated with 500 µM DXM for 15 min before determining cell surface expression by flow cytometry. Receptor expression was analyzed using mouse monoclonal anti-FLAG antibody, which was detected by goat anti-mouse Alexa 488 antibody. Significance was checked by one-way ANOVA using *Tukey's* post test or by Student's *t-test*.

Increased from 1.5-fold at 15 min incubation to almost 2-fold at 60 min quinine incubation. Human ASMCs were used as a control in desensitization assays, therefore, the effect of quinine on surface expression of endogenous T2R4 was assessed in these cells. Surface expression of T2R4 in hASMCs increased in a time-dependent manner in response to quinine (**Figure 4.3.11B**). This data was consistent with the flow cytometry data of T2R4 transiently expressed in HEK293T cells.

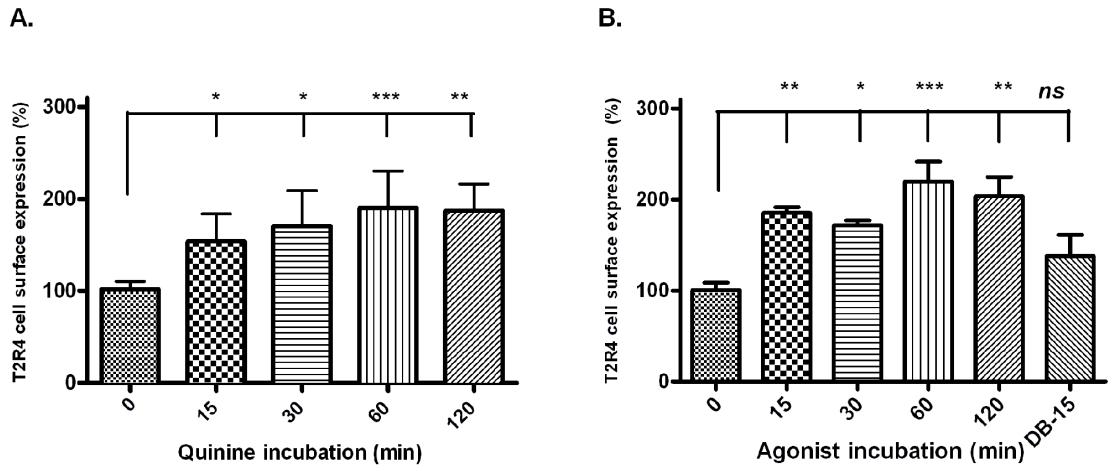

Figure 4.3.10. Time course studies of quinine incubation times on T2R4 surface expression. [**A**]. Time-dependent effect of quinine incubation on cell surface expression of T2R4 in HEK293T cells. T2R4 expressing cells were treated with quinine for 15 min, 30 min, 60 min or 120 min at 37ºC. T2R4 cell surface expression was analyzed by flow cytometry using mouse monoclonal anti-FLAG antibody. [**B**]. Time-dependent effect of quinine incubation on surface expression of endogenous T2R4 in hASMCs. T2R4 surface expression was also determined after denatonium benzoate (DB) incubation for 15 min, which produced no change in surface expression of T2R4 in hASMCs. Data represents values from three independent experiments performed in duplicates. Significance was checked by one-way ANOVA using *Tukey's* post hoc test, *$p<0.05$, **$p<0.01$, ***$p<0.001$.

4.4 Elucidation of the role of intracellular serine and threonine residues in T2R4 signaling

4.4.1 GPCR phosphorylation

An important mechanism in GPCR desensitization is receptor phosphorylation by kinases (Pitcher et al., 1998). Till now, it has been widely assumed that GRKs selectively phosphorylate active GPCRs at serine and threonine residues located predominantly within the C-terminus and 3rd ICL, thereby terminating G protein-mediated signaling by recruiting β-arrestins (Kohout and Lefkowitz, 2003; Perry et al., 2002). However, recent data suggests that members of the GRK4 protein subfamily, especially GRK5 and GRK6, effectively phosphorylate some inactive GPCRs (Li et al., 2015). This activation-independent phosphorylation leads to constitutive arrestin binding, suggesting that GRKs of this subfamily can stimulate basal receptor cycling and /or arrestin-mediated signaling in the absence of agonists. Desensitization studies of T2Rs are very scarce, and the potential residues involved in the process need to be characterized. To identify the residues involved in the desensitization of T2R4, all serine and threonine (S and T) residues in the ICLs and C-terminus were mutated to alanine in this study. The intracellular region of T2R4 consists of six serines, four in ICL1 and two in ICL2; and seven threonines, one each in ICL1 and ICL2, two in ICL3 and three in the C-terminus **(Figure 4.4.1)**. The effect of these S/T mutations on T2R4 function and surface expression was examined by measuring IP_3 generation in response to quinine and by pursuing flow cytometry and immunofluorescence studies respectively.

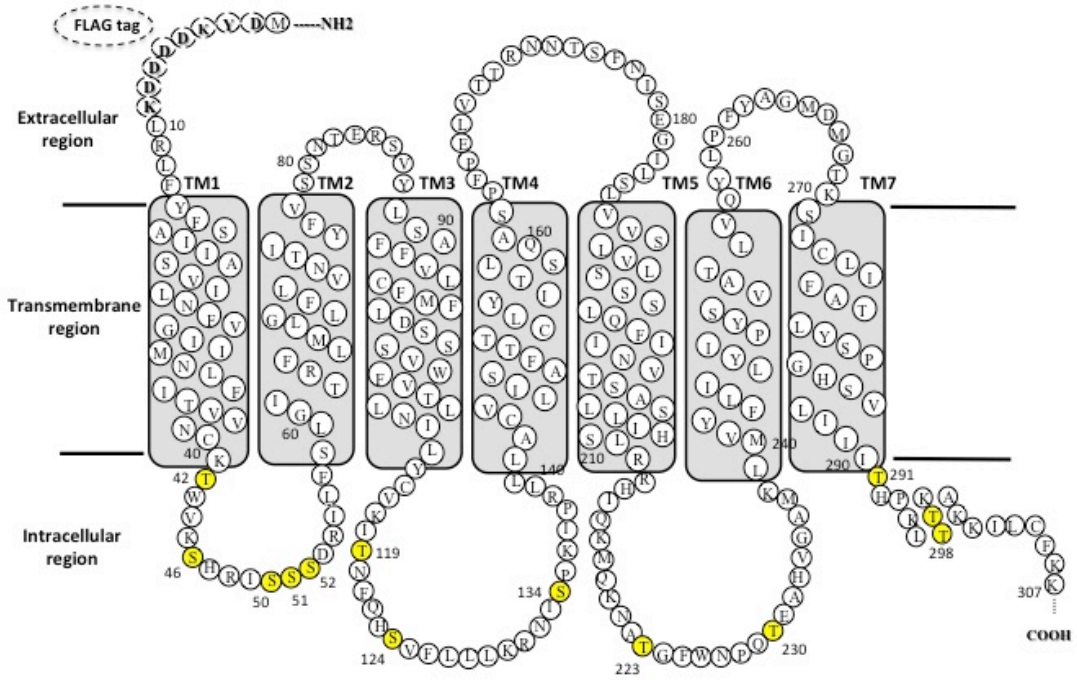

Figure 4.4.1 Amino acid sequence of the bitter taste receptor T2R4. Two-dimensional representation of the T2R4 amino acid sequence. It comprises a short extracellular N-terminus, seven transmembrane (TM) helices, three extracellular loops (ECLs), three intracellular loops (ICLs) and a short intracellular C-terminus. The intracellular serine and threonine residues are numbered and highlighted in yellow color. The intracellular region consists of six serine and seven threonine residues. Also shown is the FLAG-epitope at the N-terminus.

4.4.2 Determination of basal and quinine-mediated surface expression of serine-threonine mutants by flow cytometry

To determine the surface expression of WT-T2R4 or S/T mutants by flow cytometry, FLAG-tagged receptors were transiently expressed in HEK293T cells. Following 24 h of transfection, the cells were treated either with buffer or 5 mM quinine to assess their basal or quinine-induced surface expression respectively. The basal surface expression of S46A was higher in comparison to WT-T2R4, with a significance value of *$p<0.05$ **(Figure 4.4.2A)**. In contrast, S50A displayed a significantly reduced surface expression compared to WT-T2R4 with ***$p<0.001$. Mutants S51A, S52A, S124A and S134A displayed surface expression similar to the WT-receptor **(Figure 4.4.2A)**. To determine the effect of agonist treatment on surface expression of serine mutants, the cells were exposed to quinine for 15 min and then processed for flow cytometry studies. In agreement to previous results, quinine caused ~ 1.5-fold increase in the expression of WT-T2R4. Whereas, surface expression of S46A increased 1.5-fold over that of treated WT receptor, thus resulting in an increase of 2.5-fold over untreated WT-T2R4 **(Figure 4.4.2B)**. However, quinine could not rescue the surface expression of S50A, as no statistical difference was observed among the untreated and treated receptor**.** Surface expression of other quinine-treated mutants was similar to treated WT-T2R4. However, quinine did not cause a significant increase in surface expression of S124A and S134A **(Figure 4.4.2B)**.

Surface expression of T230A was significantly low compared to WT-T2R4 **(Figure 4.4.3A)**. Rest of the threonine mutants showed expression comparable to the WT receptor. Similar to WT-T2R4, quinine caused increase in surface expression of T42A, T119A, T223A and T291A **(Figure 4.4.3B)**. In contrast, surface expression of T230A, T297A and T298A

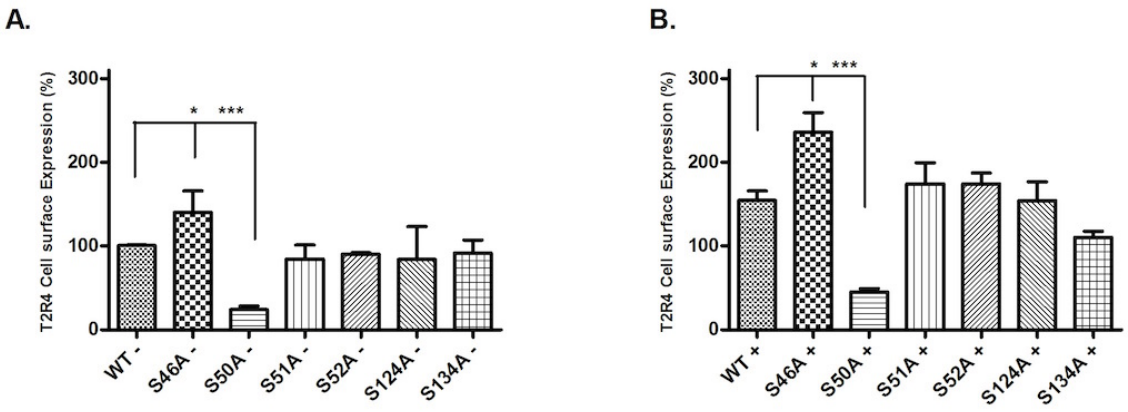

Figure 4.4.2 Cell surface expression of serine mutants of T2R4 intracellular region, in the absence and presence of quinine. A. Analysis of cell surface expression of serine mutants, expressed in HEK293T cells, in the absence of quinine. **B.** Analysis of surface expression of serine mutants, expressed in HEK293T cells, treated with 5 mM quinine for 15 min. (-) and (+) denote the absence and presence of quinine treatment. Analysis was performed by flow cytometry using the monoclonal mouse anti-FLAG antibody (1:500 dilution), which detects the FLAG-sequence at N-terminus of T2R4 and mutant receptors. The primary antibody was detected by goat anti-mouse Alexa 488 antibody (1:1000 dilution). The mean fluorescence intensities (MFI) were normalized to that of untreated WT-T2R4 (WT -), which was considered as 100%. Cells treated with isotype-specific IgG antisera were used as control. Data is representative of 3-4 independent experiments. Significance was analyzed using one way ANOVA with *Dunnette's* post hoc test, *$p<0.05$ and ***$p<0.001$.

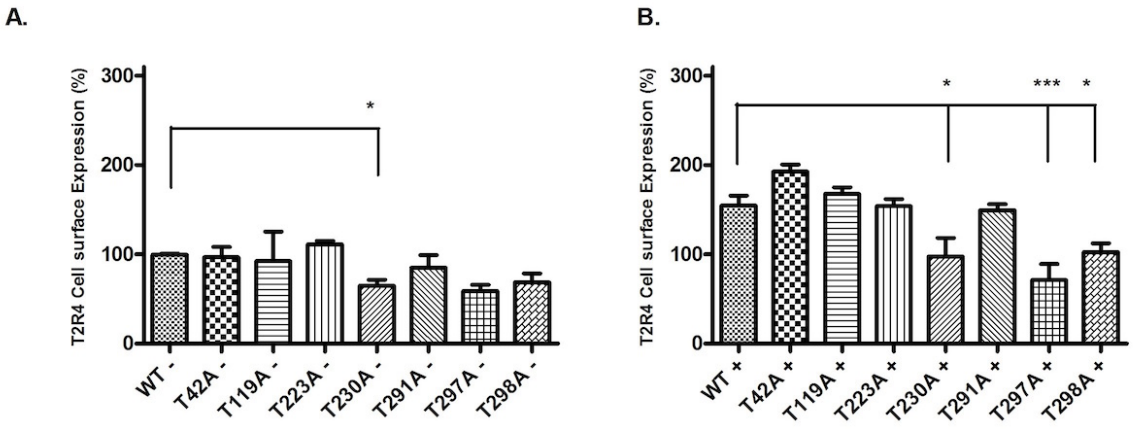

Figure 4.4.3 Cell surface expression of threonine mutants of T2R4 intracellular region, in the absence and presence of quinine. A. Analysis of cell surface expression of threonine mutants, expressed in HEK293T cells, in the absence of quinine. **B.** Analysis of surface expression of threonine mutants, expressed in HEK293T cells, treated with 5 mM quinine for 15 min. (-) and (+) denote the absence and presence of quinine treatment. Analysis was performed by flow cytometry using the monoclonal mouse anti-FLAG antibody (1:500 dilution), which detects the FLAG-sequence at N-terminus of T2R4 and mutant receptors. The primary antibody was detected by goat anti-mouse Alexa 488 antibody (1:1000 dilution). The mean fluorescence intensities (MFI) were normalized to that of untreated WT-T2R4 (WT -), which was considered as 100%. Cells treated with isotype-specific IgG antisera were used as control. Data is representative of 3-4 independent experiments. Significance was analyzed using one way ANOVA with *Dunnette's* post hoc test, *$p<0.05$ and ***$p<0.001$.

was significantly low even after quinine incubation, thus indicating that quinine did not affect the expression of these mutants **(Figure 4.4.3B)**. A comparison between untreated and treated groups showed that the chaperone activity of quinine was not effective for T230A, T297A and T298A. This data provides some insights on the S/T residues which might be responsible for the observed quinine-induced T2R4 trafficking.

4.4.3 Determination of subcellular localization of select S/T mutants by immunofluorescence

Based on surface expression studies, few mutants which displayed low surface expression and/or showed no effect of quinine on surface expression, in comparison to WT-T2R4, were selected for subcellular localization studies by immunofluorescence (IF). Mutants S50A, S134A, T297A and T298A were selected for IF study. S50A showed reduced surface expression which could not be rescued by quinine **(Figure 4.4.2A and 4.4.2B)**. Results from IF microscopy showed that S50A mutant was predominantly localized in the ER which was detected by using the ER marker calnexin **(Figure 4.4.4)**. Upon quinine incubation, there was not a significant change in the surface expression of this mutant. S134A was selected for IF study because though its surface expression was similar to WT-T2R4, quinine-treatment caused no change in expression **(Figure 4.4.4)**. As shown, no change was observed in surface expression of S134A after quinine incubation in representative HEK293T cells. The mutant was found predominantly localized to the plasma membrane, which is shown in green color detected by anti-FLAG antibody. Similar to S50A and S134A, quinine did not cause any significant change in surface localization of T297A and T298A, which displayed low expression in comparison to WT-T2R4 (**Figure 4.4.5)**. The

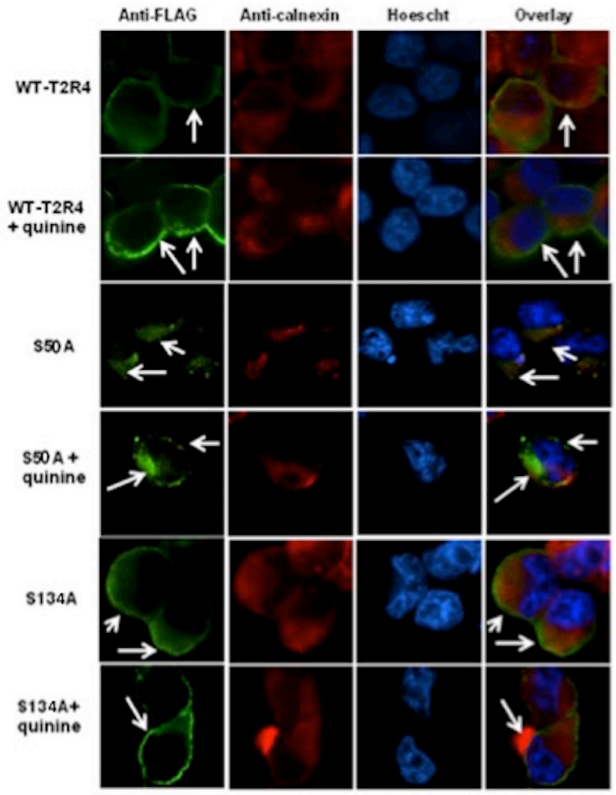

Figure 4.4.4. Immunofluorescence microscopy showing subcellular localization of WT-T2R4, S50A and S134A mutants expressed in HEK293T cells. Double label immunofluorescence was performed using mouse monoclonal anti-FLAG antibody and rabbit polyclonal anti-calnexin antibody, which localizes to the ER. The WT and mutant receptors were visualized using goat anti-mouse Alexafluor 488 secondary antibody (green), and the ER was visualized with goat anti-rabbit Alexafluor 594 secondary antibody (red). The nucleus stained with Hoechst-33342 dye is shown in blue. Overlay denotes the merge of all three colors.

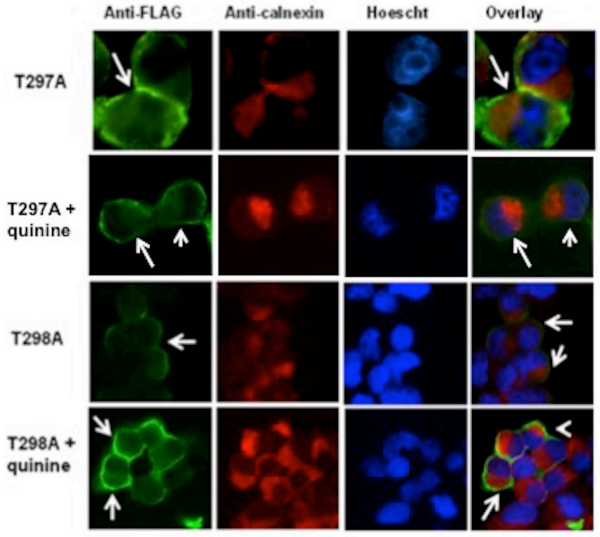

Figure 4.4.5. Immunofluorescence microscopy showing subcellular localization of T297A and T298A mutants expressed in HEK293T cells. Double label immunofluorescence was performed using mouse monoclonal anti-FLAG antibody and rabbit polyclonal anti-calnexin antibody, which localizes to the ER. The WT and mutant receptors were visualized using goat anti-mouse Alexafluor 488 secondary antibody (green), and the ER was visualized with goat anti-rabbit Alexafluor 594 secondary antibody (red). The nucleus stained with Hoechst-33342 dye is shown in blue. Overlay denotes the merge of all three colors.

IF results are thus in consistency with the flow cytometry data shown in **Figure 4.4.2** and Figure **4.4.3**.

4.4.4 Functional characterization of S/T mutants by quinine

To assess the functional characteristics of alanine mutants of S/T residues, expressed in HEK293T cells, intracellular IP_3 mobilization was measured in the absence (basal) and presence of quinine. The mobilized IP_3 was then normalized to the surface expression of mutants. The basal IP_3 of all serine mutants, except S50A, was similar to that of WT-T2R4 **(Figure 4.4.6A)**. S50A displayed significantly low basal IP_3 level, which can be accounted for by its low surface expression. In comparison to quinine-treated WT-T2R4, IP_3 generation was more pronounced in S46A and S52A **(Figure 4.4.6B)**. Whereas, quinine generated significantly low IP_3 in S50A, S124A and S134A mutants **(Figure 4.4.6B)**. IP_3 production for quinine-treated S51A was similar to the WT-receptor. Comparison of IP_3 mobilized among treated and untreated groups showed that despite of low surface expression of S50A, quinine was able to rescue its function significantly with ***$p<0.001$. Quinine produced a significant increase in IP_3 generation for all mutants.

The basal IP_3 of threonine mutants T119A, T223A and T291A was significantly high in comparison to WT-T2R4 **(Figure 4.4.7A)**, depicting that mutation of these residues disturbs the inactive conformation of the receptor. Recent studies depict that GRK5/GRK6 of GRK4 protein subfamily can phosphorylate inactive GPCRs (Li et al., 2015). Another likelihood could be that the mutant receptors are phosphorylated in their basal state by PKC (heterologous desensitization) and/or GRKs. Thus, mutation of Thr119, Thr223 and Thr291 residues might affect the desensitization mechanisms, showing higher basal activity. T42A,

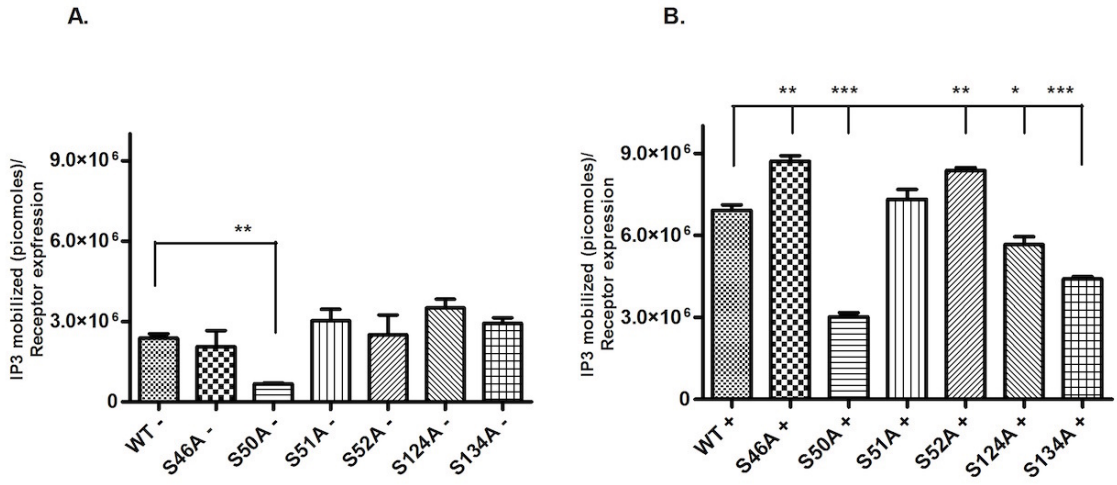

Figure 4.4.6. Functional characterization of serine mutants of T2R4 intracellular region using quinine. A. Basal IP_3 mobilization normalized to cell surface expression in serine mutants (- represents the absence of quinine). **B.** Quinine-mediated IP_3 mobilization in serine mutants (+ denotes the presence of 5 mM quinine). Responses of mock-transfected cells were subtracted from the observed receptor-specific responses. Results are from a minimum of 3 independent experiments performed in duplicates. IP_3 mobilized was normalized to cell surface expression of the receptors which was determined by flow cytometry.A one way ANOVA with *Dunnette's* post test was used to check the significance, *$p<0.05$, **$p<0.01$, ***$p<0.001$. Error bars represent mean ± SEM.

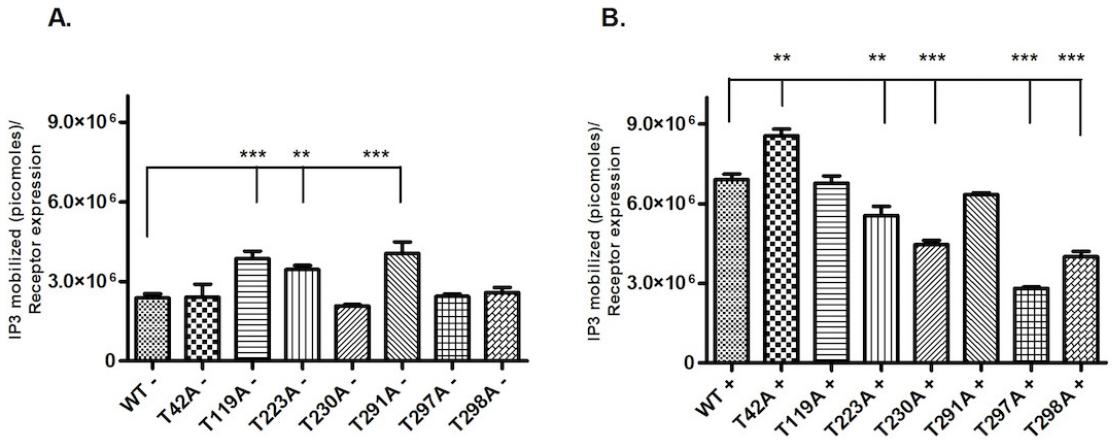

Figure 4.4.7. Functional characterization of threonine mutants of T2R4 intracellular region using quinine. A. Basal IP_3 mobilization in threonine mutants (- represents the absence of quinine). **B.** Quinine-mediated IP_3 mobilization in threonine mutants (+ denotes the presence of 5 mM quinine). Responses of mock-transfected cells were subtracted from the observed receptor-specific responses. Results are from a minimum of 3 independent experiments performed in duplicates. IP_3 mobilized was normalized to cell surface expression of the receptors which was determined by flow cytometry. A one way ANOVA with *Dunnette's* post test was used to check the significance, **p<0.01, ***p<0.001. Error bars represent mean ± SEM.

T230A, T297A and T298A displayed IP_3 mobilization similar to the WT-receptor **(Figure 4.4.7A)**. Quinine treatment caused significant IP_3 generation in T42A, whereas, significantly low IP_3 mobilization was observed for T223A, T230A, T297A and T298A **(Figure 4.4.7B)**, suggesting a loss of receptor function for these mutants. T119A, T223A and T291A displayed low function despite of high basal IP_3 levels **(Figure 4.4.7)**. All quinine-treated mutants displayed significant function compared to their untreated counterparts. An exception to this was T297A which displayed complete loss of function. Replacement of Thr298 with alanine resulted in ~ 50% loss in agonist-induced receptor signaling **(Figure 4.4.7B)**.

CHAPTER 5

5.0 DISCUSSION

5.1 Dextromethorphan mediated bitter taste receptor activation in the pulmonary circuit causes vasoconstriction

Stimulation of T2Rs in the lumen of gastrointestinal tract may condition the future avoidance of similar ingesta through the process of conditioned flavor avoidance, thus providing a second line of defense against potentially toxic compounds (Glendinning et al., 2008; Hao et al., 2009). Previous studies have found expression of T2Rs in ASM, where they caused marked relaxation in intact airways and might represent a new target for bronchodilation in asthma and obstructive airway disease (Deshpande et al., 2010; Manson et al., 2014). A recent report also identified T2Rs on motile cilia of airway epithelial cells and in the anterior nasal cavity, where they increase the ciliary beat frequency (Shah et al., 2009), promote sneezing, and regulate respiratory rate against noxious inhalants (Finger et al., 2003). The expression of four T2Rs was demonstrated in human pulmonary arteries while this study was in revision (Manson et al., 2014). However, the presence and functional significance of all T2Rs in the pulmonary vasculature remains unreported, till now (Upadhyaya et al., 2014).

In this study, a majority of the TAS2R transcripts were detected in hPASMCs. Functional screening revealed intracellular calcium responses to stimulation with a number of bitter agonists **(Figure 4.1.2.A)**. Among the 15 agonists tested, hPASMCs showed the maximum calcium mobilization response to DXM treatment, followed by quinine. Interestingly, our previous taste sensory analysis showed that quinine and DXM are the most intense bitter tasting compounds (Singh et al., 2011a; Upadhyaya et al., 2010). There were

couple of reasons for choosing DXM in the current study; compared to quinine, which activates nine T2Rs, DXM was shown to activate only T2R1 (Born et al., 2013; Meyerhof et al., 2010). In addition, recent and extensive structure-function studies pursued on T2R1 led to the pharmacological characterization of the potency of DXM, and identification of the ligand binding pocket on T2R1 (Singh et al., 2011a; Upadhyaya et al., 2010). Using different techniques including qPCR, receptor knockdown using shRNA, Western blot analysis of the decrease in T2R1 expression in knockdown cells, and immunofluorescence, the expression of T2R1 in hPASMCs was confirmed and linked to DXM mediated intracellular calcium signaling.

Despite the current lack of knowledge on endogenous ligands for T2Rs, the effect of the tested agonist(s) in the porcine arterial tissues provides relatively clear insight into which receptors are activated. DXM displays a previously unknown pharmacological activity in the pulmonary circuit, causing T2R activation leading to vasoconstrictor responses. Due to feasibility concerns in obtaining intact human lung tissues and similar expression pattern of T2R1 in human and porcine PASMCs and ASMCs, the *ex vivo* effect of DXM on porcine pulmonary arterial and airway rings was tested. It was found that DXM treatment of the pulmonary arterial rings caused vasoconstriction with an EC_{50} of 211 ± 2 μM (**Figure 4.1.8.B**). The effect of DXM on U46619 pre-contracted arterial rings was also analyzed in this study. DXM, starting from 100 μM, caused contraction of pre-contracted rings (**Figure 4.1.9**). This might be a synergistic effect of DXM and U46619 on the pulmonary artery. The role of endothelium was also analyzed in this DXM-mediated response of pulmonary arterial rings. DXM-treatment of endothelium-denuded pulmonary arterial rings did not show much change in EC_{50} value of DXM (238 ± 1 μM, **Figure 4.1.10**). Study by Manson et al. showed

that bitter agonists, chloroquine, DXM, and noscapine lead to relaxation of pre-contracted human pulmonary arteries (Manson et al., 2014). However, minimal relaxation was observed with DXM-treatment in their study following U46619 induced pre-contraction. My results contradict this recently published data on DXM in the human pulmonary artery (Manson et al., 2014). A possible explanation for the different results may be that Manson *et al*. did not use DXM concentration beyond 100 μM. Furthermore, the role of T2R1 in mediating DXM responses was not considered in that study. In contrast, chloroquine led to relaxation of pre-contracted arterial rings (**Figure 4.1.9**). This might indicate that DXM has a different mechanism of action in vascular smooth muscle than chloroquine. Interestingly, DXM caused relaxation of the airway rings with EC_{50} value of 74 ± 1 μM. This later effect of DXM in the airways, acting through T2Rs, was recently demonstrated (Manson et al., 2014). T2Rs may be developmentally regulated and/or differentially expressed among species and age groups (Foster et al., 2013). The relative expression of all TAS2Rs in porcine was not analyzed in this study, but qPCR results demonstrate similar expression pattern of TAS2R1 in human and porcine cells. Increased expression of TAS2R1 in porcine PASMCs correlates with the increased IP_3 production upon DXM treatment, which caused increase in MLC phosphorylation and contraction observed in arterial rings (**Figure 4.1.8 and 4.1.13**). Whereas, DXM treatment did not produce any significant change in IP_3 generation in porcine ASMCs which correlates with the low T2R1 expression and the observed effect of relaxation in airway rings. Hence, it is speculated that this receptor might be predominantly involved in DXM-mediated contraction of pulmonary arterial rings. Interestingly, myographic data in this study suggests that the dose of DXM plays a role in the observed effects; at low concentrations (74 μM), DXM leads to relaxation of airways, whereas, higher

concentrations (211 μM) cause contraction of the pulmonary artery. This might be a protective reflex for regulating the vascular tone when excess noxious irritants are ingested/inhaled by the body. These results suggest that DXM mediates differential effects in different body tissues.

The pulmonary arterial reactivity in vessels and airways from newborn piglets was examined. While reactivity of the neonatal pulmonary vasculature can differ from that of the adult pulmonary circuit, the neonatal pulmonary vasculature is in general more sensitive to vasospastic agents than in the adult; this vasospasm can precipitate severe pulmonary hypertension (persistent pulmonary hypertension of the newborn) in response to constrictors including hypoxia, inflammation or noxious stimuli such as bitter tastants. Porcine pulmonary vessels were used in this study as the pulmonary hypertensive model in this species has been characterized (Fediuk et al., 2012; Hinton et al., 2007). The neonatal system is unique, as the pulmonary circuit is dilating, naturally. As such, if a given drug has a vasoconstrictor effect, neonates offer a unique opportunity to test it. In this study, the observed effects of DXM on the neonatal porcine arterial rings suggest it acts as a vasoconstrictor. The presence of T2Rs in the neonatal pulmonary circuit in particular may be developmentally significant, in view of the constriction of the pulmonary circuit in utero, and its abrupt need for dilation post-birth; endogenous T2R ligands may pose a significant threat to normal neonatal pulmonary vasodilation.

To investigate the molecular mechanisms underlying the contrasting effects: DXM-induced contraction of pulmonary artery and relaxation of airway, IP_3 production was measured in both human and porcine PASMCs and ASMCs after treatment with DXM. There was no effect of DXM on IP_3 production in hASMCs, whereas, significantly increased

IP_3 production was observed in hPASMCs (**Figure 4.1.12**), which confirms that higher calcium is generated to cause a contractile response in PASMCs. Similar results were obtained in porcine cells where significantly increased IP_3 was observed after DXM-treatment of PASMCs when compared to treated ASMCs (**Figure 4.1.13A**). These contrasting effects of DXM might explain the observed difference in EC_{50} values of DXM in contracting pulmonary artery and relaxing airways. Since phosphorylation of MLC is one of the key intracellular signaling mechanisms underlying vascular smooth muscle cell contraction, the expression of MLC and phospho MLC with and without DXM treatment in porcine PASMCs was also examined. DXM treatment of PASMCs led to an increase in MLC phosphorylation (**Figure 4.1.13B**). I, thus, propose that in DXM-treated PASMCs, significant IP_3 is generated to cause phosphorylation of MLC, leading to a contractile response (**Figure 5.1.1**). The relative expression levels of T2R1 in human and porcine PASMCs correlate with the increased IP_3 production after DXM treatment (**Table 5.1.1**).

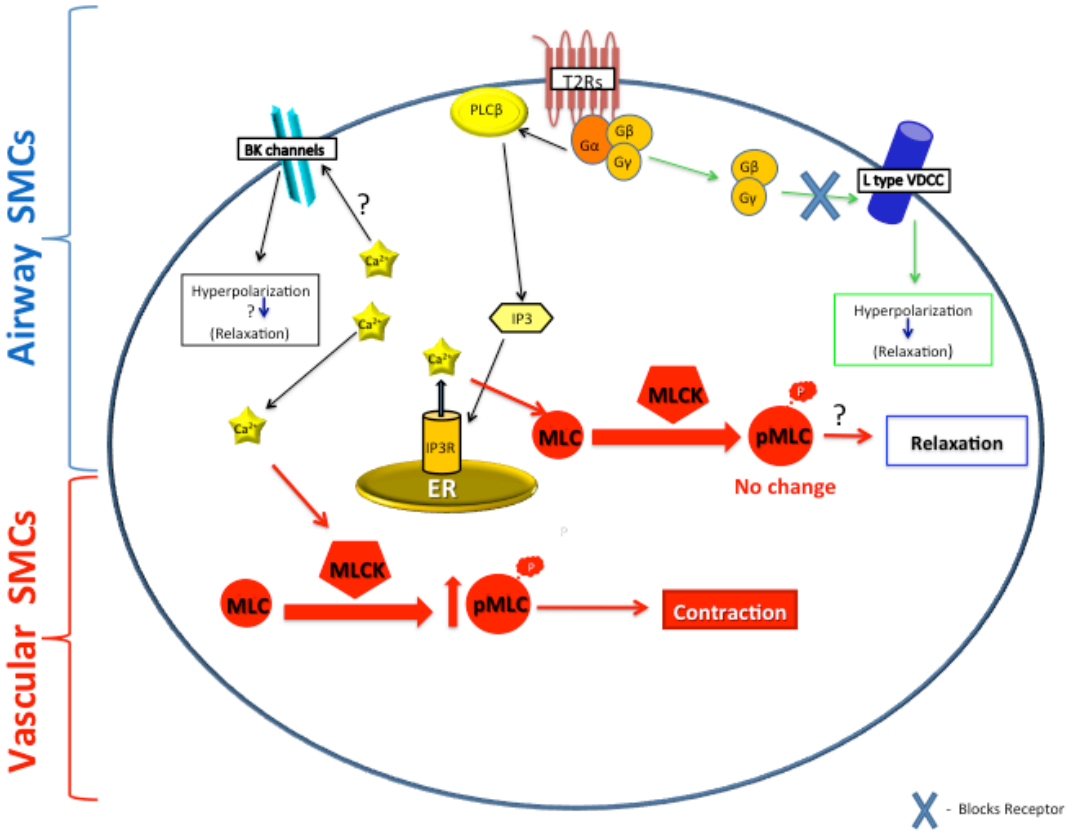

Figure 5.1.1. Schematic representation of the contrasting effects of DXM-induced vasoconstriction in PASMCs and relaxation in ASMCs. In this model, I propose that in PASMCs DXM activates the canonical T2R signaling cascade to cause significant increase in IP_3 production resulting in increase in global $[Ca^{2+}]_i$ levels. The increased $[Ca^{2+}]_i$ subsequently leads to activation of myosin light chain kinase (MLCK) thus resulting in an increase in the phosphorylated form of MLC (pMLC). Increase in pMLC ultimately leads to the constrictor effects observed in the pulmonary arterial rings. The molecular mechanism(s) underlying T2R mediated relaxation of the airways was studied by different groups. (Deshpande et al., 2010) showed that T2R activation results in localized $[Ca^{2+}]_i$ mobilization which opens up large-conductance Ca^{2+} activated K^+ (BKca) channels leading to ASM membrane hyperpolarization and relaxation. Recently, Zhang C, *et al*, demonstrated that activation of T2Rs in airways (resting state) leads to increase in global $[Ca^{2+}]_i$ levels, however, these are not sufficient to impact airway contractility (Zhang et al., 2013). In a second pathway, they proposed bitter tastants inhibit L-type voltage-dependent Ca^{2+} channels (VDCCs) via a G-protein βγ dependent process, to induce bronchodilation of pre-contracted ASM.

Table 5.1.1. DXM mediated effects on T2Rs expressed in PASMCs, ASMCs, pulmonary artery and airway rings.

Parameter	PASMCs		ASMCs	
	Neonatal pig	**Adult human**	**Neonatal pig**	**Adult human**
T2R1 mRNA level ¶ (Relative expression %)	60	100	20	30
IP_3 produced (nmoles) (DXM treated) (Basal or untreated)	565 ± 9 294 ± 28	709 ± 31 320 ± 40	333 ± 50 210 ± 27	336 ± 18 318 ± 17
***Ex vivo* effect** (Myographic studies in arterial or airway rings)	Contraction (Pulmonary arterial rings)	Not known	Relaxation (Airway rings)	Relaxation* (Airway rings)

¶ This is the only T2R characterized by structure-function studies to interact with DXM.

- Shown in previous studies (Pulkkinen et al., 2012).

5.2 Structure-function role of C-terminus in human bitter taste receptor T2R4 signaling

Sequence analysis of the human membrane protein database demonstrated the prevalence of MPBRs in the C-terminal tail in GPCRs and other receptor proteins (Okamoto et al., 2013). These MPBRs were reported to be involved in anterograde trafficking in a limited number of proteins. For example, the basic domain in C-terminus of chemokine receptor CCR5 supports optimal surface expression by co-operating with the adjacent downstream cysteine cluster (Venkatesan et al., 2001). The C-terminal MPBRs were also required for both cell surface expression and signaling of melanin-concentrating hormone receptor 1, MCH1R (Tetsuka et al., 2004). The positive role of MPBRs in anterograde trafficking was reported for the HIV coreceptor GPR15 and Golgi-resident glycosyltransferases (Giraudo and Maccioni, 2003; Okamoto et al., 2013). The C-terminal 10-12 residues following the TM segment in human GPCRs are considered the membrane proximal residues, with +1 being the most proximal to the TM (Conner et al., 2008; Okamoto et al., 2013). Majority of the mutants which displayed reduced surface expression in this study fall in the MPBR of T2R4 C-terminus, with Thr291 being the most proximal and Leu303 the most distal residue (**Figures 4.2.1 and 4.2.2A**). Interestingly L303A is the only mutant that showed increased cell surface expression but most of it is not functional as indicated by its reduced E_{max} (**Table 4.2.1**). This shows that in addition to the hydrophobic property, the bulkiness or the branched nature of the amino acid at position 303 is important for proper function. To determine whether an amino acid structurally and functionally similar to leucine is required at this position, the L303V mutation was made. As expected, the conservative substitution L303V showed wild type characteristics. L295A and K296A

mutants form part of the conserved KLK/R motif in T2Rs. Conservative substitution of these residues with valine or arginine rescued the cell surface expression equivalent to WT-T2R4, suggesting that basic and hydrophobic residues are required at the indicated positions for proper trafficking of the receptor. However, whether the differences observed in cell surface expression of the mutants are due to defective receptor trafficking or changes in levels of receptor protein expression, needs to be explored.

Di-lysine (KK) motif in GPCRs is one of the common sorting signals, which leads to ER retention (Letourneur et al., 1995; Teasdale and Jackson, 1996). There are two such motifs, Lys300, Lys301 and Lys306, Lys307 in the C-terminus of T2R4 but they are not conserved among T2Rs (**Figure 4.2.2A**). In human T2Rs, Lys300 (24% in T2Rs) is replaced by either a leucine or valine in 60% of T2Rs, whereas, Lys301 (20% in T2Rs) is replaced by an arginine in 20% of T2Rs. Interestingly, only the first KK motif of Lys300 and Lys301 is highly conserved among T2R4s in different species (**Figure 4.2.2B**). Indeed our results suggest that this KK motif is not important for activation, rather it plays a role in trafficking of T2R4 (**Table 4.2.1**). Mutations of ER retention di-lysine motifs should ideally result in increased cell surface expression. Whether the first KK motif in T2R4 is a typical retention motif or just two lysine residues found in its MPBR, remains unclear. However, analysis of the proteins that possess the di-lysine motif in their C-terminus reveals several proteins known to be localized in their mature folded state at the cell surface (Klausner et al., 1990; Letourneur et al., 1995). However, steric masking of this retention motif can lead to proper folding of the receptor. (Letourneur et al., 1995; Teasdale and Jackson, 1996). It is likely that the KK motif in mutant receptor constructs becomes exposed with altered receptor conformation, thus resulting in reduced surface expression as seen in K300A and K301A

mutants of T2R4.

There are six lysines in the C-terminus of T2R4 **(Figure 4.2.1)**. The possible role of these residues in ubiquitination, which is involved in receptor trafficking and/or degradation, cannot be ruled out and needs further investigation. Modification of proteins by ubiquitin has important functions in proteasomal degradation, transcriptional regulation, signal transduction, and trafficking within the endocytic and biosynthetic pathways. In addition to lysosomal sorting/degradation and internalization, GPCR ubiquitination also has an important role in ER quality control during biosynthesis and functions to sort misfolded receptors to the ERAD (endoplasmic reticulum associated protein degradation) pathway that involves degradation by the proteasome. Polyubiquitination and degradation of misfolded receptors by the proteasome has been demonstrated for the δ-opiod receptor (Petaja-Repo et al., 2001), rhodopsin (Illing et al., 2002; Saliba et al., 2002), TRHR (thyrotropin-releasing hormone receptor) (Cook et al., 2003) and the CaR (Huang et al., 2006). Ubiquitination of the FSHR (follitropin receptor) regulates its cell surface expression but does not affect the rate of FSHR internalization, suggesting a function in trafficking through the biosynthetic pathway. The A_{2A} adenosine receptor binds directly to USP4, a deubiquitinating enzyme, which results in enhanced cell surface expression of functionally active receptor (Milojevic et al., 2006).

A di-leucine motif (Iso302-Leu303) is situated adjacent to the di-lysine motif Lys300-Lys301) in the distal part of T2R4 C-terminus **(Figure 4.2.1)**. The I302A mutant displayed a reduced surface expression and the I303A showed an increase in receptor surface expression **(Figure 4.2.3)**. The role of di-leucine sequence has been implicated in internalization and endosome/lysosome or plasma membrane targeting of diverse proteins

(Hunziker and Fumey, 1994; Letourneur and Klausner, 1992; Schulein et al., 1998). These sequences have been shown to bind AP1and AP2 clathrin adaptor protein complexes required for intracellular protein trafficking , and this process is thought to be responsible for their assembly in clathrin-coated pits and subsequent trafficking in clathrin-coated vesicles (Heilker et al., 1996). The di-leucine motif is highly conserved in the C-terminus of GPCRs, suggesting a general role in the exit from ER for most of the membrane proteins (Duvernay et al., 2004; Schulein et al., 1998). This motif participates in regulation of receptor ER exit by association with COP II-associated proteins (Barlowe, 2003). Thus the role of T2R4 C-terminus di-leucine motif in cell surface targeting is a possibility.

The KLK/R motif is highly conserved in ICL3 within the class B secretin/glucagon GPCR subfamily (Chan et al., 2001; Takhar et al., 1996). This motif is reported to be involved in G-protein coupling for GLP-1 and secretin receptor. Alanine mutation of Lys296, an important residue of the KLK motif in T2Rs, displayed constitutive activity five-fold higher than that of WT-T2R4, indicating that this residue stabilizes an active conformation of T2R4. However, in the absence of a crystal structure of any T2R it is difficult to predict the structural mechanism(s) by which this CAM stabilizes an active conformation. CAMs in the C-terminus of Class A GPCRs, such as the 5-HT4 receptors, dopamine receptors, and P_2Y_{12} have been identified (Claeysen et al., 2001; Ding et al., 2006; Zhang et al., 2014). The CAMs in the C-terminus were suggested to have different kinetics of receptor activation compared to CAMs in the ICL3 for the 5-HT4 receptors (Claeysen et al., 2001). Several naturally occurring and disease-causing GPCR mutants with increased constitutive activity have been identified (Seifert and Wenzel-Seifert, 2002). However, naturally occurring T2R variants with high constitutive activity are yet to be reported.

Studies on G-proteins, both heterotrimeric and monomeric have shown that positive charge conferred by a polybasic domain consisting of six lysines or arginines in the C-terminus in conjunction with a second signal, such as a CAAX lipid anchoring motif (palmitoylation or isoprenylation) is sufficient to target the G-protein to plasma membrane (Hancock et al., 1991; Zhang and Casey, 1996). Even in Class A GPCRs, the CAAX motif, which tethers C-terminus to the plasma membrane forming a 4th intracellular loop, is highly conserved. However, there is no CAAX consensus motif in T2Rs. There is only one cysteine, Cys304, present in the C-terminus of T2R4. Surprisingly, there are no conserved cysteines, and many of the T2Rs have no cysteines in the C-terminus (**Figure 4.2.2A**). The C304A showed significantly reduced surface expression (**Figure 4.2.3, Table 4.2.1**). Increased EC_{50} and a right-shift in dose-response curves was observed for distal residue mutants of C-terminus, i.e., I302A, C304A, F305A, K306A and K307A. We speculate that conformational changes in the receptor brought about by these mutations, or loss of interaction with intracellular G-proteins, might have affected receptor activation and or ligand binding. T2Rs, like T1Rs and many other GPCRs, are capable of forming oligomers *in vitro* (Kuhn et al., 2010). Oligomerization of GPCRs leads to varied functional roles. It may be important for organization of receptors in the plasma membrane (Kroeger and Eidne, 2004), or for efficient and fast activation of G proteins (Herrick-Davis et al., 2005; Jastrzebska et al., 2006). Thus, it cannot be ruled out that changes in Iso302, Cys304, Phe305, Lys306 and Lys307 might be disturbing the formation of these oligomeric complexes which can affect ligand binding and receptor activation.

Another common motif found in C-termini of GPCRs is the PDZ binding motif, which is recognized by PDZ containing proteins (Saras and Heldin, 1996). A potentially large

number of mammalian family A GPCRs, have the ability to engage PDZ domain-containing proteins. The first member of this family reported to contain a PDZ motif was the β_2AR, which in addition to its signaling function was found to mediate an essential trafficking function (Cao et al., 1999). Many T2Rs possess a PDZ binding motif, but no motif is recognizable from the sequence analysis of T2R4 C-terminus. The absence of conserved cysteines and a PDZ binding motif in C-terminus, thus, depict the disparity among T2Rs. Studying the factors responsible for this low sequence conservation can provide the basis for understanding the vast diversity of the exogenous bitter ligands recognized by T2Rs and their desensitization mechanisms.

5.3 Quinine mediates desensitization but not internalization of bitter taste receptor T2R4

Desensitization of GPCRs is initiated when their cytosolic residues, containing either serine or threonine, are phosphorylated by selected kinases (Pitcher et al., 1998). Arrestin binding to the phosphorylated GPCRs uncouples them from the heterotrimeric G proteins, and may also initiate receptor internalization (Ferguson, 2001). However, in addition to these regulatory pathways, some GPCRs undergo pharmacological sequestration, which is desensitization without their actual internalization into the intracellular compartments (Mostafapour et al., 1996). These receptors may be sequestered on or near the plasma membrane without internalizing, either as insulation on the membrane (Roettger et al., 1995) or via conformational changes of receptor proteins (Mostafapour et al., 1996), thus rendering them inaccessible to their agonists. In this study, it was demonstrated that quinine causes 60% ± 5.2% desensitization of T2R4 expressed in HEK293T cells, while it causes 45% ± 2.8% desensitization of endogenous T2Rs in ASMCs (**Figure 4.3.4**). This slight discrepancy can be attributed to the ability of quinine to activate nine T2Rs with different efficacies (Meyerhof et al., 2010), which might be the case in ASMCs. In contrast, a 15 min pretreatment of T2R4-expressing HEK293T cells with yohimbine resulted in only a marginal desensitization of the receptor to a second exposure of yohimbine. A likely explanation for the differential effects of quinine and yohimbine on T2R4 desensitization may be biased-agonism. This concept was not explored for T2R agonists but biased ligands have been identified for dozens of GPCRs. A striking example of ligand-biased regulation of desensitization and endocytosis is provided by the μ-opioid receptor. The μ-opiod agonists methadone and 1-α-acetyl methadone produce disproportionate desensitization and receptor

phosphorylation (Blake et al., 1997). Similarly, methadone and buprenorphine have been shown to have desensitization properties different from those of morphine for μ –opiod receptor (Blake et al., 1997). Differences in the desensitization capabilities can also be inferred from recovery of the receptor from desensitization. For example, the recovery from prolonged activation of 5-HT_3 receptors is differential among partial agonists and full agonists (van Hooft and Vijverberg, 1996). In addition, it remains to be investigated if quinine and/or yohimbine are full agonists or partial agonists for T2R4.

There are two hypotheses regarding the desensitization mechanisms of T2Rs. The first hypothesis proposes that membrane permeant bitter tastants, such as quinine, interact with and inhibit GRKs, delaying T2R signal termination (Zubare-Samuelov et al., 2005). The second hypothesis proposes that GRKs might be involved in T2R desensitization, and causing T2R signal termination (Robinett et al., 2011). Though both studies speculate the involvement of GRKs in T2R desensitization, they did not utilize a recombinant expressed T2R or pursue knockdown of specific GRKs. Therefore, to exclude the GRK-specific effects of quinine and determine T2R4-specific desensitization in response to quinine, KD studies of endogenous GRKs in HEK293T cells were pursued. Additionally, many previous studies on GPCR regulation by GRKs have been pursued with siRNA mediated GRK-KD in HEK293 cells (Busillo et al., 2010; Kim et al., 2005a; Ren et al., 2005).

T2R signaling in heterologous systems requires complementation with Gα-proteins to successfully couple to downstream signaling pathways (Chandrashekar et al., 2000; Ueda et al., 2003). Quinine and many other amphiphilic bitter tastants are effective G-protein activators *in vitro* (Naim et al., 1994). To exclude the G-protein mediated effects of quinine, the cells were not co-transfected with any G-protein/chimera. KD of GRKs 2, 3, 5 and 6 was

selected for analyzing the contribution of endogenous GRKs in quinine-mediated T2R4 desensitization. Differences were observed in the effects of these GRKs on T2R4 function. A significant increase in the transient and sustained phases was observed in T2R4-expressing GRK3-KD and GRK6-KD cells, which is indicative of an increased sensitivity to quinine and an expected response if these GRKs have a functional role in regulating the desensitization of T2R4 (**Figure 4.3.7**). On the other hand, T2R4-expressing GRK2-KD and GRK5-KD cells did not show any significant change in either the transient or sustained phases of calcium release (**Figure 4.3.7**). The effects of different concentrations of quinine on T2R4 desensitization were also analyzed in these GRK KD cells. Concentrations of quinine starting with its EC_{50} value for T2R4 (1.0 mM) and lower, showed significant differences in GRK3 and GRK6-KD cells compared to the scrambled shRNA control. The results indicate that the receptor remains sensitized for a longer period, in response to quinine, in the absence of the involved kinases (**Figure 4.3.7**). A KD of only 40% could be achieved for GRK2 at the RNA level in HEK293T cells, as analyzed by quantitative-PCR. Whether this GRK is not involved in T2R4 desensitization or a more efficient KD is required needs to be probed. Thus the role of GRK2 in quinine-mediated desensitization cannot be ruled out. GRK2, also known as βARK, is highly specific for the agonist-activated form of the β2AR (Benovic et al., 1987; Benovic et al., 1988). It would have been worthwhile to include β_2-adrenergic receptor (β2AR) as a control GPCR to monitor GRK2 knockdown in HEK293T cells and to assess role of GRK2 in T2R4 desensitization.

In addition to this GRK-mediated effect, the role of PKC in regulation of T2R4 signaling was also assessed. The experiments with PKC activator and inhibitor, at 0.1 μM PMA and 10 μM Bis1, revealed the involvement of PKC in the regulation of T2R4 signaling

at higher concentrations of 5 mM quinine, with significance of *p<0.05 compared to untreated T2R4 (**Figure 4.3.9A and 4.3.9B**). No involvement of PKC in T2R4 desensitization was observed with 1 mM quinine (**Figure 4.3.9B**). To explore further the potential role of PKC in T2R4 desensitization, the effects of Bis1 and PMA on 1 mM quinine pretreated T2R4-expressing HEK293T cells were studied. However, no significant change was observed in quinine promoted T2R4 desensitization with PKC activation or inhibition (**Figure 4.3.9C**). A 15 min pretreatment of T2R4-expressing cells with PMA and quinine and successive exposure to quinine (PMA+qui+qui) resulted in reduced receptor desensitization (**Figure 4.3.9C**). A likely explanation for this can be that the affinity of a desensitized receptor to its agonist is weaker than of an active receptor. Given the chaperone activity observed for quinine, this results in more number of T2R4 on the cell surface. It in turn leads to increased calcium response with successive exposure of quinine. It is the second treatment of agonist which causes actual desensitization of the receptor in PMA+qui+qui treatment. The results thus indicate that GRKs are predominantly involved in T2R4 desensitization.

In many GPCRs, receptor phosphorylation leads to agonist induced internalization. Therefore, quinine-incubation was expected to cause T2R4 internalization. In contrast, quinine treatment caused an increase in cell surface trafficking of T2R4 in a time-dependent manner (**Figure 4.3.11**). However, other bitter compounds shown to activate T2R4, yohimbine, DB, dapsone and parthenolide did not cause any significant increase in T2R4 cell surface trafficking (**Figure 4.3.10A**). Interestingly, these compounds did not lead to receptor internalization either.

To assess the cause of increased T2R4 expression, it was analyzed if quinine was causing any post-translational changes. Quinine incubation, in the presence of BFA, revealed

that quinine-induced translocation of T2R4 to the plasma membrane was BFA-sensitive. Following synthesis in the endoplasmic reticulum (ER), correctly folded GPCRs traffic to the Golgi and are targeted to the plasma membrane in their mature form. ER functions as a quality control system in cells which retains the misfolded proteins for degradation (Ellgaard and Helenius, 2003). By disrupting the Golgi apparatus, BFA interrupts maturation and membrane targeting of the receptor. BFA treatment for 4 h inhibited receptor trafficking to the cell surface and showed expression of T2R4 comparable to that of control (**Figure 4.3.10B**). This data might be suggestive that only 50% of the synthesized T2Rs reach the mature form, and are targeted to the plasma membrane under basal conditions. GPCRs, except rhodopsin, are expressed at very low levels in native systems (Palczewski et al., 2000). Different strategies, like codon optimization and use of export tags at N-terminus, have been used to enhance the expression of T2Rs in heterologous systems (Pronin et al., 2004; Pydi et al., 2013). It may be concluded that quinine acts intracellularly to enhance T2R4 expression and acts as a pharmacological chaperone for T2R4.

The chaperone-like effects of agonists and antagonists have been previously reported where they can stabilize the native conformation of GPCRs and facilitate their export from ER to plasma membrane and protein maturation (Bernier et al., 2004; Chen et al., 2006). Such functional rescue suggests that pharmacological chaperones represent novel therapeutic agents for the treatment of conformational diseases (Bernier et al., 2004; Petaja-Repo et al., 2002; Petaja-Repo et al., 2000). It raises the question as to why the other T2R4 agonists tested did not result in an upregulation of its expression. Studies report that nonpeptide ligands behave as pharmacological chaperones to facilitate anterograde trafficking of the receptor along the biosynthesis pathway, indicating that membrane permeability is required

for the chaperone roles (Chen et al., 2006). Thus the agonist, like quinine, should be cell-permeable (Zubare-Samuelov et al., 2005) to act intracellularly and affect biosynthesis of the protein to produce chaperone effects. However, as data from this study indicates, this chaperone activity is both receptor and agonist-specific. In addition to its antimalarial action, quinine is capable of eliciting bronchodilation in asthmatic models (Deshpande et al., 2010; Zhang et al., 2013). Chemical chaperones were shown to have therapeutic potential in the treatment of asthma (Makhija et al., 2014). The chaperone action of quinine can, thus, have significant implications in its development as an inhalation bronchodilator drug for the treatment of asthma.

Recent studies demonstrate that residues involved in GPCR desensitization and internalization do not strictly overlap (Bray et al., 2014; Butcher et al., 2014; Ouedraogo et al., 2008). Agonists like morphine produce desensitization of mu-opiod receptors without their significant internalization (Williams et al., 2013). Data from this study supports this emerging evidence that GPCR desensitization and internalization are significantly independent processes. A summary of quinine-mediated T2R4 desensitization and trafficking is provided in **Figure 5.3.1**.

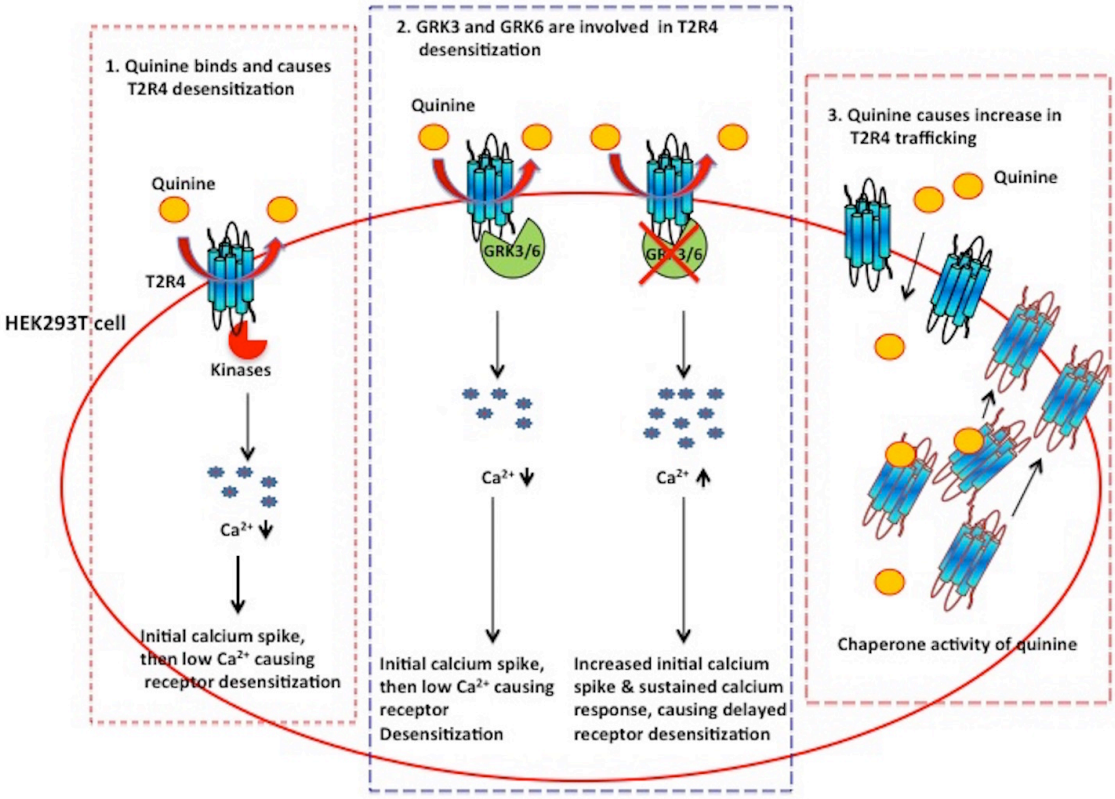

Figure 5.3.1. Schematic representation of quinine-mediated T2R4 desensitization and trafficking. The different events are divided in three parts represented by dashed boxes. [**1**]. Quinine binds to T2R4 and causes receptor desensitization. GPCRs that undergo desensitization respond to agonist with an initial Ca^{2+} spike, kinases bind to phosphorylated receptor, leading to reduction in Ca^{2+} response. [**2**]. GRK3 and GRK6 are involved in T2R4 desensitization, which is depicted by knockdown of endogenous GRKs in HEK293T cells. [**3**]. Quinine causes increase in T2R4 trafficking which is both receptor and agonist-specific. This suggests a novel pharmacochaperone activity of quinine.

5.4 Elucidation of the role of intracellular serine and threonine residues in T2R4 signaling

The potential serine and threonine residues involved in T2R4 desensitization were characterized by assessing their surface expression and IP_3 mobilization in response to quinine. The four serines in ICL1 are situated at positions 46 and 50-52, forming a triad at the latter position. In ICL2, serines are located at positions 124 and 134, with no serine residues in ICL3 or the C-terminus of T2R4 **(Figure 4.4.1)**. The seven threonines are located one each in ICLs 1 and 2, two in ICL3 and three in the C-terminus **(Figure 4.4.1)**. Replacement of Ser50 with alanine completely internalized the receptor with loss of function **(Figure 4.4.2 and Figure 4.4.6)**. Receptor localization was confirmed by IF microscopy **(Figure 4.4.4)**. Ser50 is, thus, important for both receptor expression and function. The increased function of S46A could be likely due to increase in its surface expression with quinine. Surface expression of quinine-treated T42A and S52A was similar to WT-T2R4, but both mutants displayed significant increase in IP_3 generation **(Figure 4.4.6B and 4.4.7B)**, suggesting that Thr42, Ser46 and Ser52 could be the potential residues involved in T2R4 phosphorylation. All the three residues are located in the ICL1 of T2R4. There was no significant effect of quinine on surface expression of S124A and S134A compared to the respective untreated receptors. These receptors displayed partial loss of function in comparison to WT-T2R4. Mutation of Ser124 and Ser134 might be affecting the binding of receptor to quinine, thus reducing function and affecting T2R4 trafficking to the cell surface. No effect of quinine was observed on surface expression of T223A, T230A, T291A, T297A and T298A **(figure 4.4.3B)**. Low quinine-induced expression and function of T230A, T297A and T298A could be explained by their low surface expression in transfected HEK293T cells

(Figure 4.4.3 and 4.4.7). This data is indicative of Ser124 and Ser134 (located in ICL2), and Thr223, Thr291 (located in ICL3 and C-terminus respectively) being the likely residues which affect quinine-mediated T2R4 trafficking, thus causing increase in T2R4 surface expression. Thus, in this study, the potential residues involved in T2R4 phosphorylation and quinine-induce receptor trafficking (Thr42, Ser46, Ser52, Ser124, Ser134, Thr223 and Thr291) were identified. Hence, it can be proposed that serine and threonine phosphorylation of specific intracellular residues of T2R4 is involved in receptor trafficking to the cell surface. In contrast to the downregulation of surface expression, the molecular basis for the role of phosphorylation in promoting cell surface trafficking is less well understood. Studies reveal that 14-3-3 proteins, which specifically recognize phosphorylated serine and threonine residues, mediate cell surface trafficking of various membrane proteins. The hypothetical models for the effects of 14-3-3 binding on the trafficking of membrane proteins include a masking, scaffolding or clamping of proteins (Dougherty and Morrison, 2004; Mackintosh, 2004; Mrowiec and Schwappach, 2006). Sorting signals are physically masked by 14-3-3 binding to the nearby phosphorylated serines or threonines. This blocks the access of transport machineries like COPI proteins to the sorting signal and leads to upregulation of receptors at membrane (Mant et al., 2011). In scaffolding, dimeric 14-3-3 facilitates the interaction of cargo proteins with transport machineries (Mrowiec and Schwappach, 2006). However, if these proteins are involved in regulating receptor trafficking of T2R4 is not known. Whether these S/T residues are specific for quinine-induced receptor phosphorylation and desensitization, or are potential targets with other agonists also, needs to be explored. If these residues are the potential serines or threonines involved in GRK-mediated desensitization of T2R4, needs further investigation. It would be worthwhile to analyze the

role of serine and threonine residues in T2R4 phosphorylation and desensitization by using another agonist which does not behave as a pharmacological chaperone for T2R4. Mass spectrometric analysis to determine the phosphorylation pattern of human T2R4 is a topic of future consideration.

CHAPTER 6

6.0 CONCLUSION AND FUTURE DIRECTIONS

6.1 Conclusion

Following the discovery of T2Rs a little more than a decade ago, bitter taste research was focused on T2R deorphanization, i.e., characterizing suitable bitter compounds which could activate T2Rs. Molecular modeling and structure-function studies pursued to elucidate the receptor-agonist interactions have been successful in providing novel insights into the mechanism of T2R activation. Recently, the major area of focus of bitter taste research has been elucidation of T2R function in extra-oral tissues. The discovery of T2R function in airway muscle relaxation and bronchodilation has implicated their role as potential therapeutic targets in the treatment of asthma. Considering the tremendous potential of T2Rs in extra-oral tissues, it is important to understand how these receptors are desensitized and T2R signal is terminated. In this thesis project, I have determined the expression and function of T2R1 in PASMCs, and porcine arterial and airway rings, analyzed the structure-function role of C-terminal tail in T2R4 signaling, and characterized the desensitization mechanism of T2R4 transiently expressed in HEK293T cells.

To explore the role of T2Rs in vascular tissues, PASMCs were selected for the study. The expression of 25 T2Rs in hPASMCs was characterized by RT-PCR. Majority of the T2Rs are expressed in these cells. T2R1 was selected for further study, and expression of T2R1 in hPASMCs was confirmed by different techniques. Studies for determining the function of T2R1 and the effects of DXM on pulmonary artery were pursued in a neonatal

porcine model. Novel findings from this study suggest that in the pulmonary circuit DXM acts as a vasoconstrictor, and shows that DXM mediated activation of endogenous T2R1 in pulmonary tissues leads to vasoconstrictor responses. Bitter stimuli can enter the pulmonary circuit after ingestion, during inhalation, or generated during pathological conditions. The vasoconstrictor response mediated by T2R1 activation can be an additional defensive mechanism of the body to detect and eliminate noxious and harmful stimuli. The novel role of T2Rs in vasoconstriction reported here adds to the growing body of evidence, which suggest T2Rs expressed in extra-oral tissues as mediators of off-target effects of diverse bitter tasting pharmaceuticals.

Studies aimed at deciphering the desensitization mechanism of T2Rs are very scarce. For this, using site-directed mutagenesis, the role of 16 residues of T2R4 C-terminus was examined. In this study, the effect of these C-terminus mutations on plasma membrane trafficking was analyzed, and their function in response to the T2R4 agonist quinine was characterized. This study identified both conserved and receptor specific motifs in the C-terminus of T2Rs. Residues in these motifs play different roles in receptor function. Majority of the mutants, which displayed reduced surface expression fall in the MPBR of T2R4 C-terminus. A conserved KLK/R motif in T2Rs is important for receptor trafficking and activation. Of the two dibasic KK motifs present in the C-terminus of T2R4, the KK motif present at the proximal end and made of Lys300 and Lys301 is important for cell surface expression of T2R4. Additionally, our results revealed a CAM, K296A, indicating that Lys296 of the KLK motif is important for stabilizing the active conformation of T2Rs. Taken together, results from this study provide novel insights into the role of conserved residues and MPBRs in the C-terminus of T2Rs in receptor expression and activation.

The next study of my thesis project involved characterization of desensitization and trafficking of T2R4, transiently expressed in HEK293T cells, in response to quinine. The GRKs involved in T2R4 desensitization were identified by performing GRK knockdown in HEK293T cells. Additionally, the role of PKC in this process was assessed by using PKC activator and inhibitor. The results of this study conclude that serine and threonine residues of T2R4 get rapidly phosphorylated in response to quinine stimulation. GRKs, predominantly GRK3 and GRK6, are the major players involved in the desensitization of T2R4. No involvement of PKC was observed in T2R4 desensitization with 1 mM quinine. T2R4 does not get internalized upon agonist stimulation, instead, quinine positively influences T2R4 trafficking by acting as a pharmacological chaperone. This study provides novel insights into the molecular mechanisms leading to human bitter taste signal termination.

To elucidate the intracellular residues involved in T2R4 desensitization, potential serine and threonine residues in the ICLs and C-terminus of T2R4 were characterized by measuring receptor function and surface expression. Data from this study indicates that Thr42, Ser46 and Ser52 are the potential residues likely involved in T2R4 phosphorylation. This needs to be investigated in greater detail. For example, by replacing these residues with structurally or functionally similar amino acid and pursuing structure-function and mass spectrometry.

6.2 Future directions

Since the discovery of T2Rs in the year 2000, the focus of bitter taste research has changed considerably over the years. After the successful deorphanization of the majority of human T2Rs, detailed studies on the mechanism of agonist interaction have begun to reveal how these enormously versatile receptors accommodate so many different compounds in their binding pockets. Considering the importance of T2Rs in non-gustatory tissues, more studies are needed to understand their desensitization mechanisms including phosphorylation, internalization, β-arrestin binding and ubiquitination.

The role of T2R4 C-terminus residues in quinine-mediated receptor trafficking needs to be further investigated. In comparison to other well studied GPCR classes, structure-function studies on T2Rs are hampered by a number of factors. A major limitation with pursuing structure-function analysis of T2Rs is the lack of labelled ligands, either a radioligand or fluorescent ligand. In the absence of labelled ligands, characterizing ligand binding properties, such as binding affinity for agonists and antagonists is currently not feasible. Furthermore, the large number of T2Rs, their differential expression in a number of tissues, and cross reactivity of their ligands or ability of one ligand to act on multiple T2Rs shows that a complex mechanism of signal transduction is at play. The role of intracellular serine and threonine residues in GRK and PKC-mediated desensitization of T2R4 need to be probed. Quinine has multiple actions; a pharmacological chaperone of T2R4, is cell permeable, can directly activate G-proteins, can interact with and inhibit GRKs. If a selective agonist for T2R4 could be characterized, it would prove to be an optimal choice to study receptor desensitization and phosphorylation of mutant constructs. This is crucial to the

development of T2Rs as specific therapeutic targets in the future. Few blockers of bitter taste have been discovered, however, there is an urgent need to find T2R antagonists and inverse agonists with high selectivity and efficacy, so that the consumption of healthy bitter foods and drug compliance can be increased. This will also lead to crystallization studies for these receptors which is highly required for elucidation of their three-dimensional structure. Mass spectroscopic analysis and site-directed mutagenesis studies will provide details into the phosphorylation pattern, desensitization and trafficking of human T2Rs. The detailed knowledge on bitter receptor architecture, agonist binding pockets and bitter receptor inhibitors, desensitization mechanisms may even allow the rational design of novel bitter receptor modulators which will have an impact on both applied as well as basic taste research.

CHAPTER 7

7.0 REFERENCES

Adler, E., Hoon, M.A., Mueller, K.L., Chandrashekar, J., Ryba, N.J., and Zuker, C.S. (2000). A novel family of mammalian taste receptors. Cell *100*, 693-702.

Aittaleb, M., Boguth, C.A., and Tesmer, J.J. (2010). Structure and function of heterotrimeric G protein-regulated Rho guanine nucleotide exchange factors. Molecular pharmacology *77*, 111-125.

Akao, H., Polisecki, E., Kajinami, K., Trompet, S., Robertson, M., Ford, I., Jukema, J.W., de Craen, A.J., Westendorp, R.G., Shepherd, J.*, et al.* (2012). KIF6, LPA, TAS2R50, and VAMP8 genetic variation, low density lipoprotein cholesterol lowering response to pravastatin, and heart disease risk reduction in the elderly. Atherosclerosis *220*, 456-462.

Alvarez, Y., Briones, A.M., Hernanz, R., Perez-Giron, J.V., Alonso, M.J., and Salaices, M. (2008). Role of NADPH oxidase and iNOS in vasoconstrictor responses of vessels from hypertensive and normotensive rats. British journal of pharmacology *153*, 926-935.

An, S.S., Wang, W.C., Koziol-White, C.J., Ahn, K., Lee, D.Y., Kurten, R.C., Panettieri, R.A., Jr., and Liggett, S.B. (2012). TAS2R activation promotes airway smooth muscle relaxation despite beta(2)-adrenergic receptor tachyphylaxis. American journal of physiology Lung cellular and molecular physiology *303*, L304-311.

Angus, J.A., and Wright, C.E. (2000). Techniques to study the pharmacodynamics of isolated large and small blood vessels. Journal of pharmacological and toxicological methods *44*, 395-407.

Anliker, J.A., Bartoshuk, L., Ferris, A.M., and Hooks, L.D. (1991). Children's food preferences and genetic sensitivity to the bitter taste of 6-n-propylthiouracil (PROP). The American journal of clinical nutrition *54*, 316-320.

Arakawa, M., Chakraborty, R., Upadhyaya, J., Eilers, M., Reeves, P.J., Smith, S.O., and Chelikani, P. (2011). Structural and functional roles of small group-conserved amino acids present on helix-H7 in the beta(2)-adrenergic receptor. Biochimica et biophysica acta *1808*, 1170-1178.

Barlowe, C. (2003). Signals for COPII-dependent export from the ER: what's the ticket out? Trends Cell Biol *13*, 295-300.

Bartoshuk, L.M. (2000a). Comparing sensory experiences across individuals: recent psychophysical advances illuminate genetic variation in taste perception. Chemical senses *25*, 447-460.

Bartoshuk, L.M. (2000b). Psychophysical advances aid the study of genetic variation in taste. Appetite *34*, 105.

Bartoshuk, L.M., Duffy, V.B., and Miller, I.J. (1994). PTC/PROP tasting: anatomy, psychophysics, and sex effects. Physiology & behavior *56*, 1165-1171.

Basson, M.D., Bartoshuk, L.M., Dichello, S.Z., Panzini, L., Weiffenbach, J.M., and Duffy, V.B. (2005). Association between 6-n-propylthiouracil (PROP) bitterness and colonic neoplasms. Digestive diseases and sciences *50*, 483-489.

Behrens, M., Brockhoff, A., Kuhn, C., Bufe, B., Winnig, M., and Meyerhof, W. (2004). The human taste receptor hTAS2R14 responds to a variety of different bitter compounds. Biochemical and biophysical research communications *319*, 479-485.

Behrens, M., Foerster, S., Staehler, F., Raguse, J.D., and Meyerhof, W. (2007). Gustatory expression pattern of the human TAS2R bitter receptor gene family reveals a heterogenous population of bitter responsive taste receptor cells. The Journal of neuroscience : the official journal of the Society for Neuroscience *27*, 12630-12640.

Bell, K.I., and Tepper, B.J. (2006). Short-term vegetable intake by young children classified by 6-n-propylthoiuracil bitter-taste phenotype. The American journal of clinical nutrition *84*, 245-251.

Benovic, J.L., Mayor, F., Jr., Staniszewski, C., Lefkowitz, R.J., and Caron, M.G. (1987). Purification and characterization of the beta-adrenergic receptor kinase. The Journal of biological chemistry *262*, 9026-9032.

Benovic, J.L., Staniszewski, C., Mayor, F., Jr., Caron, M.G., and Lefkowitz, R.J. (1988). beta-Adrenergic receptor kinase. Activity of partial agonists for stimulation of adenylate cyclase correlates with ability to promote receptor phosphorylation. The Journal of biological chemistry *263*, 3893-3897.

Bermak, J.C., Li, M., Bullock, C., and Zhou, Q.Y. (2001). Regulation of transport of the dopamine D1 receptor by a new membrane-associated ER protein. Nature cell biology *3*, 492-498.

Bernhardt, S.J., Naim, M., Zehavi, U., and Lindemann, B. (1996). Changes in IP3 and cytosolic Ca2+ in response to sugars and non-sugar sweeteners in transduction of sweet taste in the rat. J Physiol *490 (Pt 2)*, 325-336.

Bernier, V., Bichet, D.G., and Bouvier, M. (2004). Pharmacological chaperone action on G-protein-coupled receptors. Current opinion in pharmacology *4*, 528-533.

Biarnes, X., Marchiori, A., Giorgetti, A., Lanzara, C., Gasparini, P., Carloni, P., Born, S., Brockhoff, A., Behrens, M., and Meyerhof, W. (2010). Insights into the binding of Phenyltiocarbamide (PTC) agonist to its target human TAS2R38 bitter receptor. PloS one *5*, e12394.

Blake, A.D., Bot, G., Freeman, J.C., and Reisine, T. (1997). Differential opioid agonist regulation of the mouse mu opioid receptor. The Journal of biological chemistry *272*, 782-790.

Bohm, S.K., Khitin, L.M., Smeekens, S.P., Grady, E.F., Payan, D.G., and Bunnett, N.W. (1997). Identification of potential tyrosine-containing endocytic motifs in the carboxyl-tail and seventh transmembrane domain of the neurokinin 1 receptor. The Journal of biological chemistry *272*, 2363-2372.

Born, S., Levit, A., Niv, M.Y., Meyerhof, W., and Behrens, M. (2013). The human bitter taste receptor TAS2R10 is tailored to accommodate numerous diverse ligands. The Journal of neuroscience : the official journal of the Society for Neuroscience *33*, 201-213.

Bray, L., Froment, C., Pardo, P., Candotto, C., Burlet-Schiltz, O., Zajac, J.M., Mollereau, C., and Mouledous, L. (2014). Identification and functional characterization of the phosphorylation sites of the neuropeptide FF2 receptor. The Journal of biological chemistry *289*, 33754-33766.

Brockhoff, A., Behrens, M., Massarotti, A., Appendino, G., and Meyerhof, W. (2007). Broad tuning of the human bitter taste receptor hTAS2R46 to various sesquiterpene lactones, clerodane and labdane diterpenoids, strychnine, and denatonium. Journal of agricultural and food chemistry *55*, 6236-6243.

Brockhoff, A., Behrens, M., Niv, M.Y., and Meyerhof, W. (2010). Structural requirements of bitter taste receptor activation. Proceedings of the National Academy of Sciences of the United States of America *107*, 11110-11115.

Brockhoff, A., Behrens, M., Roudnitzky, N., Appendino, G., Avonto, C., and Meyerhof, W. (2011). Receptor agonism and antagonism of dietary bitter compounds. The Journal of neuroscience : the official journal of the Society for Neuroscience *31*, 14775-14782.

Brouwer, J.N., and Wiersma, A. (1978). Location of taste buds in intact taste papillae by a selective staining method. Histochemistry *58*, 145-151.

Bufe, B., Breslin, P.A., Kuhn, C., Reed, D.R., Tharp, C.D., Slack, J.P., Kim, U.K., Drayna, D., and Meyerhof, W. (2005). The molecular basis of individual differences in

phenylthiocarbamide and propylthiouracil bitterness perception. Current biology : CB *15*, 322-327.

Bufe, B., Hofmann, T., Krautwurst, D., Raguse, J.D., and Meyerhof, W. (2002). The human TAS2R16 receptor mediates bitter taste in response to beta-glucopyranosides. Nature genetics *32*, 397-401.

Busillo, J.M., Armando, S., Sengupta, R., Meucci, O., Bouvier, M., and Benovic, J.L. (2010). Site-specific phosphorylation of CXCR4 is dynamically regulated by multiple kinases and results in differential modulation of CXCR4 signaling. The Journal of biological chemistry *285*, 7805-7817.

Butcher, A.J., Hudson, B.D., Shimpukade, B., Alvarez-Curto, E., Prihandoko, R., Ulven, T., Milligan, G., and Tobin, A.B. (2014). Concomitant action of structural elements and receptor phosphorylation determines arrestin-3 interaction with the free fatty acid receptor FFA4. The Journal of biological chemistry *289*, 18451-18465.

Campa, D., Vodicka, P., Pardini, B., Naccarati, A., Carrai, M., Vodickova, L., Novotny, J., Hemminki, K., Forsti, A., Barale, R.*, et al.* (2010). A gene-wide investigation on polymorphisms in the taste receptor 2R14 (TAS2R14) and susceptibility to colorectal cancer. BMC Med Genet *11*, 88.

Cannon, D.S., Baker, T.B., Piper, M.E., Scholand, M.B., Lawrence, D.L., Drayna, D.T., McMahon, W.M., Villegas, G.M., Caton, T.C., Coon, H.*, et al.* (2005). Associations between phenylthiocarbamide gene polymorphisms and cigarette smoking. Nicotine & tobacco research : official journal of the Society for Research on Nicotine and Tobacco *7*, 853-858.

Cao, T.T., Deacon, H.W., Reczek, D., Bretscher, A., and von Zastrow, M. (1999). A kinase-regulated PDZ-domain interaction controls endocytic sorting of the beta2-adrenergic receptor. Nature *401*, 286-290.

Carrillo-Sepulveda, M.A., and Barreto-Chaves, M.L. (2010). Phenotypic modulation of cultured vascular smooth muscle cells: a functional analysis focusing on MLC and ERK1/2 phosphorylation. Molecular and cellular biochemistry *341*, 279-289.

Caterina, M.J., Schumacher, M.A., Tominaga, M., Rosen, T.A., Levine, J.D., and Julius, D. (1997). The capsaicin receptor: a heat-activated ion channel in the pain pathway. Nature *389*, 816-824.

Cerione, R.A., Codina, J., Benovic, J.L., Lefkowitz, R.J., Birnbaumer, L., and Caron, M.G. (1984). The mammalian beta 2-adrenergic receptor: reconstitution of functional interactions between pure receptor and pure stimulatory nucleotide binding protein of the adenylate cyclase system. Biochemistry *23*, 4519-4525.

Chakraborty, R., Bhullar, R.P., Dakshinamurti, S., Hwa, J., and Chelikani, P. (2014). Inverse agonism of SQ 29,548 and Ramatroban on Thromboxane A2 receptor. PloS one *9*, e85937.

Chakraborty, R., Pydi, S.P., Gleim, S., Dakshinamurti, S., Hwa, J., and Chelikani, P. (2012). Site-directed mutations and the polymorphic variant Ala160Thr in the human thromboxane receptor uncover a structural role for transmembrane helix 4. PloS one *7*, e29996.

Chan, K.Y., Pang, R.T., and Chow, B.K. (2001). Functional segregation of the highly conserved basic motifs within the third endoloop of the human secretin receptor. Endocrinology *142*, 3926-3934.

Chandrashekar, J., Mueller, K.L., Hoon, M.A., Adler, E., Feng, L., Guo, W., Zuker, C.S., and Ryba, N.J. (2000). T2Rs function as bitter taste receptors. Cell *100*, 703-711.

Chandrashekar, J., Yarmolinsky, D., von Buchholtz, L., Oka, Y., Sly, W., Ryba, N.J., and Zuker, C.S. (2009). The taste of carbonation. Science *326*, 443-445.

Chen, X., Gabitto, M., Peng, Y., Ryba, N.J., and Zuker, C.S. (2011). A gustotopic map of taste qualities in the mammalian brain. Science *333*, 1262-1266.

Chen, Y., Chen, C., Wang, Y., and Liu-Chen, L.Y. (2006). Ligands regulate cell surface level of the human kappa opioid receptor by activation-induced down-regulation and pharmacological chaperone-mediated enhancement: differential effects of nonpeptide and peptide agonists. The Journal of pharmacology and experimental therapeutics *319*, 765-775.

Claeysen, S., Sebben, M., Becamel, C., Parmentier, M.L., Dumuis, A., and Bockaert, J. (2001). Constitutively active mutants of 5-HT4 receptors are they in unique active states? EMBO reports *2*, 61-67.

Clark, A.A., Liggett, S.B., and Munger, S.D. (2012). Extraoral bitter taste receptors as mediators of off-target drug effects. FASEB journal : official publication of the Federation of American Societies for Experimental Biology *26*, 4827-4831.

Conner, M., Hicks, M.R., Dafforn, T., Knowles, T.J., Ludwig, C., Staddon, S., Overduin, M., Gunther, U.L., Thome, J., Wheatley, M.*, et al.* (2008). Functional and biophysical analysis of the C-terminus of the CGRP-receptor; a family B GPCR. Biochemistry *47*, 8434-8444.

Conte, C., Ebeling, M., Marcuz, A., Nef, P., and Andres-Barquin, P.J. (2002). Identification and characterization of human taste receptor genes belonging to the TAS2R family. Cytogenetic and genome research *98*, 45-53.

Cook, L.B., Zhu, C.C., and Hinkle, P.M. (2003). Thyrotropin-releasing hormone receptor processing: role of ubiquitination and proteasomal degradation. Mol Endocrinol *17*, 1777-1791.

Costa, T., and Herz, A. (1989). Antagonists with negative intrinsic activity at delta opioid receptors coupled to GTP-binding proteins. Proceedings of the National Academy of Sciences of the United States of America *86*, 7321-7325.

Cvejic, S., and Devi, L.A. (1997). Dimerization of the delta opioid receptor: implication for a role in receptor internalization. The Journal of biological chemistry *272*, 26959-26964.

Deshpande, D.A., Wang, W.C., McIlmoyle, E.L., Robinett, K.S., Schillinger, R.M., An, S.S., Sham, J.S., and Liggett, S.B. (2010). Bitter taste receptors on airway smooth muscle bronchodilate by localized calcium signaling and reverse obstruction. Nature medicine *16*, 1299-1304.

Ding, Z., Kim, S., and Kunapuli, S.P. (2006). Identification of a potent inverse agonist at a constitutively active mutant of human P2Y12 receptor. Molecular pharmacology *69*, 338-345.

Dong, C., Nichols, C.D., Guo, J., Huang, W., Lambert, N.A., and Wu, G. (2012). A triple arg motif mediates alpha(2B)-adrenergic receptor interaction with Sec24C/D and export. Traffic *13*, 857-868.

Dong, C., and Wu, G. (2007). Regulation of anterograde transport of adrenergic and angiotensin II receptors by Rab2 and Rab6 GTPases. Cellular signalling *19*, 2388-2399.

Dotson, C.D., Zhang, L., Xu, H., Shin, Y.K., Vigues, S., Ott, S.H., Elson, A.E., Choi, H.J., Shaw, H., Egan, J.M.*, et al.* (2008). Bitter taste receptors influence glucose homeostasis. PloS one *3*, e3974.

Dougherty, M.K., and Morrison, D.K. (2004). Unlocking the code of 14-3-3. J Cell Sci *117*, 1875-1884.

Drewnowski, A., Henderson, S.A., and Cockroft, J.E. (2007). Genetic sensitivity to 6-n-propylthiouracil has no influence on dietary patterns, body mass indexes, or plasma lipid profiles of women. Journal of the American Dietetic Association *107*, 1340-1348.

Duffy, V.B., Davidson, A.C., Kidd, J.R., Kidd, K.K., Speed, W.C., Pakstis, A.J., Reed, D.R., Snyder, D.J., and Bartoshuk, L.M. (2004). Bitter receptor gene (TAS2R38), 6-n-propylthiouracil (PROP) bitterness and alcohol intake. Alcoholism, clinical and experimental research *28*, 1629-1637.

Duvernay, M.T., Zhou, F., and Wu, G. (2004). A conserved motif for the transport of G protein-coupled receptors from the endoplasmic reticulum to the cell surface. The Journal of biological chemistry *279*, 30741-30750.

Edelstein, B.L., and Douglass, C.W. (1995). Dispelling the myth that 50 percent of U.S. schoolchildren have never had a cavity. Public health reports *110*, 522-530; discussion 521, 531-523.

Ellgaard, L., and Helenius, A. (2003). Quality control in the endoplasmic reticulum. Nature reviews Molecular cell biology *4*, 181-191.

Essick, G.K., Chopra, A., Guest, S., and McGlone, F. (2003). Lingual tactile acuity, taste perception, and the density and diameter of fungiform papillae in female subjects. Physiology & behavior *80*, 289-302.

Fediuk, J., Gutsol, A., Nolette, N., and Dakshinamurti, S. (2012). Thromboxane-induced actin polymerization in hypoxic pulmonary artery is independent of Rho. American journal of physiology Lung cellular and molecular physiology *302*, L13-26.

Ferguson, S.S. (2001). Evolving concepts in G protein-coupled receptor endocytosis: the role in receptor desensitization and signaling. Pharmacological reviews *53*, 1-24.

Finger, T.E., Bottger, B., Hansen, A., Anderson, K.T., Alimohammadi, H., and Silver, W.L. (2003). Solitary chemoreceptor cells in the nasal cavity serve as sentinels of respiration. Proceedings of the National Academy of Sciences of the United States of America *100*, 8981-8986.

Finger, T.E., Danilova, V., Barrows, J., Bartel, D.L., Vigers, A.J., Stone, L., Hellekant, G., and Kinnamon, S.C. (2005). ATP signaling is crucial for communication from taste buds to gustatory nerves. Science *310*, 1495-1499.

Fischer, R., Griffin, F., and Rockey, M.A. (1966). Gustatory chemoreception in man: multidisciplinary aspects and perspectives. Perspectives in biology and medicine *9*, 549-577.

Floriano, W.B., Hall, S., Vaidehi, N., Kim, U., Drayna, D., and Goddard, W.A., 3rd (2006). Modeling the human PTC bitter-taste receptor interactions with bitter tastants. Journal of molecular modeling *12*, 931-941.

Foster, S.R., Porrello, E.R., Purdue, B., Chan, H.W., Voigt, A., Frenzel, S., Hannan, R.D., Moritz, K.M., Simmons, D.G., Molenaar, P.*, et al.* (2013). Expression, regulation and putative nutrient-sensing function of taste GPCRs in the heart. PloS one *8*, e64579.

Fotiadis, D., Liang, Y., Filipek, S., Saperstein, D.A., Engel, A., and Palczewski, K. (2003). Atomic-force microscopy: Rhodopsin dimers in native disc membranes. Nature *421*, 127-128.

Fox, A.L. (1932). The Relationship between Chemical Constitution and Taste. Proceedings of the National Academy of Sciences of the United States of America *18*, 115-120.

Fredriksson, R., Lagerstrom, M.C., Lundin, L.G., and Schioth, H.B. (2003). The G-protein-coupled receptors in the human genome form five main families. Phylogenetic analysis, paralogon groups, and fingerprints. Molecular pharmacology *63*, 1256-1272.

Geiss, G.K., Bumgarner, R.E., Birditt, B., Dahl, T., Dowidar, N., Dunaway, D.L., Fell, H.P., Ferree, S., George, R.D., Grogan, T.*, et al.* (2008). Direct multiplexed measurement of gene expression with color-coded probe pairs. Nature biotechnology *26*, 317-325.

Gilbertson, T.A., Damak, S., and Margolskee, R.F. (2000). The molecular physiology of taste transduction. Current opinion in neurobiology *10*, 519-527.

Giraudo, C.G., and Maccioni, H.J. (2003). Endoplasmic reticulum export of glycosyltransferases depends on interaction of a cytoplasmic dibasic motif with Sar1. Molecular biology of the cell *14*, 3753-3766.

Glendinning, J.I., Yiin, Y.M., Ackroff, K., and Sclafani, A. (2008). Intragastric infusion of denatonium conditions flavor aversions and delays gastric emptying in rodents. Physiology & behavior *93*, 757-765.

Goldstein, G.L., Daun, H., and Tepper, B.J. (2005). Adiposity in middle-aged women is associated with genetic taste blindness to 6-n-propylthiouracil. Obesity research *13*, 1017-1023.

Gong, Y., Yi, M., Fediuk, J., Lizotte, P.P., and Dakshinamurti, S. (2010). Hypoxic neonatal pulmonary arterial myocytes are sensitized to ROS-generated 8-isoprostane. Free radical biology & medicine *48*, 882-894.

Greene, T.A., Alarcon, S., Thomas, A., Berdougo, E., Doranz, B.J., Breslin, P.A., and Rucker, J.B. (2011). Probenecid inhibits the human bitter taste receptor TAS2R16 and suppresses bitter perception of salicin. PloS one *6*, e20123.

Guo, Q., Subramanian, H., Gupta, K., and Ali, H. (2011). Regulation of C3a receptor signaling in human mast cells by G protein coupled receptor kinases. PloS one *6*, e22559.

Habibian, M., Roberts, G., Lawson, M., Stevenson, R., and Harris, S. (2001). Dietary habits and dental health over the first 18 months of life. Community dentistry and oral epidemiology *29*, 239-246.

Hancock, J.F., Cadwallader, K., Paterson, H., and Marshall, C.J. (1991). A CAAX or a CAAL motif and a second signal are sufficient for plasma membrane targeting of ras proteins. The EMBO journal *10*, 4033-4039.

Hansen, J.L., and Sheikh, S.P. (2004). Functional consequences of 7TM receptor dimerization. Eur J Pharm Sci *23*, 301-317.

Hao, S., Dulake, M., Espero, E., Sternini, C., Raybould, H.E., and Rinaman, L. (2009). Central Fos expression and conditioned flavor avoidance in rats following intragastric administration of bitter taste receptor ligands. American journal of physiology Regulatory, integrative and comparative physiology *296*, R528-536.

He, W., Danilova, V., Zou, S., Hellekant, G., Max, M., Margolskee, R.F., and Damak, S. (2002). Partial rescue of taste responses of alpha-gustducin null mice by transgenic expression of alpha-transducin. Chemical senses *27*, 719-727.

Hebert, T.E., Moffett, S., Morello, J.P., Loisel, T.P., Bichet, D.G., Barret, C., and Bouvier, M. (1996). A peptide derived from a beta2-adrenergic receptor transmembrane domain inhibits both receptor dimerization and activation. The Journal of biological chemistry *271*, 16384-16392.

Heck, G.L., Mierson, S., and DeSimone, J.A. (1984). Salt taste transduction occurs through an amiloride-sensitive sodium transport pathway. Science *223*, 403-405.

Hedge, A.M., and Sharma, A. (2008). Genetic sensitivity to 6-n-propylthiouracil (PROP) as a screening tool for obesity and dental caries in children. The Journal of clinical pediatric dentistry *33*, 107-111.

Heilker, R., Manning-Krieg, U., Zuber, J.F., and Spiess, M. (1996). In vitro binding of clathrin adaptors to sorting signals correlates with endocytosis and basolateral sorting. The EMBO journal *15*, 2893-2899.

Herrick-Davis, K., Grinde, E., Harrigan, T.J., and Mazurkiewicz, J.E. (2005). Inhibition of serotonin 5-hydroxytryptamine2c receptor function through heterodimerization: receptor dimers bind two molecules of ligand and one G-protein. The Journal of biological chemistry *280*, 40144-40151.

Hinton, M., Gutsol, A., and Dakshinamurti, S. (2007). Thromboxane hypersensitivity in hypoxic pulmonary artery myocytes: altered TP receptor localization and kinetics. American journal of physiology Lung cellular and molecular physiology *292*, L654-663.

Horn, F., Bettler, E., Oliveira, L., Campagne, F., Cohen, F.E., and Vriend, G. (2003). GPCRDB information system for G protein-coupled receptors. Nucleic acids research *31*, 294-297.

Huang, Y., Niwa, J., Sobue, G., and Breitwieser, G.E. (2006). Calcium-sensing receptor ubiquitination and degradation mediated by the E3 ubiquitin ligase dorfin. The Journal of biological chemistry *281*, 11610-11617.

Hunziker, W., and Fumey, C. (1994). A di-leucine motif mediates endocytosis and basolateral sorting of macrophage IgG Fc receptors in MDCK cells. The EMBO journal *13*, 2963-2969.

Illing, M.E., Rajan, R.S., Bence, N.F., and Kopito, R.R. (2002). A rhodopsin mutant linked to autosomal dominant retinitis pigmentosa is prone to aggregate and interacts with the ubiquitin proteasome system. The Journal of biological chemistry *277*, 34150-34160.

Inoue, H., Nojima, H., and Okayama, H. (1990). High efficiency transformation of Escherichia coli with plasmids. Gene *96*, 23-28.

Janssen, S., Laermans, J., Verhulst, P.J., Thijs, T., Tack, J., and Depoortere, I. (2011). Bitter taste receptors and alpha-gustducin regulate the secretion of ghrelin with functional effects on food intake and gastric emptying. Proceedings of the National Academy of Sciences of the United States of America *108*, 2094-2099.

Jastrzebska, B., Fotiadis, D., Jang, G.F., Stenkamp, R.E., Engel, A., and Palczewski, K. (2006). Functional and structural characterization of rhodopsin oligomers. The Journal of biological chemistry *281*, 11917-11922.

Jones, K.A., Borowsky, B., Tamm, J.A., Craig, D.A., Durkin, M.M., Dai, M., Yao, W.J., Johnson, M., Gunwaldsen, C., Huang, L.Y.*, et al.* (1998). GABA(B) receptors function as a heteromeric assembly of the subunits GABA(B)R1 and GABA(B)R2. Nature *396*, 674-679.

Karrer, T., and Bartoshuk, L. (1991). Capsaicin desensitization and recovery on the human tongue. Physiology & behavior *49*, 757-764.

Keller, K.L., Steinmann, L., Nurse, R.J., and Tepper, B.J. (2002). Genetic taste sensitivity to 6-n-propylthiouracil influences food preference and reported intake in preschool children. Appetite *38*, 3-12.

Keller, K.L., and Tepper, B.J. (2004). Inherited taste sensitivity to 6-n-propylthiouracil in diet and body weight in children. Obesity research *12*, 904-912.

Kim, J., Ahn, S., Ren, X.R., Whalen, E.J., Reiter, E., Wei, H., and Lefkowitz, R.J. (2005a). Functional antagonism of different G protein-coupled receptor kinases for beta-arrestin-mediated angiotensin II receptor signaling. Proceedings of the National Academy of Sciences of the United States of America *102*, 1442-1447.

Kim, M.R., Kusakabe, Y., Miura, H., Shindo, Y., Ninomiya, Y., and Hino, A. (2003a). Regional expression patterns of taste receptors and gustducin in the mouse tongue. Biochemical and biophysical research communications *312*, 500-506.

Kim, U., Wooding, S., Ricci, D., Jorde, L.B., and Drayna, D. (2005b). Worldwide haplotype diversity and coding sequence variation at human bitter taste receptor loci. Human mutation *26*, 199-204.

Kim, U.K., Jorgenson, E., Coon, H., Leppert, M., Risch, N., and Drayna, D. (2003b). Positional cloning of the human quantitative trait locus underlying taste sensitivity to phenylthiocarbamide. Science *299*, 1221-1225.

Kinnamon, S.C., Dionne, V.E., and Beam, K.G. (1988). Apical localization of K+ channels in taste cells provides the basis for sour taste transduction. Proceedings of the National Academy of Sciences of the United States of America *85*, 7023-7027.

Klausner, R.D., Lippincott-Schwartz, J., and Bonifacino, J.S. (1990). The T cell antigen receptor: insights into organelle biology. Annu Rev Cell Biol *6*, 403-431.

Kohout, T.A., and Lefkowitz, R.J. (2003). Regulation of G protein-coupled receptor kinases and arrestins during receptor desensitization. Molecular pharmacology *63*, 9-18.

Kroeger, K.M., and Eidne, K.A. (2004). Study of G-protein-coupled receptor-protein interactions by bioluminescence resonance energy transfer. Methods Mol Biol *259*, 323-333.

Kuhn, C., Bufe, B., Batram, C., and Meyerhof, W. (2010). Oligomerization of TAS2R bitter taste receptors. Chemical senses *35*, 395-406.

Kuhn, C., Bufe, B., Winnig, M., Hofmann, T., Frank, O., Behrens, M., Lewtschenko, T., Slack, J.P., Ward, C.D., and Meyerhof, W. (2004). Bitter taste receptors for saccharin and acesulfame K. The Journal of neuroscience : the official journal of the Society for Neuroscience *24*, 10260-10265.

Kuner, R., Kohr, G., Grunewald, S., Eisenhardt, G., Bach, A., and Kornau, H.C. (1999). Role of heteromer formation in GABAB receptor function. Science *283*, 74-77.

Kunishima, N., Shimada, Y., Tsuji, Y., Sato, T., Yamamoto, M., Kumasaka, T., Nakanishi, S., Jingami, H., and Morikawa, K. (2000). Structural basis of glutamate recognition by a dimeric metabotropic glutamate receptor. Nature *407*, 971-977.

Kurihara, K., Katsuragi, Y., Matsuoka, I., Kashiwayanagi, M., Kumazawa, T., and Shoji, T. (1994). Receptor mechanisms of bitter substances. Physiology & behavior *56*, 1125-1132.

Lalonde, E.R., and Eglitis, J.A. (1961). Number and distribution of taste buds on the epiglottis, pharynx, larynx, soft palate and uvula in a human newborn. The Anatomical record *140*, 91-95.

Ledda, M., Kutalik, Z., Souza Destito, M.C., Souza, M.M., Cirillo, C.A., Zamboni, A., Martin, N., Morya, E., Sameshima, K., Beckmann, J.S.*, et al.* (2013). GWAS of human bitter taste perception identifies new loci and reveals additional complexity of bitter taste genetics. Human molecular genetics.

Lee, R.J., Chen, B., Redding, K.M., Margolskee, R.F., and Cohen, N.A. (2013). Mouse nasal epithelial innate immune responses to Pseudomonas aeruginosa quorum-sensing molecules require taste signaling components. Innate immunity *20*, 606-617.

Lee, R.J., and Cohen, N.A. (2013). The emerging role of the bitter taste receptor T2R38 in upper respiratory infection and chronic rhinosinusitis. American journal of rhinology & allergy *27*, 283-286.

Lee, R.J., Xiong, G., Kofonow, J.M., Chen, B., Lysenko, A., Jiang, P., Abraham, V., Doghramji, L., Adappa, N.D., Palmer, J.N.*, et al.* (2012). T2R38 taste receptor polymorphisms underlie susceptibility to upper respiratory infection. The Journal of clinical investigation *122*, 4145-4159.

Lefkowitz, R.J., Pitcher, J., Krueger, K., and Daaka, Y. (1998). Mechanisms of beta-adrenergic receptor desensitization and resensitization. Advances in pharmacology *42*, 416-420.

Letourneur, F., Hennecke, S., Demolliere, C., and Cosson, P. (1995). Steric masking of a dilysine endoplasmic reticulum retention motif during assembly of the human high affinity receptor for immunoglobulin E. The Journal of cell biology *129*, 971-978.

Letourneur, F., and Klausner, R.D. (1992). A novel di-leucine motif and a tyrosine-based motif independently mediate lysosomal targeting and endocytosis of CD3 chains. Cell *69*, 1143-1157.

Li, L., Homan, K.T., Vishnivetskiy, S.A., Manglik, A., Tesmer, J.J., Gurevich, V.V., and Gurevich, E.V. (2015). G Protein-coupled Receptor Kinases of the GRK4 Protein Subfamily Phosphorylate Inactive G Protein-coupled Receptors (GPCRs). The Journal of biological chemistry *290*, 10775-10790.

Li, X., Staszewski, L., Xu, H., Durick, K., Zoller, M., and Adler, E. (2002). Human receptors for sweet and umami taste. Proceedings of the National Academy of Sciences of the United States of America *99*, 4692-4696.

Lund, T.C., Kobs, A.J., Kramer, A., Nyquist, M., Kuroki, M.T., Osborn, J., Lidke, D.S., Low-Nam, S.T., Blazar, B.R., and Tolar, J. (2013). Bone marrow stromal and vascular smooth muscle cells have chemosensory capacity via bitter taste receptor expression. PloS one *8*, e58945.

Lyu, R.M., Germano, P.M., Choi, J.K., Le, S.V., and Pisegna, J.R. (2000). Identification of an essential amino acid motif within the C terminus of the pituitary adenylate cyclase-activating polypeptide type I receptor that is critical for signal transduction but not for receptor internalization. The Journal of biological chemistry *275*, 36134-36142.

Mackintosh, C. (2004). Dynamic interactions between 14-3-3 proteins and phosphoproteins regulate diverse cellular processes. The Biochemical journal *381*, 329-342.

Maehashi, K., Matano, M., Wang, H., Vo, L.A., Yamamoto, Y., and Huang, L. (2008). Bitter peptides activate hTAS2Rs, the human bitter receptors. Biochemical and biophysical research communications *365*, 851-855.

Maggio, R., Novi, F., Scarselli, M., and Corsini, G.U. (2005). The impact of G-protein-coupled receptor hetero-oligomerization on function and pharmacology. FEBS J *272*, 2939-2946.

Makhija, L., Krishnan, V., Rehman, R., Chakraborty, S., Maity, S., Mabalirajan, U., Chakraborty, K., Ghosh, B., and Agrawal, A. (2014). Chemical chaperones mitigate experimental asthma by attenuating endoplasmic reticulum stress. American journal of respiratory cell and molecular biology *50*, 923-931.

Manson, M.L., Safholm, J., Al-Ameri, M., Bergman, P., Orre, A.C., Sward, K., James, A., Dahlen, S.E., and Adner, M. (2014). Bitter taste receptor agonists mediate relaxation of human and rodent vascular smooth muscle. European journal of pharmacology *740C*, 302-311.

Mant, A., Elliott, D., Eyers, P.A., and O'Kelly, I.M. (2011). Protein kinase A is central for forward transport of two-pore domain potassium channels K2P3.1 and K2P9.1. The Journal of biological chemistry *286*, 14110-14119.

Margolskee, R.F. (2002). Molecular mechanisms of bitter and sweet taste transduction. The Journal of biological chemistry *277*, 1-4.

Masuho, I., Tateyama, M., and Saitoh, O. (2005). Characterization of bitter taste responses of intestinal STC-1 cells. Chemical senses *30*, 281-290.

Matsunami, H., Montmayeur, J.P., and Buck, L.B. (2000). A family of candidate taste receptors in human and mouse. Nature *404*, 601-604.

Mattes, R.D. (2001). The taste of fat elevates postprandial triacylglycerol. Physiology & behavior *74*, 343-348.

Maudsley, S., Martin, B., and Luttrell, L.M. (2005). The origins of diversity and specificity in g protein-coupled receptor signaling. The Journal of pharmacology and experimental therapeutics *314*, 485-494.

McKemy, D.D., Neuhausser, W.M., and Julius, D. (2002). Identification of a cold receptor reveals a general role for TRP channels in thermosensation. Nature *416*, 52-58.

McLaughlin, S.K., McKinnon, P.J., and Margolskee, R.F. (1992). Gustducin is a taste-cell-specific G protein closely related to the transducins. Nature *357*, 563-569.

Mennella, J.A., Pepino, M.Y., and Reed, D.R. (2005). Genetic and environmental determinants of bitter perception and sweet preferences. Pediatrics *115*, e216-222.

Mennella, J.A., Spector, A.C., Reed, D.R., and Coldwell, S.E. (2013). The bad taste of medicines: overview of basic research on bitter taste. Clin Ther *35*, 1225-1246.

Meyerhof, W. (2005). Elucidation of mammalian bitter taste. Reviews of physiology, biochemistry and pharmacology *154*, 37-72.

Meyerhof, W., Batram, C., Kuhn, C., Brockhoff, A., Chudoba, E., Bufe, B., Appendino, G., and Behrens, M. (2010). The molecular receptive ranges of human TAS2R bitter taste receptors. Chemical senses *35*, 157-170.

Miller, I.J. (1995). Handbook of olfaction and gustation (New York: Marcel Dekker).

Miller, I.J., Jr. (1986). Variation in human fungiform taste bud densities among regions and subjects. The Anatomical record *216*, 474-482.

Miller, I.J., Jr., and Preslar, A.J. (1975). Spatial distribution of rat fungiform papillae. The Anatomical record *181*, 679-684.

Milojevic, T., Reiterer, V., Stefan, E., Korkhov, V.M., Dorostkar, M.M., Ducza, E., Ogris, E., Boehm, S., Freissmuth, M., and Nanoff, C. (2006). The ubiquitin-specific protease Usp4 regulates the cell surface level of the A2A receptor. Molecular pharmacology *69*, 1083-1094.

Mostafapour, S., Kobilka, B.K., and von Zastrow, M. (1996). Pharmacological sequestration of a chimeric beta 3/beta 2 adrenergic receptor occurs without a corresponding amount of receptor internalization. Receptors & signal transduction *6*, 151-163.

Mrowiec, T., and Schwappach, B. (2006). 14-3-3 proteins in membrane protein transport. Biol Chem *387*, 1227-1236.

Mueller, K.L., Hoon, M.A., Erlenbach, I., Chandrashekar, J., Zuker, C.S., and Ryba, N.J. (2005). The receptors and coding logic for bitter taste. Nature *434*, 225-229.

Mulvany, M.J., and Halpern, W. (1977). Contractile properties of small arterial resistance vessels in spontaneously hypertensive and normotensive rats. Circulation research *41*, 19-26.

Munzel, T., Afanas'ev, I.B., Kleschyov, A.L., and Harrison, D.G. (2002). Detection of superoxide in vascular tissue. Arteriosclerosis, thrombosis, and vascular biology *22*, 1761-1768.

Naim, M., Seifert, R., Nurnberg, B., Grunbaum, L., and Schultz, G. (1994). Some taste substances are direct activators of G-proteins. The Biochemical journal *297 (Pt 3)*, 451-454.

Namba, T., Sugimoto, Y., Negishi, M., Irie, A., Ushikubi, F., Kakizuka, A., Ito, S., Ichikawa, A., and Narumiya, S. (1993). Alternative splicing of C-terminal tail of prostaglandin E receptor subtype EP3 determines G-protein specificity. Nature *365*, 166-170.

Nelson, G., Chandrashekar, J., Hoon, M.A., Feng, L., Zhao, G., Ryba, N.J., and Zuker, C.S. (2002). An amino-acid taste receptor. Nature *416*, 199-202.

Nelson, G., Hoon, M.A., Chandrashekar, J., Zhang, Y., Ryba, N.J., and Zuker, C.S. (2001). Mammalian sweet taste receptors. Cell *106*, 381-390.

Okamoto, Y., Bernstein, J.D., and Shikano, S. (2013). Role of C-terminal membrane-proximal basic residues in cell surface trafficking of HIV coreceptor GPR15 protein. The Journal of biological chemistry *288*, 9189-9199.

Oldham, W.M., and Hamm, H.E. (2008). Heterotrimeric G protein activation by G-protein-coupled receptors. Nature reviews Molecular cell biology *9*, 60-71.

Ouedraogo, M., Lecat, S., Rochdi, M.D., Hachet-Haas, M., Matthes, H., Gicquiaux, H., Verrier, S., Gaire, M., Glasser, N., Mely, Y.*, et al.* (2008). Distinct motifs of neuropeptide Y receptors differentially regulate trafficking and desensitization. Traffic *9*, 305-324.

Ozeck, M., Brust, P., Xu, H., and Servant, G. (2004). Receptors for bitter, sweet and umami taste couple to inhibitory G protein signaling pathways. European journal of pharmacology *489*, 139-149.

Palczewski, K., Kumasaka, T., Hori, T., Behnke, C.A., Motoshima, H., Fox, B.A., Le Trong, I., Teller, D.C., Okada, T., Stenkamp, R.E., *et al.* (2000). Crystal structure of rhodopsin: A G protein-coupled receptor. Science *289*, 739-745.

Pankevych, H., Korkhov, V., Freissmuth, M., and Nanoff, C. (2003). Truncation of the A1 adenosine receptor reveals distinct roles of the membrane-proximal carboxyl terminus in receptor folding and G protein coupling. The Journal of biological chemistry *278*, 30283-30293.

Park, P.S., and Palczewski, K. (2005). Diversifying the repertoire of G protein-coupled receptors through oligomerization. Proceedings of the National Academy of Sciences of the United States of America *102*, 8793-8794.

Perez, C.A., Huang, L., Rong, M., Kozak, J.A., Preuss, A.K., Zhang, H., Max, M., and Margolskee, R.F. (2002). A transient receptor potential channel expressed in taste receptor cells. Nature neuroscience *5*, 1169-1176.

Perry, S.J., Baillie, G.S., Kohout, T.A., McPhee, I., Magiera, M.M., Ang, K.L., Miller, W.E., McLean, A.J., Conti, M., Houslay, M.D., *et al.* (2002). Targeting of cyclic AMP degradation to beta 2-adrenergic receptors by beta-arrestins. Science *298*, 834-836.

Petaja-Repo, U.E., Hogue, M., Bhalla, S., Laperriere, A., Morello, J.P., and Bouvier, M. (2002). Ligands act as pharmacological chaperones and increase the efficiency of delta opioid receptor maturation. The EMBO journal *21*, 1628-1637.

Petaja-Repo, U.E., Hogue, M., Laperriere, A., Bhalla, S., Walker, P., and Bouvier, M. (2001). Newly synthesized human delta opioid receptors retained in the endoplasmic

reticulum are retrotranslocated to the cytosol, deglycosylated, ubiquitinated, and degraded by the proteasome. The Journal of biological chemistry *276*, 4416-4423.

Petaja-Repo, U.E., Hogue, M., Laperriere, A., Walker, P., and Bouvier, M. (2000). Export from the endoplasmic reticulum represents the limiting step in the maturation and cell surface expression of the human delta opioid receptor. The Journal of biological chemistry *275*, 13727-13736.

Pidamale, R., Sowmya, B., Thomas, A., and Jose, T. (2012). Genetic sensitivity to bitter taste of 6-n Propylthiouracil: A useful diagnostic aid to detect early childhood caries in pre-school children. Indian journal of human genetics *18*, 101-105.

Pierce, K.L., Premont, R.T., and Lefkowitz, R.J. (2002). Seven-transmembrane receptors. Nature reviews Molecular cell biology *3*, 639-650.

Pin, J.P., Galvez, T., and Prezeau, L. (2003). Evolution, structure, and activation mechanism of family 3/C G-protein-coupled receptors. Pharmacology & therapeutics *98*, 325-354.

Pitcher, J.A., Freedman, N.J., and Lefkowitz, R.J. (1998). G protein-coupled receptor kinases. Annual review of biochemistry *67*, 653-692.

Prescott, J., Soo, J., Campbell, H., and Roberts, C. (2004). Responses of PROP taster groups to variations in sensory qualities within foods and beverages. Physiology & behavior *82*, 459-469.

Prescott, J., and Swain-Campbell, N. (2000). Responses to repeated oral irritation by capsaicin, cinnamaldehyde and ethanol in PROP tasters and non-tasters. Chemical senses *25*, 239-246.

Pronin, A.N., Tang, H., Connor, J., and Keung, W. (2004). Identification of ligands for two human bitter T2R receptors. Chemical senses *29*, 583-593.

Pronin, A.N., Xu, H., Tang, H., Zhang, L., Li, Q., and Li, X. (2007). Specific alleles of bitter receptor genes influence human sensitivity to the bitterness of aloin and saccharin. Current biology : CB *17*, 1403-1408.

Pulkkinen, V., Manson, M.L., Safholm, J., Adner, M., and Dahlen, S.E. (2012). The bitter taste receptor (TAS2R) agonists denatonium and chloroquine display distinct patterns of relaxation of the guinea pig trachea. American journal of physiology Lung cellular and molecular physiology *303*, L956-966.

Pydi, S.P., Bhullar, R.P., and Chelikani, P. (2012). Constitutively active mutant gives novel insights into the mechanism of bitter taste receptor activation. Journal of neurochemistry *122*, 537-544.

Pydi, S.P., Chakraborty, R., Bhullar, R.P., and Chelikani, P. (2013). Role of rhodopsin N-terminus in structure and function of rhodopsin-bitter taste receptor chimeras. Biochemical and biophysical research communications *430*, 179-182.

Pydi, S.P., Singh, N., Upadhyaya, J., Bhullar, R.P., and Chelikani, P. (2014a). The third intracellular loop plays a critical role in bitter taste receptor activation. Biochimica et biophysica acta *1838*, 231-236.

Pydi, S.P., Sobotkiewicz, T., Billakanti, R., Bhullar, R.P., Loewen, M.C., and Chelikani, P. (2014b). Amino acid derivatives as bitter taste receptor (T2R) blockers. The Journal of biological chemistry *289*, 25054-25066.

Ramon, E., del Valle, L.J., and Garriga, P. (2003). Unusual thermal and conformational properties of the rhodopsin congenital night blindness mutant Thr-94 --> Ile. The Journal of biological chemistry *278*, 6427-6432.

Reed, D.R., Nanthakumar, E., North, M., Bell, C., Bartoshuk, L.M., and Price, R.A. (1999). Localization of a gene for bitter-taste perception to human chromosome 5p15. American journal of human genetics *64*, 1478-1480.

Reiter, E., and Lefkowitz, R.J. (2006). GRKs and beta-arrestins: roles in receptor silencing, trafficking and signaling. Trends in endocrinology and metabolism: TEM *17*, 159-165.

Ren, X.R., Reiter, E., Ahn, S., Kim, J., Chen, W., and Lefkowitz, R.J. (2005). Different G protein-coupled receptor kinases govern G protein and beta-arrestin-mediated signaling of V2 vasopressin receptor. Proceedings of the National Academy of Sciences of the United States of America *102*, 1448-1453.

Robinett, K.S., Deshpande, D.A., Malone, M.M., and Liggett, S.B. (2011). Agonist-promoted homologous desensitization of human airway smooth muscle bitter taste receptors. American journal of respiratory cell and molecular biology *45*, 1069-1074.

Roettger, B.F., Rentsch, R.U., Hadac, E.M., Hellen, E.H., Burghardt, T.P., and Miller, L.J. (1995). Insulation of a G protein-coupled receptor on the plasmalemmal surface of the pancreatic acinar cell. The Journal of cell biology *130*, 579-590.

Rozengurt, E. (2006). Taste receptors in the gastrointestinal tract. I. Bitter taste receptors and alpha-gustducin in the mammalian gut. American journal of physiology Gastrointestinal and liver physiology *291*, G171-177.

Rupesh, S., and Nayak, U.A. (2006). Genetic sensitivity to the bitter taste of 6-n propylthiouracil: a new risk determinant for dental caries in children. Journal of the Indian Society of Pedodontics and Preventive Dentistry *24*, 63-68.

Sainz, E., Cavenagh, M.M., Gutierrez, J., Battey, J.F., Northup, J.K., and Sullivan, S.L. (2007). Functional characterization of human bitter taste receptors. The Biochemical journal *403*, 537-543.

Sainz, E., Korley, J.N., Battey, J.F., and Sullivan, S.L. (2001). Identification of a novel member of the T1R family of putative taste receptors. Journal of neurochemistry *77*, 896-903.

Sakurai, T., Misaka, T., Ishiguro, M., Masuda, K., Sugawara, T., Ito, K., Kobayashi, T., Matsuo, S., Ishimaru, Y., Asakura, T.*, et al.* (2010). Characterization of the beta-D-glucopyranoside binding site of the human bitter taste receptor hTAS2R16. The Journal of biological chemistry *285*, 28373-28378.

Saliba, R.S., Munro, P.M., Luthert, P.J., and Cheetham, M.E. (2002). The cellular fate of mutant rhodopsin: quality control, degradation and aggresome formation. J Cell Sci *115*, 2907-2918.

Saras, J., and Heldin, C.H. (1996). PDZ domains bind carboxy-terminal sequences of target proteins. Trends in biochemical sciences *21*, 455-458.

Schioth, H.B., and Fredriksson, R. (2005). The GRAFS classification system of G-protein coupled receptors in comparative perspective. General and comparative endocrinology *142*, 94-101.

Schulein, R., Hermosilla, R., Oksche, A., Dehe, M., Wiesner, B., Krause, G., and Rosenthal, W. (1998). A dileucine sequence and an upstream glutamate residue in the intracellular carboxyl terminus of the vasopressin V2 receptor are essential for cell surface transport in COS.M6 cells. Molecular pharmacology *54*, 525-535.

Sclafani, A., Ackroff, K., and Abumrad, N.A. (2007). CD36 gene deletion reduces fat preference and intake but not post-oral fat conditioning in mice. American journal of physiology Regulatory, integrative and comparative physiology *293*, R1823-1832.

Seifert, R., and Wenzel-Seifert, K. (2002). Constitutive activity of G-protein-coupled receptors: cause of disease and common property of wild-type receptors. Naunyn-Schmiedeberg's archives of pharmacology *366*, 381-416.

Shah, A.S., Ben-Shahar, Y., Moninger, T.O., Kline, J.N., and Welsh, M.J. (2009). Motile cilia of human airway epithelia are chemosensory. Science *325*, 1131-1134.

Sharman, J.L., Benson, H.E., Pawson, A.J., Lukito, V., Mpamhanga, C.P., Bombail, V., Davenport, A.P., Peters, J.A., Spedding, M., Harmar, A.J.*, et al.* (2013). IUPHAR-DB: updated database content and new features. Nucleic acids research *41*, D1083-1088.

Shepard, T.H. (1961). Phenylthiocarbamide Non-Tasting among Congenital Athyrotic Cretins: Further Studies in an Attempt to Explain the Increased Incidence. The Journal of clinical investigation *40*, 1751-1757.

Shiffman, D., O'Meara, E.S., Bare, L.A., Rowland, C.M., Louie, J.Z., Arellano, A.R., Lumley, T., Rice, K., Iakoubova, O., Luke, M.M.*, et al.* (2008). Association of gene variants with incident myocardial infarction in the Cardiovascular Health Study. Arteriosclerosis, thrombosis, and vascular biology *28*, 173-179.

Shimoda, L.A., Sham, J.S., Shimoda, T.H., and Sylvester, J.T. (2000). L-type Ca(2+) channels, resting [Ca(2+)](i), and ET-1-induced responses in chronically hypoxic pulmonary myocytes. American journal of physiology Lung cellular and molecular physiology *279*, L884-894.

Shindo, Y., Miura, H., Carninci, P., Kawai, J., Hayashizaki, Y., Ninomiya, Y., Hino, A., Kanda, T., and Kusakabe, Y. (2008). G alpha14 is a candidate mediator of sweet/umami signal transduction in the posterior region of the mouse tongue. Biochemical and biophysical research communications *376*, 504-508.

Silver, P.J. (1986). Pharmacological modulation of cardiac and vascular contractile protein function. Journal of cardiovascular pharmacology *8 Suppl 9*, S34-46.

Singh, N., Chakraborty, R., Bhullar, R.P., and Chelikani, P. (2014). Differential expression of bitter taste receptors in non-cancerous breast epithelial and breast cancer cells. Biochemical and biophysical research communications *446*, 499-503.

Singh, N., Pydi, S.P., Upadhyaya, J., and Chelikani, P. (2011a). Structural basis of activation of bitter taste receptor T2R1 and comparison with Class A G-protein-coupled receptors (GPCRs). The Journal of biological chemistry *286*, 36032-36041.

Singh, N., Vrontakis, M., Parkinson, F., and Chelikani, P. (2011b). Functional bitter taste receptors are expressed in brain cells. Biochemical and biophysical research communications *406*, 146-151.

Slack, J.P., Brockhoff, A., Batram, C., Menzel, S., Sonnabend, C., Born, S., Galindo, M.M., Kohl, S., Thalmann, S., Ostopovici-Halip, L.*, et al.* (2010). Modulation of bitter taste perception by a small molecule hTAS2R antagonist. Current biology : CB *20*, 1104-1109.

Spielman, A.I. (1998). Gustducin and its role in taste. Journal of dental research *77*, 539-544.

Spielman, A.I., Nagai, H., Sunavala, G., Dasso, M., Breer, H., Boekhoff, I., Huque, T., Whitney, G., and Brand, J.G. (1996). Rapid kinetics of second messenger production in bitter taste. The American journal of physiology *270*, C926-931.

Stewart, J.E., Feinle-Bisset, C., Golding, M., Delahunty, C., Clifton, P.M., and Keast, R.S. (2010). Oral sensitivity to fatty acids, food consumption and BMI in human subjects. The British journal of nutrition *104*, 145-152.

Takhar, S., Gyomorey, S., Su, R.C., Mathi, S.K., Li, X., and Wheeler, M.B. (1996). The third cytoplasmic domain of the GLP-1[7-36 amide] receptor is required for coupling to the adenylyl cyclase system. Endocrinology *137*, 2175-2178.

Tan, J., Abrol, R., Trzaskowski, B., and Goddard, W.A., 3rd (2012). 3D Structure Prediction of TAS2R38 Bitter Receptors Bound to Agonists Phenylthiocarbamide (PTC) and 6-n-Propylthiouracil (PROP). Journal of chemical information and modeling *52*, 1875-1885.

Teasdale, R.D., and Jackson, M.R. (1996). Signal-mediated sorting of membrane proteins between the endoplasmic reticulum and the golgi apparatus. Annual review of cell and developmental biology *12*, 27-54.

Tepper, B.J., and Nurse, R.J. (1997). Fat perception is related to PROP taster status. Physiology & behavior *61*, 949-954.

Terrillon, S., and Bouvier, M. (2004). Roles of G-protein-coupled receptor dimerization. EMBO reports *5*, 30-34.

Tetsuka, M., Saito, Y., Imai, K., Doi, H., and Maruyama, K. (2004). The basic residues in the membrane-proximal C-terminal tail of the rat melanin-concentrating hormone receptor 1 are required for receptor function. Endocrinology *145*, 3712-3723.

Timpson, N.J., Christensen, M., Lawlor, D.A., Gaunt, T.R., Day, I.N., Ebrahim, S., and Davey Smith, G. (2005). TAS2R38 (phenylthiocarbamide) haplotypes, coronary heart disease traits, and eating behavior in the British Women's Heart and Health Study. The American journal of clinical nutrition *81*, 1005-1011.

Tizzano, M., Cristofoletti, M., Sbarbati, A., and Finger, T.E. (2011). Expression of taste receptors in solitary chemosensory cells of rodent airways. BMC pulmonary medicine *11*, 3.

Tizzano, M., Dvoryanchikov, G., Barrows, J.K., Kim, S., Chaudhari, N., and Finger, T.E. (2008). Expression of Galpha14 in sweet-transducing taste cells of the posterior tongue. BMC Neurosci *9*, 110.

Tizzano, M., Gulbransen, B.D., Vandenbeuch, A., Clapp, T.R., Herman, J.P., Sibhatu, H.M., Churchill, M.E., Silver, W.L., Kinnamon, S.C., and Finger, T.E. (2010). Nasal chemosensory cells use bitter taste signaling to detect irritants and bacterial signals. Proceedings of the National Academy of Sciences of the United States of America *107*, 3210-3215.

Tomhave, E.D., Richardson, R.M., Didsbury, J.R., Menard, L., Snyderman, R., and Ali, H. (1994). Cross-desensitization of receptors for peptide chemoattractants. Characterization of a new form of leukocyte regulation. Journal of immunology *153*, 3267-3275.

Ueda, T., Ugawa, S., Yamamura, H., Imaizumi, Y., and Shimada, S. (2003). Functional interaction between T2R taste receptors and G-protein alpha subunits expressed in taste receptor cells. The Journal of neuroscience : the official journal of the Society for Neuroscience *23*, 7376-7380.

Ugawa, S., Minami, Y., Guo, W., Saishin, Y., Takatsuji, K., Yamamoto, T., Tohyama, M., and Shimada, S. (1998). Receptor that leaves a sour taste in the mouth. Nature *395*, 555-556.

Upadhyaya, J., Pydi, S.P., Singh, N., Aluko, R.E., and Chelikani, P. (2010). Bitter taste receptor T2R1 is activated by dipeptides and tripeptides. Biochemical and biophysical research communications *398*, 331-335.

Upadhyaya, J., Singh, N., Bhullar, R.P., and Chelikani, P. (2015). The structure-function role of C-terminus in human bitter taste receptor T2R4 signaling. Biochimica et biophysica acta *1848*, 1502-1508.

Upadhyaya, J.D., Singh, N., Sikarwar, A.S., Chakraborty, R., Pydi, S.P., Bhullar, R.P., Dakshinamurti, S., and Chelikani, P. (2014). Dextromethorphan mediated bitter taste receptor activation in the pulmonary circuit causes vasoconstriction. PloS one *9*, e110373.

van Hooft, J.A., and Vijverberg, H.P. (1996). Selection of distinct conformational states of the 5-HT3 receptor by full and partial agonists. British journal of pharmacology *117*, 839-846.

VanLeeuwen, D., Steffey, M.E., Donahue, C., Ho, G., and MacKenzie, R.G. (2003). Cell surface expression of the melanocortin-4 receptor is dependent on a C-terminal di-isoleucine sequence at codons 316/317. The Journal of biological chemistry *278*, 15935-15940.

Venkatesan, S., Petrovic, A., Locati, M., Kim, Y.O., Weissman, D., and Murphy, P.M. (2001). A membrane-proximal basic domain and cysteine cluster in the C-terminal tail of CCR5 constitute a bipartite motif critical for cell surface expression. The Journal of biological chemistry *276*, 40133-40145.

Verma, P., Shetty, V., and Hegde, A.M. (2006). Propylthiouracil (PROP)--a tool to determine taster status in relation to caries experience, streptococcus mutans levels and dietary preferences in children. The Journal of clinical pediatric dentistry *31*, 113-117.

Wang, J.C., Hinrichs, A.L., Bertelsen, S., Stock, H., Budde, J.P., Dick, D.M., Bucholz, K.K., Rice, J., Saccone, N., Edenberg, H.J.*, et al.* (2007). Functional variants in TAS2R38 and TAS2R16 influence alcohol consumption in high-risk families of African-American origin. Alcoholism, clinical and experimental research *31*, 209-215.

Wang, Y., Erickson, R.P., and Simon, S.A. (1995). Modulation of rat chorda tympani nerve activity by lingual nerve stimulation. Journal of neurophysiology *73*, 1468-1483.

Whitehead, M.C., Ganchrow, J.R., Ganchrow, D., and Yao, B. (1999). Organization of geniculate and trigeminal ganglion cells innervating single fungiform taste papillae: a study with tetramethylrhodamine dextran amine labeling. Neuroscience *93*, 931-941.

Williams, J.T., Ingram, S.L., Henderson, G., Chavkin, C., von Zastrow, M., Schulz, S., Koch, T., Evans, C.J., and Christie, M.J. (2013). Regulation of mu-opioid receptors: desensitization, phosphorylation, internalization, and tolerance. Pharmacological reviews *65*, 223-254.

Wong, G.T., Gannon, K.S., and Margolskee, R.F. (1996). Transduction of bitter and sweet taste by gustducin. Nature *381*, 796-800.

Wu, J., and Aluko, R.E. (2007). Quantitative structure-activity relationship study of bitter di- and tri-peptides including relationship with angiotensin I-converting enzyme inhibitory activity. Journal of peptide science : an official publication of the European Peptide Society *13*, 63-69.

Wu, S.V., Rozengurt, N., Yang, M., Young, S.H., Sinnett-Smith, J., and Rozengurt, E. (2002). Expression of bitter taste receptors of the T2R family in the gastrointestinal tract and enteroendocrine STC-1 cells. Proceedings of the National Academy of Sciences of the United States of America *99*, 2392-2397.

Wu, T.C., Chao, C.Y., Lin, S.J., and Chen, J.W. (2012). Low-dose dextromethorphan, a NADPH oxidase inhibitor, reduces blood pressure and enhances vascular protection in experimental hypertension. PloS one *7*, e46067.

Xu, J., Cao, J., Iguchi, N., Riethmacher, D., and Huang, L. (2013). Functional characterization of bitter-taste receptors expressed in mammalian testis. Molecular human reproduction *19*, 17-28.

Zhang, B., Albaker, A., Plouffe, B., Lefebvre, C., and Tiberi, M. (2014). Constitutive activities and inverse agonism in dopamine receptors. Advances in pharmacology *70*, 175-214.

Zhang, C.H., Lifshitz, L.M., Uy, K.F., Ikebe, M., Fogarty, K.E., and ZhuGe, R. (2013). The cellular and molecular basis of bitter tastant-induced bronchodilation. PLoS biology *11*, e1001501.

Zhang, F.L., and Casey, P.J. (1996). Protein prenylation: molecular mechanisms and functional consequences. Annual review of biochemistry *65*, 241-269.

Zhang, W., Qin, L., Wang, T., Wei, S.J., Gao, H.M., Liu, J., Wilson, B., Liu, B., Zhang, W., Kim, H.C*., et al.* (2005). 3-hydroxymorphinan is neurotrophic to dopaminergic neurons and is also neuroprotective against LPS-induced neurotoxicity. FASEB journal : official publication of the Federation of American Societies for Experimental Biology *19*, 395-397.

Zhang, Y., Hoon, M.A., Chandrashekar, J., Mueller, K.L., Cook, B., Wu, D., Zuker, C.S., and Ryba, N.J. (2003). Coding of sweet, bitter, and umami tastes: different receptor cells sharing similar signaling pathways. Cell *112*, 293-301.

Zubare-Samuelov, M., Shaul, M.E., Peri, I., Aliluiko, A., Tirosh, O., and Naim, M. (2005). Inhibition of signal termination-related kinases by membrane-permeant bitter and sweet

tastants: potential role in taste signal termination. American journal of physiology Cell physiology *289*, C483-492.